UNIVERSITY OF ÇUKUROVA
INSTITUTE OF NATURAL AND APPLIED SCIENCES

PhD THESIS

Şule ÇOLAK

ANTENNA ARRAYS IN ULTRA WIDEBAND COMMUNICATIONS

DEPARTMENT OF ELECTRICAL AND ELECTRONICS ENGINEERING

ADANA, 2007

ÇUKUROVA ÜNİVERSİTESİ
FEN BİLİMLERİ ENSTİTÜSÜ

ANTENNA ARRAYS IN ULTRA WIDEBAND COMMUNICATIONS

Şule ÇOLAK

DOKTORA TEZİ

ELEKTRİK-ELEKTRONİK MÜHENDİSLİĞİ ANABİLİM DALI

Bu tez …./…./ 2007 Tarihinde Aşağıdaki Jüri Üyeleri Tarafından Oybirliği / Oyçokluğu İle Kabul Edilmiştir.

İmza............……..……..	İmza................………..	İmza...............………….
Prof. Dr. A.Hamit SERBEST	Prof. Dr. Gülsen ÖNENGÜT	Prof. Dr. Arif NACAROĞLU
DANIŞMAN	ÜYE	ÜYE

İmza……….........………	İmza……....................….
Doç. Dr. Turgut İKİZ	Yrd. Doç. Dr. Sami ARICA
ÜYE	ÜYE

Bu tez Enstitümüz Elektrik Elektronik Mühendisliği Anabilim Dalında hazırlanmıştır.

Kod No:

Prof. Dr. Aziz ERTUNÇ
Enstitü Müdürü
İmza-Mühür

ABSTRACT

PhD THESIS

ANTENNA ARRAYS IN ULTRA WIDEBAND COMMUNICATIONS

Şule ÇOLAK

DEPARTMENT OF ELECTRICAL AND ELECTRONICS ENGINEERING
INSTITUTE OF NATURAL AND APPLIED SCIENCES
UNIVERSITY OF ÇUKUROVA

Supervisor: Prof. Dr. A. Hamit SERBEST
Year: 2007, **Pages**:118

Jury: Prof. Dr. A. Hamit SERBEST
Prof. Dr. Gülsen ÖNENGÜT
Prof. Dr. Arif NACAROĞLU
Assc. Prof. Dr. Turgut İKİZ
Asst. Prof. Dr. Sami ARICA

In this study, characteristics for radiation of ultra wideband (UWB) signals from an array of dipoles and reception of the transmitted pulse by a receiving dipole are investigated. Analysis is performed in the frequency domain. Mathematical formulations for radiated and received energy and correlation coefficient expressions are derived using analytical approach in the frequency domain. Computer programs based on these mathematical operations are created and computed results are presented.

The approach is first applied to a single dipole considering that it is the basic element of the array and mathematically simple. Then, the behavior of an array of dipoles with equally spaced same length elements and different length elements are analyzed, respectively. Additionally, beam scanning for UWB arrays is investigated. Effects of changing various antenna parameters such as element spacing and the number of antenna elements are illustrated.

Key Words: Antenna Array, Correlation Coefficient, Dipole Antenna, Energy, UWB

ÖZ

DOKTORA TEZİ

ULTRA GENİŞ BANDLI HABERLEŞME SİSTEMLERİNDE ANTEN DİZİLERİ

Şule ÇOLAK

ELEKTRİK ELEKTRONİK MÜHENDİSLİĞİ ANABİLİM DALI
FEN BİLİMLERİ ENSTİTÜSÜ
ÇUKUROVA ÜNİVERSİTESİ

Danışman: Prof. Dr. A. Hamit SERBEST
Yıl: 2007, **Sayfa**:118

Jüri: Prof. Dr. A. Hamit SERBEST
Prof. Dr. Gülsen ÖNENGÜT
Prof. Dr. Arif NACAROĞLU
Doç. Dr. Turgut İKİZ
Yrd. Doç. Dr. Sami ARICA

Bu çalışmada ultra geniş bandlı (UWB) sinyallerin bir dipol dizisinden yayılması ve gönderilen sinyallerin alıcı dipol tarafından alınma karakteristiği incelenmiştir. Analiz frekans domaininde gerçekleştirilmiştir. Yayılan ve alınan enerji, ve korelasyon katsayısı ifadelerinin matematiksel formülleri frekans domaininde analitik yaklaşım kullanılarak elde edilmiştir. Bu matematiksel işlemler temel alınarak bilgisayar programları geliştirilmiş ve hesaplanan sonuçlar gösterilmiştir.

Yaklaşım ilk olarak dizinin temel elemanı olduğu ve matematiksel olarak basit olduğu gözönüne alınarak tek dipol elemanına uygulanmıştır. Daha sonra da, sırasıyla, eşit aralıklı aynı uzunluklu dipol dizilerinin ve eşit aralıklı farklı uzunluklu dipol dizilerinin davranışları analiz edilmiştir. Ayrıca, UWB anten dizilerinde ışın tarama incelenmiştir. Eleman aralığı ve eleman sayısı gibi çeşitli anten parametrelerinin değişiminin etkileri gösterilmiştir.

Anahtar Kelimeler: Anten Dizisi, Korelasyon Katsayısı, Dipol Anten, Enerji, UWB.

ACKNOWLEDGEMENTS

I would first like to acknowledge my supervisor Prof. Dr. A. Hamit SERBEST and co-supervisor Assc. Prof. Dr. Tan F. WONG. Without their guidance and encouragement, this dissertation could not have been completed.

I would also like to acknowledge my committee members Prof. Dr. Gülsen ÖNENGÜT, Prof. Dr. Arif NACAROĞLU, Assc. Prof. Dr. Turgut İKİZ, and Asst. Prof. Dr. Sami ARICA for their time and support. My educational experience as a doctoral student has also been enriched by the other faculty and graduate students in our department. I furthermore thank to PhD students and faculty members in Wireless Information Networking Group of Electrical and Computer Enginnering Department at University of Florida, especially Sarva Vijayakumaran, for their valuable help and support.

I am grateful to my husband Selçuk for his unconditional love, patience and encouragement, also to my son Arda Bora for his inspiration. And last but certainly not least, I am ever thankful to my parents and my sisters for their continuous love and support.

TABLE OF CONTENTS **PAGE**

NOTATIONS AND ABBREVIATIONS

c	: Speed of Light
CC	: Correlation Coefficient
$\mathbf{E}$	: Electric Field Vector
FCC	: United States Federal Communications Commission
T	: Pulse Duration
f_c	: Center Frequency
$\mathbf{h}_{eff}$	: Effective Length
θ	: Observation Angle
θ_s	: Scan Angle
UWB	: Ultra Wideband
W_{rad}	: Radiated Energy
W_{rec}	: Received Energy
Z	: Characteristic Impedance of Transmission Line
Z_L	: Load Impedance
Ω	: Antenna Parameter
$I(z,f)$	: Current Distribution along the Dipole
ζ_0	: Free Space Impedance
V_g	: Generator Voltage
V_L	: Load Voltage
λ_c	: Wavelength Corresponding to the Center Frequency
$2l$	: Dipole Length
M	: (2N+1) Number of Dipoles in an Antenna Array

LIST OF FIGURES **PAGE**

1. INTRODUCTION

Ultra Wideband (UWB) technology is the transmission and reception of ultra-short pulses whose characteristic spectrum extends over a wide frequency range. UWB systems operate at very low power and the information transmission is carried out by using short impulses over a large bandwidth.

According to the definition established by the OSD/DARPA (Office of the Secretary of Defense, Defense Advanced Research Projects Agency) UWB radar review panel (July 13, 1990), the term ultra-wideband refers to electromagnetic signal waveforms having -20 dB fractional bandwidths that are greater than 25% with respect to the center frequency or that occupy 1.5 GHz or more of spectrum (FCC, 2002).

In February 2002, the Federal Communications Commission (FCC) introduced a modified definition which is based on -10 dB bandwidth, instead of the -20 dB bandwidth used by the OSD/DARPA. This definition is proposed because ultra wideband devices operate close to noise level, and therefore, it would be a problem to measure the -20 dB bandwidth (FCC, 2002).

According to the FCC rules, a signal whose -10 dB fractional bandwidth is larger than 20% or whose -10 dB absolute bandwidth is larger than 500 MHz is classified as ultra wideband signal. Fractional bandwidth B_f is defined as

$$B_f = 2\frac{f_h - f_l}{f_h + f_l}, \tag{1}$$

where f_h and f_l are the upper and lower 10 dB points of the signal spectrum, respectively.

The proponents of the ultra wideband technology have claimed that the system has the ability to utilize the frequency spectrum without causing any interference problem to other conventional communication systems, because it has a low power spectral density. Figure 1.1 (Reed, 2005) shows spectrum utilization of UWB system and conventional narrowband system.

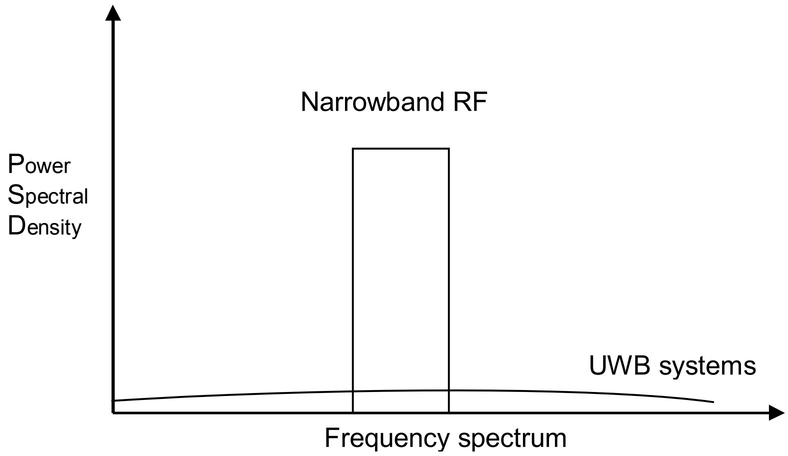

Figure1.1. Illustration of spectrum utilization by UWB systems

Ultra-wideband appears as an attractive technology for indoor wireless networks with high data-rate. Instead of transmitting and receiving modulated sinusoidal waveforms, a UWB communication system transmits GHz pulses which occupy a wide portion of the frequency spectrum.

UWB has become an attractive option for researchers in both industry and academia due to its low power, low interference and low regulation for present and future wireless applications. The system shares the frequency spectrum with other systems and extends over the same range with many licensed frequency bands. Therefore; due to these advantages, there has been an increasing interest in UWB communication systems recently.

Historically, UWB radar systems were developed mainly for military applications because of its penetration capabilities. Nowadays, UWB technology has also been in use for consumer electronics and communications.

1.1. Overview of Ultra-Wideband Communications

In today's world, although it is most common to use sinusoidal signals in wireless communication systems, the earliest electromagnetic communication systems were actually based on pulses (Ghavami et. al., 2004).

The spark gap generator is known to be the first UWB radio that was used by Hertz and Marconi in the late 1800's (Weightman, 2003). Heinrich Hertz used the spark gap to produce electromagnetic waves for his experiments in 1893. Similarly, Marconi used spark gap generator for electromagnetic data communications (Molisch, 2006). Marconi's spark-gap transmission experiments in 1901 were one of the first experiments about impulse radio. Additionally, Sommerfeld first analyzed the diffraction of a short pulse by a half-plane which is known to be one of the fundamental problems in UWB wave propagation (Qiu, 2005). Therefore, it can be assumed that the first practical UWB systems and theoretical research on UWB radiation goes back to more than one century ago. Nevertheless, the signals generated by the spark-gap transmitters had low spectral efficiency and low bit rate but large bandwidth (Molisch, 2006). During that period, researchers could not utilize this issue and it was perceived as a failure. Therefore, the communications became mainly narrowband after 1910, and ultra wideband research did not get any more interest until the 1960s when the studies began again for time domain electromagnetics with the innovative work of Gerald F. Ross.

In his studies, Ross described the transient behavior of microwave networks through their characteristic impulse responses. Also around this time, the sampling oscilloscope was developed by Hewlett Packard and some techniques were built up for subnanosecond (baseband) pulse generation. This allowed the analysis of short-duration signals in the time domain experimentally and provided the direct observation and measurement of the impulse response for microwave networks. When the techniques for impulse measurement were developed also for designing wideband antenna structures, researchers recognized that short pulse radar and communication systems could be built up utilizing the same equipments.

Afterwards, the main interest moved towards the techniques for the development of radar and communication devices. Designing high power, short pulse generators for UWB radar systems was investigated by the military. In particular, radar got a lot of interest because it was possible to obtain results with good accuracy. The low-frequency components were useful in penetrating objects, and ground penetrating radar was developed (Ghavami et. al., 2004).

In the 1970s, ultra wideband communications started to get more attention (Harmuth, 1981). Ross developed various applications for radar and communications at the Sperry Research Center. In April 1973, he was awarded the first UWB communications patent. Therefore, in the 1970s and 1980s, most of the research and development were in the military or in the works funded by the US Government.

UWB research fields continued to expand towards new areas. Several applications, such as automobile collision avoidance, positioning systems, and liquid-level sensing were developed (Ghavami et. al., 2004). Through the 1980s, UWB was employed by the radar research community to develop short-range, high-resolution sensing applications. One of the earliest applications of UWB technology was high power military radar. Also, low probability of intercept capability of UWB signals is utilized for covert communications and use of a very wide band of frequencies allowed detection of buried mines in ground penetrating radar applications. The term *ultra-wideband* was first applied around 1989 by the U.S. Department of Defense and this technology was earlier referred to as baseband carrier-free or impulse radar.

Small companies such as Multispectral Solutions, Inc., Aether Wire and Location, and Pulson Communications (Time Domain Corporation) also started basic research and development on communications and positioning systems, specializing in UWB technology, beginning in the late 1980s (Sholtz et. al., 2005).

By the mid-1990's, University of Southern California's UltRa Lab was established. UltRa Lab lobbied FCC to allow commercializing the UWB technology. In May 1998, a workshop sponsored by US Army Research Office and USC UltRa Lab was organized and soon after this conference, the companies working on UWB technology decided to band together and formed an informal industry association, Ultra-Wideband Working Group (http://www.uwb.org).

In the late 1990s, there has been a lot of interest regarding the application of UWB technology for wireless communications. Companies such as Time Domain Corporation, US Radar, Zircon Corporation had requested for permission from FCC to develop a small number of commercialized UWB devices. At the same time, USC's UltRa Lab acquired a license from FCC for experimental studies on UWB radio transmissions.

Since UWB signals occupy a large frequency range, they violate the frequency regulations assigned to other conventional narrowband systems all over the world. However, proponents of the technology in both industry and academia insisted that UWB emissions would not interfere with those other narrowband services. Then, after lengthy deliberations, the FCC issued its first report and order on UWB technology in April 2002 (FCC, 2002). In this ruling, it is specified that the UWB emission is allowed between the frequency ranges of 3.1 GHz and 10.6 GHz.

Since the late 1990s, the research and development of ultra wideband technology have widely emerged and become a promising technology which came to be known as *impulse radio*.

1.2. Literature on Ultra-Wideband Antennas

Transient radiation from antennas has been studied extensively in the literature (Franceschetti and Papas, 1974), (Samaddar, 1992), (Mokole, 1996) etc. Franceschetti and Papas (1974) introduced various heuristic procedures relating to the computation of transient radiation from elementary sources, such as coaxial apertures, infinitely long cylindrical antennas, finite cylindrical antennas and loop antennas. An approximate analysis of transient radiation from linear antennas and loops of arbitrary dimensions were presented in which transmission line techniques were used for modeling currents and voltages. This approximation has also been used for investigating the behavior of the radiated electric field from a half-wave dipole in free space excited by a single-cycle sinusoidal voltage (Samaddar, 1992), and for analyzing ultra-wideband arrays considering a linear array of thin dipoles that are excited by a single-cycle sine (Mokole, 1996). In this transmission line technique, the zero-order approximate solution for the current along the antenna is used in the frequency domain. This way, time-dependent current and the radiated electrical field could be calculated and interpreted easily.

Lamensdorf and Susman (1994) presented the concepts of pulse fidelity and correlation energy patterns for characterization of antennas in time domain. Pulse fidelity is a measure of the performance of the antenna, and time-domain correlation pattern shows the relationship between radiated pulses in different directions. In a recent study by McLean et.al., (2004, 2005) three UWB antenna performance descriptors were proposed: energy pattern, correlated energy pattern and correlation coefficient pattern. Dissanayake and Esselle (2006) used these definitions in a correlation based study to create new parameters to characterize and quantify performance of ultra wideband antennas and demonstrate their use through practical applications. Although the study also concerns pulse correlation coefficient concepts, it is carried out in the frequency domain.

Different techniques for optimizing the feed voltage, the transient radiation, and energy for dipole antenna and arrays were proposed by Pozar et. al. (1983, 1985) and Kang and Pozar (1986). Taha and Chagg (2002) developed algorithms for designing optimal template waveforms for UWB impulse radio in the presence of multipath.

Another frequency domain study was based on optimizing source pulses and detection templates in ultra wideband radio systems (Shan et. al., 2005). In this study, differential evolution, an improved version of the genetic algorithm was used to optimize the UWB signals for a narrow band thin wire dipole antenna system and a wide band planar antenna system.

Chen et al. (2003) presented the basic design considerations for transmitting and receiving antennas in the UWB systems by using the finite difference time domain (FDTD) method. In the paper, it is emphasized that the overall performances of UWB systems can be optimized by choosing the antennas and the source pulses appropriately. Another design consideration for a transmitting and receiving antenna system was presented by Wu et al. (2003) analyzing two identical planar bowtie antennas numerically and experimentally in both time and frequency domains. Authors in this study also utilized an EM software package (XFDTD) for numerical analysis.

The dependence of the power radiated from ultra wideband antennas both on frequency and direction is presented experimentally by Malik et al.(2006). The variation of antenna radiation patterns with frequency is first established with the simple example of a dipole antenna, and is then evaluated experimentally using discone and Vivaldi antennas that represent the general cases of omni directional and directional UWB antennas separately.

Another study based on the selection of proper template pulse waveform in UWB pulse communications is presented by Li et al. (2006). The authors concern the BER (bit error rate) for receiving at various different direction angles. Therefore, proper design of the template pulse waveform would help to obtain low BER and improve the overall system performance.

Heidary (2001) discussed the radiation characteristics of UWB mono-pulse arrays which radiate coded mono-pulse sequences with considerably low duty cycle. In this research, for spreading the signal spectrum even more, pseudo-random time-hopping spread spectrum technique is applied. At the receiver side, pseudo-random code is used to sift the desired signals among other interfering signals. Sörgel et. al. (2005) analyzed UWB antenna arrays using the arrays transient response that gives information about radiation and reception characteristics. The performed analysis was independent of applied input signal. Wu et. al. (2005) investigated a planar UWB dipole antenna array using FDTD and method of moments (MOM). Another antenna-array concept was introduced by Ni and Grabel (2005, 2006), implying that the workable frequency range of the array was determined by the individual elements' bandwidths numerically using FDTD and MOM methods.

1.3. The UWB Technology

As noted earlier, Ultra-Wideband (UWB) technology is the transmission and reception of ultra short impulses whose characteristic spectrum occupies a wide range of frequencies. The enormous wide bandwidth is a considerably important difference between UWB systems and conventional narrowband wireless systems.

Gaussian monocycle is the basic element of the UWB communication system. Figure 1.2 shows the monocycle in both the time and frequency domains (“PulsON Technology Overview”, http://www.timedomain.com , July 2000).

The general expression of a Gaussian monocycle is defined as follows

$$V_g(t) = \frac{t}{T}\exp\left(-\frac{1}{2}(\frac{t}{T})^2\right) \tag{2}$$

The center frequency is the reciprocal of the monocycle’s duration.

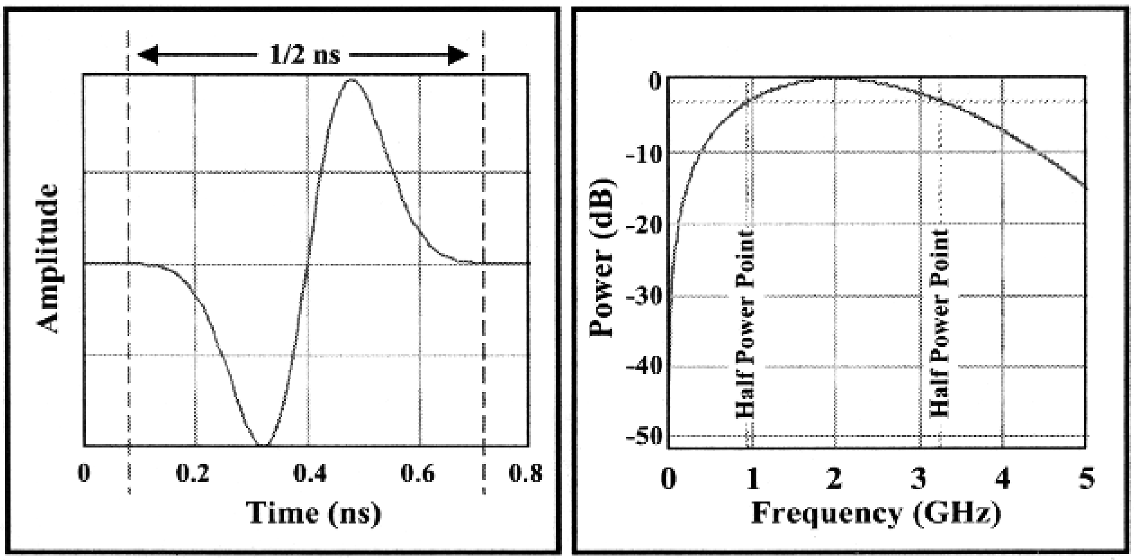

Figure 1.2. 2 GHz center frequency Gaussian monocycle in time and frequency domains (http://www.timedomain.com, 2000)

The UWB monocycle is a wide bandwidth signal. The center frequency and the bandwidth are determined by the monocycle’s width. The pulse duration and the center frequency are inversely related with each other and the bandwidth is 116% of monocycle’s center frequency. The frequency spectrum of pulse ranges from near dc to several gigahertz and consequently the transmitted signal in such a system occupies an extremely large bandwidth even in the absence of data modulation. The expression for the monocycle is denoted as the first derivative of a Gaussian function.

In the UWB system design, it is important to decide operational frequency range of the system. The frequency regulations could be different for different countries and the transmit signals have to satisfy country's rules. Until the end of 1990's, the intentional broadband radiation was prohibited all over the world since the broadband emission can interfere with conventional narrowband systems. The proponents of the UWB claimed and lobbied that UWB systems minimize this interference by spreading the power over a very large bandwidth. After long discussions, the FCC issued its "report and order" in 2002. In this report and order, emission of intentional UWB radiation was permitted with restrictions on the emitted power spectral density (FCC, 2002). These restrictions are specified according to the application areas of the operating devices.

In order to eliminate the interference of various systems over the same and nearby frequency ranges, different rules are enforced for the communication systems and regulations are applied for power output. Since ultra wideband systems cover a large spectrum and interfere with existing users, the FCC and other regulatory groups form spectral masks for different applications. Spectral masks indicate the allowed power output in certain frequency ranges to minimize this interference.

In Figure 1.3, an example of the FCC spectral mask is shown (Ghavami et. al., 2004) for indoor UWB systems. As seen in the figure, a maximum power output of -41.3 dBm/MHz is allowed in the range between 3.1 GHz and 10.6 GHz. In the frequency bands 0.96 GHz-1.61GHz a very small power output is allowed because of the already existing services like mobile telephony, global positioning system, and military applications.

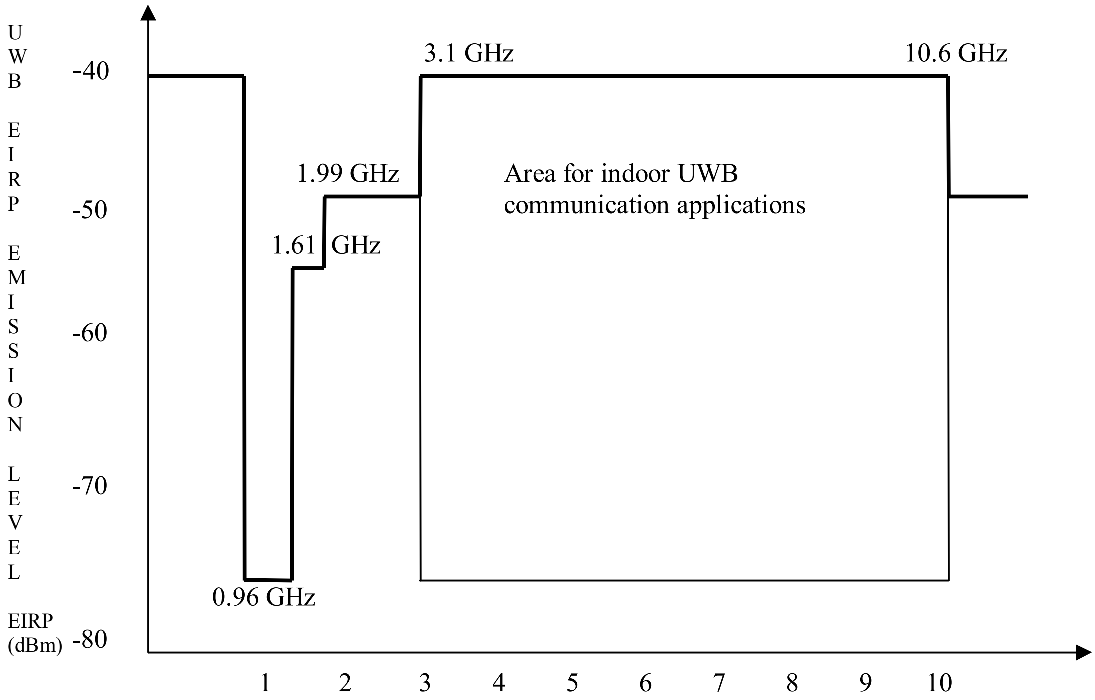

Figure 1.3. Spectral mask mandated by FCC 15.517 (b,c) for indoor UWB systems (Ghavami et. al., 2004)

1.4. Advantages and Limitations of UWB

The main advantages and benefits of UWB systems can be summarized as follows:

In military communications, there are many potential threats about the security of the signal. Ultra wideband signals are usually at noise floor level due to the very large spreading factor. Therefore they provide low probability of detection for military communication and cannot be detected using conventional receivers. Also, UWB signals immune to jamming and interference from other radio systems because of the large spreading factor.

In UWB communication system, the pulses can easily penetrate walls, doors, and other objects. Since UWB signals contain significant low frequency components, it has the ability to penetrate materials that are normally more resistive to higher frequencies.

The extremely high transmission bandwidth of an UWB signal provides very accurate timing information to be resolved. Accurate range measurements and positioning can be achieved due to the resolving capability of multipath. This ability combined with the penetration through materials makes UWB suitable for accurate positioning applications.

Multiple users can transmit simultaneously on the same frequency range as long as they use different spreading codes. Due to the very large spreading gain of UWB systems, it can enable multiple access capability and a large number of users can be fitted in a UWB system.

Since the UWB technology is the transmission and reception of baseband signals, its complexity is relatively low and it provides inexpensive implementation compared to conventional narrowband systems. UWB systems do not require RF modulators and demodulators in the transmitter and receiver design. The absence of RF & IF stages, linear amplifiers, and the required filters reduces the complexity and the cost of the system.

Another advantage of UWB transmission for communications is its high data rate. Higher data rates can enable new applications and devices. The extremely large bandwidth occupied by UWB gives this potential.

The main disadvantages and limitations of UWB systems can be summarized as follows:

UWB antennas need to be optimized over a wide range of frequencies such that the antennas employed in UWB systems are required to efficiently radiate electromagnetic signals over several gigahertz bandwidth. This makes the design procedure more complicated than for other conventional narrowband antennas.

The transmission range of an UWB radio is very limited without use of a power amplifier. Designing small-size, efficient wideband power amplifiers and directional antennas is still a challenge even though medium-range communications using low-power UWB signals is claimed to be possible.

Since UWB extends over an extremely wide bandwidth, many other wireless systems would be affected and need to be convinced that UWB will not cause too much interference to their existing services. Although it has been claimed that the interference between UWB and other systems is minimal, a large amount of UWB transmissions could still cause a problem for systems such as GPS. Moreover, if higher power UWB signals are used for longer range transmissions, the interference problem may arise.

1.5. UWB Applications

FCCs First Report and Order (FCC, 2002) permits the marketing and operation of certain type of new products incorporating ultra-wideband technology. Depending on the operational characteristics and the potential for causing interference to other services, each system is allowed to operate in their allocated frequency bands. According to these restrictions, the FCC report categorizes UWB devices into following categories: imaging systems, communications and measurement systems, and vehicular radar systems.

Ground penetrating radar systems (GPRs), wall imaging systems, through-wall imaging systems, and medical systems can be included in the imaging systems (FCC, 2002).

GPRs are used for detecting the buried objects. The operational frequencies are required to be below 960 MHz or in between 3.1-10.6 GHz. Law enforcement, fire and rescue, scientific research institutions, mining companies, and construction companies are placed in this category.

Wall imaging systems are designed for the detection of objects located within a wall. The frequencies for operating wall imaging systems must be below 960 MHz or in the frequency band 3.1-10.6 GHz. This category also includes law enforcement, fire and rescue, scientific research institutions, mining companies, and construction companies.

Through-wall imaging systems detect the location or movement of objects located on the other side of a structure. The operational frequency is below 960 MHz or in the frequency band 1.99-10.6 GHz. Operation is restricted to law enforcement and fire and rescue.

Medical systems are used for health care applications to observe the location or movement of objects inside the body of a human or animal. These systems must operate in the frequency band 3.1-10.6 GHz. Operation must be carried out under the guidance of licensed health care practitioners.

Communication and measurement systems include devices that are subject to certain frequency and power limitations under the Part 15 of the FCC's rules. UWB high-speed home and business networking devices, storage tank measurement can be included in this group. The operational frequency band is 3.1-10.6 GHz.

Vehicular radar system devices are used to detect the location and movement of objects near a vehicle. They operate in 24 GHz band using directional antennas on terrestrial transportation vehicles. The center frequency of the emission and the frequency at which the highest radiated emission occurs are greater than 24.075 GHz. (FCC, 2002)

1.6. UWB Antenna Concept and Design Considerations

Antenna has an important role in the overall system of transmitting and receiving ultra short pulses for UWB communications, therefore there has been an ever-increasing interest for antenna design in UWB signaling. Enormous wide bandwidth of the system causes antenna design to be a crucial task, since the antenna is required to radiate electromagnetic signals efficiently over a wide range of frequencies. This, of course, makes the design procedure more complicated than for other conventional narrowband antennas. Therefore, the design of ultra wideband antennas requires special considerations.

Since there is not a single operating frequency in UWB, the wavelengths for this type of signals are usually specified in terms of the lower and upper wavelengths in the system (Ghavami et. al., 2004). While the conventional antenna parameters are appropriate for narrowband systems, they may not be suitable for use in ultra wideband systems (Wu et.al., 2003). Many well known narrowband antenna parameters should be reconsidered since the entire frequency spectrum of the UWB range needs to be taken into account.

The radiation pattern of the antenna is a function of both frequency and direction. Additionally, antenna distorts the pulse and causes change in the shape of the incoming pulse. Therefore, the pulse waveform arriving at the receiver usually does not look like input pulse at the transmitter. This makes detection process of the applied pulse much more complicated. On the other hand, pulse detection at the receiver is accomplished effectively by choosing an appropriate template. Hence, the characteristic of the pulses at the receiver is important for understanding the overall performance of the antenna system. Such abovementioned issues make antenna design one of the main challenges for UWB signal radiation and reception, and behavior of antennas for UWB signals should be examined from different aspects for the design considerations of UWB antennas.

The classical descriptions for antenna parameters need to be generalized considering the overall spectrum of the pulse signal. To describe the antennas, energy-based concepts are proposed to define numerical terms, rather than using frequency dependent power concepts (Lamensdorf and Susman, 1994).

For a wideband signal, the transmitted energy pattern is specified as the illustration of the radiated energy with respect to angle for a specified input excitation. Similarly, as the energy is received at the terminals of the receiver, the received energy pattern with respect to angle is described considering the incident plane wave (Lamensdorf and Susman, 1994).

The main reasons for using the total energy are claimed to be based on the fact that; a matched-filter processor can produce an output proportional to this energy, and it is suitable for mathematical treatments (Lamensdorf and Susman, 1994). At the receiver, proper selection of the template signal enables to capture the energy of the received signal effectively (Taha and Chugg, 2002). This is significant, because the pulse experiences distortion in the presence of multipath and the received pulse shape is degenerated as a result of different frequency components (Taha and Chugg, 2002), (Qui, 1998), (Qui and Lu, 1999). Therefore, selection of the optimum template signal which is matched to the received signal at the receiver needs special consideration.

Wu et. al. (2003) state clearly the pulse detection mechanism difference between UWB and narrowband systems as follows: In narrowband systems, in the presence of an additive white Gaussian noise (AWGN) channel, if the signal to noise ratio (SNR) is large enough, then the received pulses can easily be detected. The presence of the carrier enables the capturing of the transmitted signals easily. On the other hand, pulse detection is carried out in a different way in UWB systems because there is not a carrier. Since UWB systems operate very close to noise floor, they need to deal with interference problems. Due to the absence of the carrier, an alternate template pulse needs to be introduced. Therefore, to evaluate the detection capability of the receiver, correlation coefficient concept is specified. The magnitude of the correlation coefficient varies in between 0 and 1, and a large correlation coefficient means that detection can easily be achieved at the receiver. If a fixed template is used at the receiver, the correlation coefficient varies along different directions. Therefore, a correlation coefficient pattern needs to be described in order to figure out the detection of received pulses for different angles. The received pulse could not be detected unless both the energy and the correlation coefficient are sufficiently large (Wu et. al., 2003).

A variety of theoretical and experimental techniques in frequency and time domain can be utilized to analyze the characteristics of pulsed antennas. In time domain, numerical techniques such as finite difference time domain (FDTD) have been mostly used to investigate the behavior of those antennas. Computer programming in these methods need considerable hard work and additionally, it is not a simple task to extract physical meanings from the obtained results. (Boryssenko and Tarasuk, 1999).

On the other hand, it is easier to obtain physical meaning from the results when analytical methods are used in examining the characteristics of the antenna structure. Additionally, analytical techniques play a more significant role in deducing general conclusions on the problems. Moreover, analytically treated antennas can be implemented easily by using current computer programs (Boryssenko and Tarasuk, 1999).

In the literature, there are studies made with dipole for UWB pulse radiation and reception in which various numerical techniques such as FDTD and MoM have been generally used to examine the antenna behavior (McLean et. al., 2005; Chen et. al., 2003). UWB dipole arrays are also investigated as an option to deal with the challenging properties of UWB systems and improve the radiation and detection characteristics utilizing adjustable parameters of the array.

This study obtains results analytically in frequency domain rather than using numerical techniques in time domain. The main focus of the study is to examine the behavior and performance of various antenna structures such as one dipole, array of same length dipoles and array of different length dipoles.

In this study, radiated energy expression from transmitting antenna and received energy expression by the load at the terminals of the receiving antenna are derived. Radiated and received energy patterns which are normalized by the energy at broadside direction value are plotted with respect to observation angle. Of course, the pattern definitions are described by considering the total spectrum of the UWB signal. As noted earlier, detection process at the receiver also needs special consideration to capture the incoming signal effectively. For this purpose, correlation coefficient is investigated to examine the correlation detection behavior of the receiving antenna. Frequency domain correlation coefficient between the generator voltage applied to the transmitting antenna and load voltage at the terminals of the receiving antenna are determined and correlation coefficient graphs are plotted with respect to the observation angle. Also, the effects of array parameters, such as element number and spacing on the abovementioned concepts are considered.

The beam scanning concept for UWB arrays is also examined. The radiated energy expression is derived and the energy pattern is obtained with respect to observation angle for different scan directions.

Also, a program is coded in MATLAB programming language to find the optimal antenna array parameters that gives the maximum correlation coefficient for the different length dipoles array.

This analysis which is carried out in the frequency domain as an alternative to usual time-domain analysis provides a new perspective and will be a useful step for the design consideration of UWB antennas. The main point for performing the analysis in the frequency domain is that it is numerically simple, and it is possible to obtain explicit expressions in most cases and achieve reasonably accurate results. This is significant because the proposed frequency domain analysis can be easily applied to many different antenna structures and the promising ones could be chosen for fine tuning to employ the much slower but more accurate methods.

2. ULTRA WIDEBAND ANTENNAS

2.1. Introduction

Antenna design plays a significant role in transmitting and receiving ultra wideband short pulses. As noted earlier, design issue is an important challenge for ultra wideband radio communications and remains as one of the major concerns for improvement in UWB technology.

UWB antennas should be designed attentively to transmit and receive pulses of very short time duration. Many well known narrowband antenna parameters should be reconsidered since the entire frequency spectrum of the UWB range needs to be taken into account.

The dipole is usually used as a reference for examining general behavior and for comparison with other antennas. Since it is important to understand the behavior of antennas for ultra wideband signals, examining the thin dipole would be reasonable to obtain a general idea for the characteristics of the pulsed antennas. The thin dipole is chosen because the mathematical operations can be conducted easily when the induced current distribution along the dipole is expressed as the modified zero-order approximation (Mokole, 1996), (Samaddar, 1992).

2.2. Theory of Radiation from a Thin Dipole Antenna

A center-fed thin dipole of length 2*l* and radius *a* is considered in Fig. 2.1. The coordinate system is chosen with its origin at the center of the antenna. When the dipole is assumed to be very thin, that is 2*l* >>a, then the current distribution along the thin dipole can be expressed in the frequency domain as follows (Franceschietti and Papas, 1974), (Samaddar,1992)

$$I(z,f) = \frac{2jVg(f)}{Z_0(1+\alpha)} \frac{\sin\frac{2\pi f}{c}(l-|z|)}{1+\Gamma\exp(-j\frac{2\pi f}{c}l)} \exp(-j\frac{2\pi f}{c}l), \qquad (3)$$

which can be regarded as the current distribution along a two-wire open-circuited transmission line of length l, characteristic impedance $Z_0=\Omega.(\zeta_0/2\pi)=(\zeta_0/\pi)\ln(2l/a)$ where $\Omega=2\ln(2l/a)$ is the antenna parameter and ζ_0 is the free space impedance. The generator impedance is taken as $Z_g=\alpha Z_0=(1-\Gamma)Z_0/(1+\Gamma)$, where α is real and Γ is the reflection coefficient from the antenna to the generator. For the matched case $\Gamma=0$ and $\alpha=1$. Then the current distribution becomes

$$I(z,f)=\frac{jVg(f)}{Z_0}\sin\frac{2\pi f}{c}\left(1-|z|\right)\exp(-j\frac{2\pi fl}{c}) \quad (4)$$

This model is applicable as long as the observation point is considered to be far away from the thin dipole.

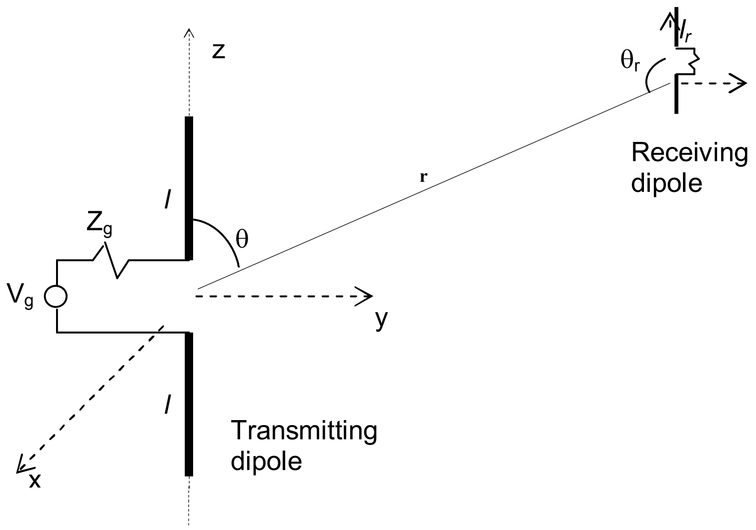

Figure 2.1. Geometry of transmitting and receiving thin dipole antenna

It should be noted that the electric field expression from an arbitrary distribution of current is given by (Collin, 1985)

$$\mathbf{E}(\mathbf{r},f)=\frac{j(2\pi f/c)\zeta_0}{4\pi r}e^{-j\frac{2\pi fr}{c}}\int_V[\mathbf{a_r}.\mathbf{J(r')}\mathbf{a_r}-\mathbf{J(r')}]e^{j\frac{2\pi f}{c}\mathbf{a_r}.\mathbf{r'}}dV'. \tag{5}$$

When the current is a line current I along a contour *C*, then Eqn. (5) can be expressed in the form

$$\mathbf{E}(\mathbf{r},f)=\frac{j(2\pi f/c)\zeta_0}{4\pi r}e^{-j\frac{2\pi fr}{c}}\int_C[(\mathbf{a_r}.\mathbf{a})\mathbf{a_r}-\mathbf{a}]I(l')e^{j\frac{2\pi f}{c}\mathbf{a_r}.\mathbf{r'}}dl' \tag{6}$$

where **a** is a unit vector along C in the direction of the current.

Then, according to Fig. 2.1, it can be seen that the unit vector $\mathbf{a}=\mathbf{a_z}$, $\mathbf{r'}=z'\mathbf{a_z}$, and $\mathbf{a_r}.\mathbf{a_z}=\cos\theta$.

Therefore, the electric field expression for the dipole is given by

$$\mathbf{E}(\mathbf{r},f)=\frac{j(2\pi f/c)\zeta_0}{4\pi r}e^{-j\frac{2\pi fr}{c}}\int_{-1}^{1}(\mathbf{a_r}\cos\theta-\mathbf{a_z})I(z,f)e^{j\frac{2\pi f}{c}z'\cos\theta}dz' \tag{7}$$

Substituting Eqn. (4) into Eqn. (7) and using the relationship between unit vectors in rectangular coordinates which is shown below,

$$\mathbf{a_z}=\mathbf{a_r}\cos\theta-\mathbf{a_\theta}\sin\theta\Rightarrow\mathbf{a_r}\cos\theta-\mathbf{a_z}=\mathbf{a_\theta}\sin\theta \tag{8}$$

yields (Collin, 1985)

$$\mathbf{E}(\mathbf{r},f)=\mathbf{a_\theta}\frac{j(2\pi f/c)\zeta_0}{4\pi r}\sin\theta\frac{jV(f)}{Z_0}e^{-j\frac{2\pi f(r+l)}{c}}\int_{-1}^{1}\sin\frac{2\pi f}{c}(l-|z'|)e^{j\frac{2\pi fz'\cos\theta}{c}}dz'$$

$$=-\mathbf{a_\theta}\frac{(2\pi f/c)\zeta_0}{4\pi r}\sin\theta\frac{V(f)}{Z_0}e^{-j\frac{2\pi f(r+l)}{c}}\frac{1}{2j}\int_{-1}^{1}[e^{j\frac{2\pi f}{c}(l-|z'|)}-e^{-j\frac{2\pi f}{c}(l-|z'|)}]e^{j\frac{2\pi fz'\cos\theta}{c}}dz'$$

$$= -\mathbf{a}_\theta \frac{(2\pi f/c)\zeta_0 \sin\theta V(f)}{4\pi r Z_0} e^{-j\frac{2\pi f(r+l)}{c}} \frac{1}{2j} \underbrace{\int_{-l}^{l} [e^{j\frac{2\pi f}{c}l} . e^{j\frac{2\pi f}{c}(z'\cos\theta - |z'|)} - e^{-j\frac{2\pi f}{c}l} . e^{j\frac{2\pi f}{c}(z'\cos\theta + |z'|)}] dz'}_{E_A}$$

$$E_A = e^{j\frac{2\pi f}{c}l} \int_0^l e^{j\frac{2\pi f}{c}z'(\cos\theta-1)} dz' + e^{j\frac{2\pi f}{c}l} \int_{-l}^0 e^{j\frac{2\pi f}{c}z'(\cos\theta+1)} dz'$$

$$-e^{-j\frac{2\pi f}{c}l} \int_0^l e^{j\frac{2\pi f}{c}z'(\cos\theta+1)} dz' - e^{-j\frac{2\pi f}{c}l} \int_{-l}^0 e^{j\frac{2\pi f}{c}z'(\cos\theta-1)} dz'$$

$$= \frac{e^{j\frac{2\pi f}{c}l}[e^{j\frac{2\pi f}{c}(\cos\theta-1)} - 1]}{\frac{j2\pi f}{c}(\cos\theta - 1)} + \frac{e^{j\frac{2\pi f}{c}l}[1 - e^{-j\frac{2\pi f}{c}(\cos\theta+1)}]}{\frac{j2\pi f}{c}(\cos\theta + 1)}$$

$$-\frac{e^{-j\frac{2\pi f}{c}l}[e^{j\frac{2\pi f}{c}(\cos\theta+1)} - 1]}{\frac{j2\pi f}{c}(\cos\theta + 1)} - \frac{e^{-j\frac{2\pi f}{c}l}[1 - e^{-j\frac{2\pi f}{c}(\cos\theta+1)}]}{\frac{j2\pi f}{c}(\cos\theta - 1)}$$

$$= \frac{[e^{j\frac{2\pi fl\cos\theta}{c}} - e^{j\frac{2\pi fl}{c}} - e^{-j\frac{2\pi fl}{c}} + e^{-j\frac{2\pi fl\cos\theta}{c}}]}{\frac{j2\pi f}{c}(\cos\theta - 1)} + \frac{[e^{j\frac{2\pi fl}{c}} - e^{-j\frac{2\pi fl\cos\theta}{c}} - e^{j\frac{2\pi fl\cos\theta}{c}} + e^{-j\frac{2\pi fl}{c}}]}{\frac{j2\pi f}{c}(\cos\theta + 1)}$$

$$= \frac{2[\cos\frac{2\pi fl\cos\theta}{c} - \cos\frac{2\pi fl}{c}]}{\frac{j2\pi f}{c}(\cos\theta - 1)} + \frac{2[\cos\frac{2\pi fl}{c} - \cos\frac{2\pi fl\cos\theta}{c}]}{\frac{j2\pi f}{c}(\cos\theta + 1)}$$

$$= \frac{2}{\frac{j2\pi f}{c}}[\cos\frac{2\pi fl\cos\theta}{c} - \cos\frac{2\pi fl}{c}][\frac{1}{(\cos\theta - 1)} - \frac{1}{(\cos\theta + 1)}]$$

$$E_A = \frac{-4}{\frac{j2\pi f}{c}\sin^2\theta}[\cos\frac{2\pi fl\cos\theta}{c} - \cos\frac{2\pi fl}{c}] \tag{9}$$

Then radiated electric field becomes

$$\mathbf{E}(\mathbf{r},f) = -\vec{\mathbf{a}}_\theta \frac{\zeta_0 V(f)}{2\pi r Z_0 \sin\theta}\left[\cos\frac{2\pi f l\cos\theta}{c} - \cos\frac{2\pi f l}{c}\right]\exp\left(-j\frac{2\pi f}{c}(r+l)\right). \quad (10)$$

When the generator voltage $V_g(t)$ is a monopulse, which is the 1st derivative of Gaussian pulse:

$$Vg(t) = \frac{t}{T}\exp\left(-\frac{1}{2}(\frac{t}{T})^2\right) \Rightarrow Vg(f) = (2\pi)^{3/2}T^2 f\exp\left(-2\pi^2T^2f^2\right), \quad (11)$$

then the radiated far field in the frequency domain, due to this center-fed cylindrical thin dipole is found as follows

$$\mathbf{E}(\mathbf{r},f) = -\vec{\mathbf{a}}_\theta \frac{\zeta_0\sqrt{2\pi}T^2 f\exp\left(-2\pi^2T^2f^2\right)}{rZ_0\sin\theta}\left[\cos\frac{2\pi f l\cos\theta}{c} - \cos\frac{2\pi f l}{c}\right]\exp\left(-j\frac{2\pi f}{c}(r+l)\right).$$

(12)

2.3. Radiated Energy

As noted earlier, radiation pattern is an important specification for the antenna design. In order to obtain the radiation pattern for the thin dipole, radiated energy is formulated by considering the total spectrum as follows

$$W_{rad} = \frac{1}{\zeta_0}\int_{-\infty}^{\infty}\left|\mathbf{E}_T(\mathbf{r},f)\right|^2 df \quad (13)$$

$$W_{rad} = \int_{-\infty}^{\infty}\left|-\vec{\mathbf{a}}_\theta \frac{\zeta_0 V(f)}{2\pi r Z_0 \sin\theta}\left[\cos\frac{2\pi f l\cos\theta}{c} - \cos\frac{2\pi f l}{c}\right]\exp\left(-j\frac{2\pi f}{c}(r+l)\right)\right|^2 df$$

$$= \int_{-\infty}^{\infty} \frac{\zeta_0^2 \left|V_g(f)\right|^2}{(2\pi r Z_0 \sin\theta)^2} \left[\cos\frac{2\pi f l \cos\theta}{c} - \cos\frac{2\pi f l}{c}\right]^2 df$$

Substituting the Gaussian monopulse expression for $V_g(f)$ and $Z_0 = (\zeta_0/\pi)\ln(2l/a)$ into the equation, W_{rad} becomes

$$W_{rad} = \frac{(2\pi)^3 T^4 \zeta_0^2}{(2\pi)^2 r^2 Z_0^{\ 2} \sin^2\theta} \int_0^{\infty} f^2 e^{-(2\pi f T)^2} \left[\cos\frac{2\pi f l \cos\theta}{c} - \cos\frac{2\pi f l}{c}\right]^2 df \tag{14}$$

and it reduces to

$$W_{rad} = \frac{4\pi^3 T^4}{[r \ln(\frac{2l}{a}) \sin\theta]^2} \int_0^{\infty} f^2 e^{-(2\pi f T)^2} \left[\cos\frac{2\pi f l \cos\theta}{c} - \cos\frac{2\pi f l}{c}\right]^2 df\ . \tag{15}$$

Parenthesis in Eq. (15) can be expanded to obtain an explicit expression for the radiated energy W_{rad} as follows

$$W_{rad} = \frac{4\pi^3 T^4}{[r \ln(\frac{2l}{a}) \sin\theta]^2} \int_0^{\infty} f^2 e^{-(2\pi f T)^2} \left[\cos^2\frac{2\pi f l \cos\theta}{c} - -2\cos\frac{2\pi f l \cos\theta}{c}\cos\frac{2\pi f l}{c} + \cos^2\frac{2\pi f l}{c}\right] df \tag{16}$$

The integral in Eq. (16) can be evaluated using the expressions given below (Gradshteyn, 1980),

$$\int_0^{\infty} x^2 e^{-(px)^2} \cos ax.dx = \sqrt{\pi}\frac{2p^2 - a^2}{8p^5} e^{-(\frac{a^2}{4p^2})^2} \tag{17}$$

$$\int_0^{\infty} x^{2n} e^{-px^2} dx = \frac{(2n-1)!!}{2(2p)^n}\sqrt{\frac{\pi}{p}}, p > 0 \qquad 1!! = 1\ . \tag{18}$$

Then, each expression in paranthesis can be determined in the following manner:

$$A=\int_0^\infty f^2 e^{-(2\pi Tf)^2}\cos^2\frac{2\pi fl\cos\theta}{c}df$$

$$A=\int_0^\infty f^2 e^{-(2\pi Tf)^2}\frac{1+\cos\dfrac{4\pi fl\cos\theta}{c}}{2}df=\int_0^\infty\frac{f^2 e^{-(2\pi Tf)^2}}{2}df+\int_0^\infty f^2 e^{-(2\pi Tf)^2}\frac{\cos\dfrac{4\pi fl\cos\theta}{c}}{2}df$$

$$A=\frac{1}{2}[\frac{1}{2(2.4\pi^2T^2)}\sqrt{\frac{\pi}{4\pi^2T^2}}+\sqrt{\pi}\frac{2(2\pi T)^2-\left(\dfrac{4\pi l\cos\theta}{c}\right)^2}{8(2\pi T)^5}e^{-\frac{(4\pi l\cos\theta)^2}{c^2 4(2\pi T)^2}}]$$

$$A=\frac{1}{2}[\frac{\sqrt{\pi}}{4(2\pi T)^3}+\sqrt{\pi}\frac{8(\pi Tc)^2-(4\pi l\cos\theta)^2}{8c^2(2\pi T)^5}e^{-\left(\frac{l\cos\theta}{cT}\right)^2}]$$

$$B=\int_0^\infty f^2 e^{-(2\pi Tf)^2}\cos\frac{2\pi fl\cos\theta}{c}.\cos\frac{2\pi fl}{c}df$$

$$B=\int_0^\infty f^2 e^{-(2\pi Tf)^2}\frac{1}{2}[\cos\frac{2\pi fl(\cos\theta+1)}{c}.\cos\frac{2\pi fl(\cos\theta-1)}{c}df$$

$$B=\sqrt{\pi}\frac{1}{2}[\frac{2(2\pi T)^2-\left(\dfrac{2\pi l(\cos\theta+1)}{c}\right)^2}{8(2\pi T)^5}e^{-\frac{(2\pi l(\cos\theta+1))^2}{c^2 4(2\pi T)^2}}$$

$$+\frac{2(2\pi T)^2-\left(\dfrac{2\pi l(\cos\theta-1)}{c}\right)^2}{8(2\pi T)^5}e^{-\frac{(2\pi l(\cos\theta-1))^2}{c^2 4(2\pi T)^2}}]$$

$$B=\sqrt{\pi}\,\frac{1}{2}[\frac{8(\pi Tc)^2-\left(2\pi l(\cos\theta+1)\right)^2}{8c^2(2\pi T)^5}e^{-\left(\frac{l(\cos\theta+1)}{2cT}\right)^2}$$

$$+\frac{8(\pi Tc)^2-\left(2\pi l(\cos\theta-1)\right)^2}{8c^2(2\pi T)^5}e^{-\left(\frac{l(\cos\theta-1)}{2cT}\right)^2}]$$

$$C=\int_0^\infty f^2e^{-(2\pi Tf)^2}\cos^2\frac{2\pi fl}{c}df$$

$$C=\int_0^\infty f^2e^{-(2\pi Tf)^2}\frac{1+\cos\frac{4\pi fl}{c}}{2}df=\frac{1}{2}[\int_0^\infty f^2e^{-(2\pi Tf)^2}df+\int_0^\infty f^2e^{-(2\pi Tf)^2}\cos\frac{4\pi fl}{c}df]$$

$$C=\frac{1}{2}[\frac{1}{2(2.4\pi^2T^2)}\sqrt{\frac{\pi}{4\pi^2T^2}}+\sqrt{\pi}\,\frac{2(2\pi T)^2-\left(\frac{4\pi l}{c}\right)^2}{8(2\pi T)^5}e^{-\frac{(4\pi l)^2}{c^2 4(2\pi T)^2}}]$$

$$C=\frac{1}{2}[\frac{\sqrt{\pi}}{4(2\pi T)^3}+\sqrt{\pi}\,\frac{8(\pi Tc)^2-\left(4\pi l\right)^2}{8c^2(2\pi T)^5}e^{-\left(\frac{1}{cT}\right)^2}]$$

Then final form of W_{rad} can be expressed simply as shown below

$$W_{rad}=\frac{4\pi^3T^4}{[r\ln(\frac{2l}{a})\sin\theta]^2}\left[A-2B+C\right]. \qquad (19)$$

2.4. Receiving Dipole

When the radiated field from the transmitting antenna is incident on a receiving dipole of length $2l_r$ and radius b in the far field region of the transmitting antenna in Figure 2.1., the induced open-circuit voltage across the terminals of the receiving dipole is calculated as follows (Samaddar,1993)

$$V(f) = \mathbf{E}(r,f) \cdot \mathbf{h}_{eff}(f) \tag{20}$$

where, $\mathbf{h}_{eff}$ is the effective length of the receiving antenna and it's general expression is defined as (Samaddar,1993)

$$h_{eff}(f) = \frac{[\mathbf{1} - \hat{r}_r \hat{r}_r]}{I_{in,r}} \cdot \iiint_{V_r} \mathbf{J}_r(\mathbf{r}_r, f) \exp\left\{\frac{2\pi f}{c}(\hat{r}_r . \mathbf{r}_r)\right\} dv_r \ . \tag{21}$$

Here, $\hat{r}_r$ and $\mathbf{r}_r$ represent the unit vector in a radial direction and the position vector of a source element that is measured from the coordinate system of the receiving antenna, respectively; **1** is a unit dyadic; $\mathbf{J}_r(\mathbf{r}_r,f)$ and $I_{in,r}$ are the induced current density and short-circuit current on the receiving antenna. By substituting these parameters and considering that the receiving dipole is oriented along the z axis, effective length $\mathbf{h}_{eff}(f)$ takes the form,

$$\mathbf{h}_{eff}(f) = -\vec{\mathbf{a}}_{\theta_r} \frac{\sin\theta_r}{I_{in,r}} \int_{-l}^{l} I(z,f) \exp(j\frac{2\pi f}{c} z_r \cos\theta_r) dz \tag{22}$$

where I(z,f) is the induced current density on thin dipole. Note that the same transmission line analogy as in the transmitting dipole is used in the receiving dipole (Samaddar, 1993). Then the effective length is determined as

$$\mathbf{h}_{eff}(f) = -\vec{\mathbf{a}}_{\theta r} \frac{2\left[\cos\frac{2\pi f l_r \cos\theta_r}{c} - \cos\frac{2\pi f l_r}{c}\right]}{(\frac{2\pi f}{c})\sin\theta_r \sin\frac{2\pi f l_r}{c}} \ . \tag{23}$$

The open circuit voltage V(f) then becomes

$$V(f) = \hat{\mathbf{a}}_{\theta}\hat{\mathbf{a}}_{\theta r}\frac{\zeta_0 V_g(f)e^{-\frac{j2\pi f}{c}(r+l)}}{2\pi r Z_0 \sin\theta \sin\theta_r}\frac{[\cos\frac{2\pi f l\cos\theta}{c} - \cos\frac{2\pi f l}{c}][\cos\frac{2\pi f l_r\cos\theta_r}{c} - \cos\frac{2\pi f l_r}{c}]}{(\frac{2\pi f}{c})\sin\frac{2\pi f l_r}{c}}. \tag{24}$$

The voltage $V_L(f)$ across the load Z_L connected across the terminals of the receiving dipole is given by the expression

$$V_L(f) = \frac{V(f)}{Z_L + Z_{in,r}} Z_L \tag{25}$$

where $Z_{in,r}$ is the input impedance of the receiving dipole. $V_L(f)$ then becomes as follows

$$V_L(f) = \frac{\zeta_0\sqrt{2\pi}cT^2 e^{-(2\pi f T)^2} Z_L[\cos\frac{2\pi f l\cos\theta}{c} - \cos\frac{2\pi f l}{c}][\cos\frac{2\pi f l_r\cos\theta_r}{c} - \cos\frac{2\pi f l_r}{c}]}{\pi r\sin\theta\sin\theta_r Z_0[Z_L - j\frac{\zeta_0}{\pi}\ln(\frac{2l}{a})\cot\frac{2\pi f l_r}{c}]f\sin\frac{2\pi f l_r}{c}} e^{-\frac{j2\pi f}{c}(r+l)}. \tag{26}$$

2.5. Received Energy

Characteristic of the received energy by the load at the receiver is also important and needs to be considered for understanding the behavior of UWB antennas. The energy received by the load at the terminals of the receiving dipole can be obtained from

$$W_{rec} = \int_{-\infty}^{\infty}\frac{|V_L(f)|^2}{Z_L^*}df. \tag{27}$$

Substituting $V_L(f)$ into Eqn. (27), we obtain

$$W_{rec} = \frac{1}{Z_L}\int_{-\infty}^{\infty}\left|\frac{\zeta_0\sqrt{2\pi}cT^2e^{-(2\pi fT)^2}Z_L[\cos\frac{2\pi fl\cos\theta}{c}-\cos\frac{2\pi fl}{c}][\cos\frac{2\pi fl_r\cos\theta_r}{c}-\cos\frac{2\pi fl_r}{c}]}{\pi r\sin\theta\sin\theta_r Z_0[Z_L - j\frac{\zeta_0}{\pi}\ln(\frac{2l}{a})\cot\frac{2\pi fl_r}{c}]f\sin\frac{2\pi fl_r}{c}}e^{-\frac{j2\pi f}{c}(r+1)}\right|^2 df.$$

Received energy then takes the form

$$W_{rec} = \frac{(\zeta_0 c)^2 2\pi T^4}{[\pi r Z_0\sin\theta\sin\theta_r]^2}\int_{-\infty}^{\infty}\frac{e^{-(2\pi Tf)^2}}{\sin^2\left(\frac{2\pi fl_r}{c}\right)}\frac{[\cos\frac{2\pi fl\cos\theta}{c}-\cos\frac{2\pi fl}{c}]^2[\cos\frac{2\pi fl_r\cos\theta_r}{c}-\cos\frac{2\pi fl_r}{c}]^2}{Z_L^2+[\frac{\zeta_0}{\pi}\ln(\frac{2l}{a})\cot\frac{2\pi fl_r}{c}]^2}df$$

which reduces to

$$W_{rec} = \frac{4\pi Z_L c^2T^4}{[r\ln(\frac{2l}{a})\sin\theta\sin\theta_r]^2}\int_{0}^{\infty}\frac{e^{-(2\pi Tf)^2}}{\sin^2\left(\frac{2\pi fl_r}{c}\right)}\frac{\left[\cos\frac{2\pi fl\cos\theta}{c}-\cos\frac{2\pi fl}{c}\right]^2\left[\cos\frac{2\pi fl_r\cos\theta_r}{c}-\cos\frac{2\pi fl_r}{c}\right]^2}{Z_L^2+[\frac{\zeta_0}{\pi}\ln(\frac{2l}{a})\cot\frac{2\pi fl_r}{c}]^2}df \quad (28)$$

which can easily be solved numerically by using computer programs.

2.6. Correlation Coefficient

For UWB applications, in addition to assessing the radiated and received energies, it is also important to figure out how an antenna changes the shape of a waveform when transmitting or receiving. This could be achieved by employing a correlation between the transmitted or received waveform and a template.

When correlation detection is used at the receiver, it is appropriate to define the correlation between the transmitted or received signal and a template function and then observe the correlation pattern. It has been stated that different detection schemes can also be modeled in this way even though they do not actually employ a correlation detector (Mclean et al, 2005).

When the aim is to perform signal recognition, mainly the shape of the signal is concerned rather than the magnitude of the signal. In this case, the normalized correlation coefficient is defined as a function of direction (Mclean et al, 2005). The template function is selected considering the aim of the application. When the detection mechanism has already been specified for a communication system, it is reasonable to choose a template corresponding to the optimum input waveform. If the objective is to see how well an antenna keeps the shape of the waveform with respect to angle, it is reasonable to choose the template function that matches the waveform radiated in a reference direction; for example, the direction of maximum radiated energy density (Mclean et al., 2005).

Therefore, firstly, in order to observe how well the dipole maintains signal shape with respect to direction, correlation coefficient is obtained between the field expression and a template (Mclean et al., 2005), which is the field expression at broadside direction as follows

$$CC = \frac{\int_0^\infty \mathbf{E}(\mathbf{r},f,\theta)\mathbf{E}^*(\mathbf{r},f,\frac{\pi}{2})df}{\sqrt{\int_0^\infty |\mathbf{E}(\mathbf{r},f,\theta)|^2 df}\sqrt{\int_0^\infty \left|\mathbf{E}(\mathbf{r},f,\frac{\pi}{2})\right|^2 df}} \tag{29}$$

The electric field expression has already been obtained as

$$\mathbf{E}(\mathbf{r},f) = -\vec{\mathbf{a}}_\theta \frac{\zeta_0 V(f)}{2\pi r Z_0 \sin\theta}\left[\cos\frac{2\pi f l\cos\theta}{c} - \cos\frac{2\pi f l}{c}\right]\exp\left(-j\frac{2\pi f}{c}(r+l)\right).$$

$$= -\vec{\mathbf{a}}_\theta \frac{V(f)}{2r\ln(\frac{2l}{a})\sin\theta}\left[\cos\frac{2\pi f l\cos\theta}{c} - \cos\frac{2\pi f l}{c}\right]\exp\left(-j\frac{2\pi f}{c}(r+l)\right). \tag{30}$$

If the field expression at $\pi/2$ direction is represented by $\mathbf{E}(\mathbf{r},f,\pi/2)$, then $\mathbf{E}(\mathbf{r},f,\pi/2)$ can be evaluated as

$$\mathbf{E}(\mathbf{r},\mathrm{f},\frac{\pi}{2}) = -\vec{\mathbf{a}}_\theta \frac{\mathrm{V_g(f)}}{2\mathrm{r}\ln(\frac{2\mathrm{l}}{\mathrm{a}})\sin\frac{\pi}{2}}[\cos\frac{2\pi\mathrm{fl}\cos\frac{\pi}{2}}{\mathrm{c}} - \cos\frac{2\pi\mathrm{fl}}{\mathrm{c}}]\exp\left(-\mathrm{j}\frac{2\pi\mathrm{f}}{\mathrm{c}}(\mathrm{r}+\mathrm{l})\right).$$

$$= -\vec{\mathbf{a}}_\theta \frac{\mathrm{V_g(f)}}{2\mathrm{r}\ln(\frac{2\mathrm{l}}{\mathrm{a}})}\left[\cos 0 - \cos\frac{2\pi\mathrm{fl}}{\mathrm{c}}\right]\exp\left(-\mathrm{j}\frac{2\pi\mathrm{f}}{\mathrm{c}}(\mathrm{r}+\mathrm{l})\right).$$

$$\mathbf{E}(\mathbf{r},\mathrm{f},\frac{\pi}{2}) = -\vec{\mathbf{a}}_\theta \frac{\mathrm{V_g(f)}}{2\mathrm{r}\ln(\frac{2\mathrm{l}}{\mathrm{a}})}\left[1 - \cos\frac{2\pi\mathrm{fl}}{\mathrm{c}}\right]\exp\left(-\mathrm{j}\frac{2\pi\mathrm{f}}{\mathrm{c}}(\mathrm{r}+\mathrm{l})\right). \tag{31}$$

First, correlation between electric field and the field at $\pi/2$ direction which is the template in this case is obtained as follows

$$\int_{-\infty}^{\infty}\mathbf{E}(\mathbf{r},\mathrm{f},\theta).\mathbf{E}(\mathbf{r},\mathrm{f},\frac{\pi}{2})\mathrm{df} = \int_{-\infty}^{\infty}\frac{-\mathrm{a}_\theta \mathrm{V_g(f)}}{2\mathrm{r}\ln(\frac{2\mathrm{l}}{\mathrm{a}})\sin\theta}\left[\cos\frac{2\pi\mathrm{fl}\cos\theta}{\mathrm{c}} - \cos\frac{2\pi\mathrm{fl}}{\mathrm{c}}\right]\exp\left(-\mathrm{j}\frac{2\pi\mathrm{f}}{\mathrm{c}}(\mathrm{r}+\mathrm{l})\right)$$

$$\times\frac{-\mathrm{a}_\theta \mathrm{V_g(f)}}{2\mathrm{r}\ln(\frac{2\mathrm{l}}{\mathrm{a}})}\left[1 - \cos\frac{2\pi\mathrm{fl}}{\mathrm{c}}\right]\exp\left(\mathrm{j}\frac{2\pi\mathrm{f}}{\mathrm{c}}(\mathrm{r}+\mathrm{l})\right).$$

$$= \int_{-\infty}^{\infty}\frac{|\mathrm{V_g(f)}|^2}{[2\mathrm{r}\ln(\frac{2\mathrm{l}}{\mathrm{a}})]^2\sin\theta}\left[\cos\frac{2\pi\mathrm{fl}\cos\theta}{\mathrm{c}} - \cos\frac{2\pi\mathrm{fl}}{\mathrm{c}}\right]\left[1 - \cos\frac{2\pi\mathrm{fl}}{\mathrm{c}}\right]\mathrm{df} \tag{32}$$

Substituting Gaussian Monocycle expression into the Eqn. (32) and expanding the terms in parentheses, correlation between the two terms becomes

$$\mathrm{C} = \int_{-\infty}^{\infty}\frac{(2\pi)^3\mathrm{T}^4\mathrm{f}^2\mathrm{e}^{-(2\pi\mathrm{fT})^2}}{[2\mathrm{r}\ln(\frac{2\mathrm{l}}{\mathrm{a}})]^2\sin\theta}\left[\cos\frac{2\pi\mathrm{fl}\cos\theta}{\mathrm{c}} - \cos\frac{2\pi\mathrm{fl}\cos\theta}{\mathrm{c}}\cos\frac{2\pi\mathrm{fl}}{\mathrm{c}} - \cos\frac{2\pi\mathrm{fl}}{\mathrm{c}} + \cos^2\frac{2\pi\mathrm{fl}}{\mathrm{c}}\right]\mathrm{df}$$

Next step in evaluating correlation coefficient is the determination of square root of energies for normalizing the fields. Therefore, square root of the radiated energy is obtained as shown below:

$$\sqrt{\int_{-\infty}^{\infty} |\mathbf{E}(\mathbf{r},f,\theta)|^2 .df} = \sqrt{\int_{-\infty}^{\infty} \frac{|V_g(f)|^2}{2r\ln(\frac{2l}{a})\sin\theta}\left[\cos\frac{2\pi fl\cos\theta}{c} - \cos\frac{2\pi fl}{c}\right]^2 .df}$$

$$= \frac{(2\pi)^{3/2}T^2}{2r\ln(\frac{2l}{a})\sin\theta}\sqrt{\int_{-\infty}^{\infty} f^2 e^{-(2\pi fT)^2}\left[\cos\frac{2\pi fl\cos\theta}{c} - \cos\frac{2\pi fl}{c}\right]^2 .df} \quad (33)$$

Similarly, square root of radiated energy at broadside direction is formulated as follows:

$$\sqrt{\int_{-\infty}^{\infty} \left|\mathbf{E}(\mathbf{r},f,\frac{\pi}{2})\right|^2 .df} = \sqrt{\int_{-\infty}^{\infty} \frac{|V_g(f)|^2}{\left[2r\ln(\frac{2l}{a})\right]^2}\left[1 - \cos\frac{2\pi fl}{c}\right]^2 .df}$$

$$= \frac{(2\pi)^{3/2}T^2}{2r\ln(\frac{2l}{a})}\sqrt{\int_{-\infty}^{\infty} f^2 e^{-(2\pi fT)^2}\left[1 - \cos\frac{2\pi fl}{c}\right]^2 .df} \quad (34)$$

Then, correlation coefficient is obtained after normalizing the two field expressions by their energy, respectively as below

$$CC = \frac{\int_0^{\infty} \mathbf{E}(\mathbf{r},f,\theta)\mathbf{E}^*(\mathbf{r},f,\frac{\pi}{2})df}{\sqrt{\int_0^{\infty} |\mathbf{E}(\mathbf{r},f,\theta)|^2 df}\sqrt{\int_0^{\infty} \left|\mathbf{E}(\mathbf{r},f,\frac{\pi}{2})\right|^2 df}} \quad (35)$$

Substituting corresponding field expressions into Eqn. (35), the correlation coefficient expression below is obtained.

$$CC = \frac{\dfrac{(2\pi)^3 T^4}{[2r\ln(\frac{2l}{a})]^2 \sin\theta} \displaystyle\int_0^\infty f^2 e^{-(2\pi Tf)^2} \cdot [\cos\frac{2\pi fl\cos\theta}{c} - \cos\frac{2\pi fl\cos\theta}{c}\cos\frac{2\pi fl}{c} - \cos\frac{2\pi fl}{c} + \cos^2\frac{2\pi fl}{c}]df}{\dfrac{(2\pi)^{3/2} T^2}{2r\ln(\frac{2l}{a})\sin\theta}\sqrt{\displaystyle\int_0^\infty f^2 e^{-(2\pi Tf)^2} \cdot [\cos\frac{2\pi fl\cos\theta}{c} - \cos\frac{2\pi fl}{c}]^2 df} \times \dfrac{(2\pi)^{3/2} T^2}{2r\ln(\frac{2l}{a})}\sqrt{\displaystyle\int_0^\infty f^2 e^{-(2\pi Tf)^2} \cdot [1-\cos\frac{2\pi fl}{c}]^2 df}}$$

(36)

For ease of mathematical treatment in evaluating the correlation coefficient, expression in numerator is denoted by N and expressions in denominator are denoted by D1, and D2, respectively. Then, the correlation coefficient can be written in the form

$$CC = \frac{N}{D1 * D2} \tag{37}$$

Parenthesis in N can be expanded to obtain an explicit expression as follows

$$N = 2\left\{\int_0^\infty f^2 e^{-(2\pi Tf)^2}\cos\frac{2\pi fl\cos\theta}{c}df - \int_0^\infty f^2 e^{-(2\pi Tf)^2}\cos\frac{2\pi fl\cos\theta}{c}\cos\frac{2\pi fl}{c}df - \int_0^\infty f^2 e^{-(2\pi Tf)^2}\cos\frac{2\pi fl}{c}df + \int_0^\infty f^2 e^{-(2\pi Tf)^2}\cos^2\frac{2\pi fl}{c}df\right\}$$

$$=2\int_0^\infty f^2 e^{-(2\pi Tf)^2}\cos\frac{2\pi fl\cos\theta}{c}df-2\int_0^\infty f^2 e^{-(2\pi Tf)^2}\frac{1}{2}\left[\cos\frac{2\pi fl(\cos\theta+1)}{c}+\cos\frac{2\pi fl(\cos\theta-1)}{c}\right]df$$

$$-2\int_0^\infty f^2 e^{-(2\pi Tf)^2}\cos\frac{2\pi fl}{c}df+2\int_0^\infty f^2 e^{-(2\pi Tf)^2}\frac{1}{2}\left[1+\cos\frac{2.2\pi fl}{c}\right]df$$

$$=2\int_0^\infty f^2 e^{-(2\pi Tf)^2}\cos\frac{2\pi fl\cos\theta}{c}df-\int_0^\infty f^2 e^{-(2\pi Tf)^2}\cos\frac{2\pi fl(\cos\theta+1)}{c}df-\int_0^\infty f^2 e^{-(2\pi Tf)^2}\cos\frac{2\pi fl(\cos\theta-1)}{c}df$$

$$-2\int_0^\infty f^2 e^{-(2\pi Tf)^2}\cos\frac{2\pi fl}{c}df+\int_0^\infty f^2 e^{-(2\pi Tf)^2}df+\int_0^\infty f^2 e^{-(2\pi Tf)^2}\cos\frac{4\pi fl}{c}df \tag{38}$$

The integrals in Eqn. (38) can be evaluated using the expressions given below (Gradshteyn, 1980),

$$\int_0^\infty x^2 e^{-(px)^2}\cos ax.dx=\sqrt{\pi}\,\frac{2p^2-a^2}{8p^5}e^{-(\frac{a^2}{4p^2})^2}$$

$$\int_0^\infty x^{2n}e^{-px^2}dx=\frac{(2n-1)!!}{2(2p)^n}\sqrt{\frac{\pi}{p}},p>0 \qquad 1!!=1$$

which were used for evaluating the integrals in Eqn. (16). Then, explicit expression for each integral can be obtained in the following manner:

$$A=\int_0^\infty f^2 e^{-(2\pi Tf)^2}\cos\frac{2\pi fl\cos\theta}{c}df=\sqrt{\pi}\,\frac{2(2\pi T)^2-\left(\frac{2\pi l\cos\theta}{c}\right)^2}{8(2\pi T)^5}e^{-\frac{(2\pi l\cos\theta)^2}{c^2 4(2\pi T)^2}}$$

$$=\sqrt{\pi}\,\frac{8(\pi Tc)^2-(2\pi l\cos\theta)^2}{8c^2(2\pi T)^5}e^{-\left(\frac{l\cos\theta}{2cT}\right)^2}$$

$$B = \int_0^\infty f^2 e^{-(2\pi Tf)^2} \cos\frac{2\pi fl\left(\cos\theta+1\right)}{c} df = \sqrt{\pi}\,\frac{2(2\pi T)^2 - \left(\dfrac{2\pi l\left(\cos\theta+1\right)}{c}\right)^2}{8(2\pi T)^5} e^{-\frac{\left(2\pi l(\cos\theta+1)\right)^2}{c^2 4(2\pi T)^2}}$$

$$= \sqrt{\pi}\,\frac{8(\pi Tc)^2 - \left(2\pi l\left(\cos\theta+1\right)\right)^2}{8c^2(2\pi T)^5} e^{-\left(\frac{l(\cos\theta+1)}{2cT}\right)^2}$$

$$C = \int_0^\infty f^2 e^{-(2\pi Tf)^2} \cos\frac{2\pi fl\left(\cos\theta-1\right)}{c} df = \sqrt{\pi}\,\frac{8(\pi Tc)^2 - \left(2\pi l\left(\cos\theta-1\right)\right)^2}{8c^2(2\pi T)^5} e^{-\left(\frac{l(\cos\theta-1)}{2cT}\right)^2}$$

$$D = \int_0^\infty f^2 e^{-(2\pi Tf)^2} \cos\frac{2\pi fl}{c} df = \sqrt{\pi}\,\frac{8(\pi Tc)^2 - \left(2\pi l\right)^2}{8c^2(2\pi T)^5} e^{-\left(\frac{1}{2cT}\right)^2}$$

$$E = \int_0^\infty f^2 e^{-(2\pi Tf)^2} df = \frac{\left(2.1-1\right)!!}{2\left(2(2\pi T)^2\right)} \sqrt{\frac{\pi}{(2\pi T)^2}} = \frac{\sqrt{\pi}}{4(2\pi T)^3}$$

$$F = \int_0^\infty f^2 e^{-(2\pi Tf)^2} \cos\frac{4\pi fl}{c} df = \sqrt{\pi}\,\frac{8(\pi Tc)^2 - \left(4\pi l\right)^2}{8c^2(2\pi T)^5} e^{-\left(\frac{1}{2cT}\right)^2}$$

Therefore, the final form of N can be denoted as shown below

$$N = 2A - B - C - 2D + E + F. \qquad (39)$$

Similarly, parenthesis in D1 can be expanded to obtain the explicit form of the integrals as follows

$$D1 = \sqrt{2\int_0^\infty f^2 e^{-(2\pi Tf)^2} \left[\cos^2\frac{2\pi fl\cos\theta}{c} - 2\cos\frac{2\pi fl\cos\theta}{c}\cos\frac{2\pi fl}{c} + \cos^2\frac{2\pi fl}{c}\right] df} \qquad (40)$$

$$=\sqrt{2\int_0^\infty f^2 e^{-(2\pi Tf)^2}\left[\frac{1+\cos\frac{4\pi fl\cos\theta}{c}}{2}-2\frac{1}{2}\left[\cos\frac{2\pi fl(\cos\theta+1)}{c}+\cos\frac{2\pi fl(\cos\theta-1)}{c}\right]+\frac{1+\cos\frac{4\pi fl}{c}}{2}\right]df}$$

$$=\sqrt{\begin{array}{l}\int_0^\infty f^2 e^{-(2\pi Tf)^2}df+\int_0^\infty f^2 e^{-(2\pi Tf)^2}\cos\frac{4\pi fl\cos\theta}{c}df-2\int_0^\infty f^2 e^{-(2\pi Tf)^2}\cos\frac{2\pi fl(\cos\theta+1)}{c}df\\ \qquad -2\int_0^\infty f^2 e^{-(2\pi Tf)^2}\cos\frac{2\pi fl(\cos\theta-1)}{c}df+\int_0^\infty f^2 e^{-(2\pi Tf)^2}df+\int_0^\infty f^2 e^{-(2\pi Tf)^2}\cos\frac{4\pi fl}{c}df\end{array}}$$

$$=\sqrt{\begin{array}{l}2\int_0^\infty f^2 e^{-(2\pi Tf)^2}df+\int_0^\infty f^2 e^{-(2\pi Tf)^2}\cos\frac{4\pi fl\cos\theta}{c}df-2\int_0^\infty f^2 e^{-(2\pi Tf)^2}\cos\frac{2\pi fl(\cos\theta+1)}{c}df\\ \qquad -\int_0^\infty f^2 e^{-(2\pi Tf)^2}\cos\frac{2\pi fl(\cos\theta-1)}{c}df+\int_0^\infty f^2 e^{-(2\pi Tf)^2}\cos\frac{4\pi fl}{c}df\end{array}}$$

$$G=\int_0^\infty f^2 e^{-(2\pi Tf)^2}df=\frac{\sqrt{\pi}}{4(2\pi T)^3}\text{, which is same as E}$$

$$H=\int_0^\infty f^2 e^{-(2\pi Tf)^2}\cos\frac{4\pi fl\cos\theta}{c}df==\sqrt{\pi}\,\frac{8(\pi Tc)^2-(4\pi l\cos\theta)^2}{8c^2(2\pi T)^5}e^{-\left(\frac{l\cos\theta}{2cT}\right)^2}$$

$$I=\int_0^\infty f^2 e^{-(2\pi Tf)^2}\cos\frac{2\pi fl(\cos\theta+1)}{c}df=\sqrt{\pi}\,\frac{8(\pi Tc)^2-(2\pi l(\cos\theta+1))^2}{8c^2(2\pi T)^5}e^{-\left(\frac{l(\cos\theta+1)}{2cT}\right)^2},$$

which is same as B.

$$J=\int_0^\infty f^2 e^{-(2\pi Tf)^2}\cos\frac{2\pi fl(\cos\theta-1)}{c}df=\sqrt{\pi}\,\frac{8(\pi Tc)^2-(2\pi l(\cos\theta-1))^2}{8c^2(2\pi T)^5}e^{-\left(\frac{l(\cos\theta-1)}{2cT}\right)^2},$$

which is same as C.

$$K=\int_0^\infty f^2 e^{-(2\pi Tf)^2}\cos\frac{4\pi fl}{c}df=\sqrt{\pi}\,\frac{8(\pi Tc)^2-\left(4\pi l\right)^2}{8c^2(2\pi T)^5}\,e^{-\left(\frac{1}{2cT}\right)^2}$$, which is same as D.

Then, D1 can be expressed as

$$D1=\sqrt{2G+H-2I-2J+K} \tag{41}$$

Finally, D2 is also found in a straightforward manner as follows

$$D2=\sqrt{2\int_0^\infty f^2 e^{-(2\pi Tf)^2}\left[1-2\cos\frac{2\pi fl}{c}+\cos^2\frac{2\pi fl}{c}\right]df} \tag{42}$$

$$=\sqrt{2\int_0^\infty f^2 e^{-(2\pi Tf)^2}df-2\int_0^\infty f^2 e^{-(2\pi Tf)^2}.2.\cos\frac{2\pi fl}{c}df+2\int_0^\infty f^2 e^{-(2\pi Tf)^2}\frac{[1+\cos\frac{4\pi fl}{c}]}{2}df}$$

$$=\sqrt{2\int_0^\infty f^2 e^{-(2\pi Tf)^2}df-4\int_0^\infty f^2 e^{-(2\pi Tf)^2}\cos\frac{2\pi fl}{c}df+\int_0^\infty f^2 e^{-(2\pi Tf)^2}df+\int_0^\infty f^2 e^{-(2\pi Tf)^2}\cos\frac{4\pi fl}{c}df}$$

$$=\sqrt{3\int_0^\infty f^2 e^{-(2\pi Tf)^2}df-4\int_0^\infty f^2 e^{-(2\pi Tf)^2}\cos\frac{2\pi fl}{c}df+\int_0^\infty f^2 e^{-(2\pi Tf)^2}\cos\frac{4\pi fl}{c}df}$$

$$L=\int_0^\infty f^2 e^{-(2\pi Tf)^2}df=\frac{\sqrt{\pi}}{4(2\pi T)^3}$$

$$M=\int_0^\infty f^2 e^{-(2\pi Tf)^2}\cos\frac{2\pi fl}{c}df=\sqrt{\pi}\,\frac{8(\pi Tc)^2-\left(2\pi l\right)^2}{8c^2(2\pi T)^5}\,e^{-\left(\frac{1}{2cT}\right)^2}$$

$$N = \int_0^\infty f^2 e^{-(2\pi Tf)^2} \cos\frac{4\pi fl}{c} df = \sqrt{\pi}\,\frac{8(\pi Tc)^2 - (4\pi l)^2}{8c^2(2\pi T)^5}\, e^{-\left(\frac{1}{2cT}\right)^2}$$

Then, D2 can be written as

$$D2 = \sqrt{3L - 4M + N}\ . \tag{43}$$

As a result, after these mathematical manipulations, correlation coefficient can be expressed as follows

$$CC = \frac{2A - B - C - 2D + E + F}{\sqrt{2G + H - 2I - 2J + K}\sqrt{3L - 4M + N}}\ . \tag{44}$$

In the paper of Mclean et. al. (2005), correlation coefficient has been described as the square of the correlation coefficient definition presented in this study. In that paper, the definitions were given in time domain and the computations were performed using method of moments (MoM). The input excitation was Gaussian pulse. They chose three different pulse widths in terms of the dipole transit time *l*/c, where *l* is the overall length of the dipole and *c* is the free space wave velocity. The three natural widths of the Gaussian pulses were stated to be $2.98\times10^{-1}\times l/c$, $1.49\times10^{-1}\times l/c$, and $7.45\times10^{-2}\times l/c$.

For comparison purposes, the analysis presented in this study is repeated using the Gaussian pulse as input signal and selecting the pulse widths in terms of the dipole transit time and correlation coefficient graph is obtained. The results are in agreement with the results obtained in the paper (Mclean et. al., 2005) and it is seen in the following figure (Figure 2.2). This comparison is presented for the verification of analysis performed here.

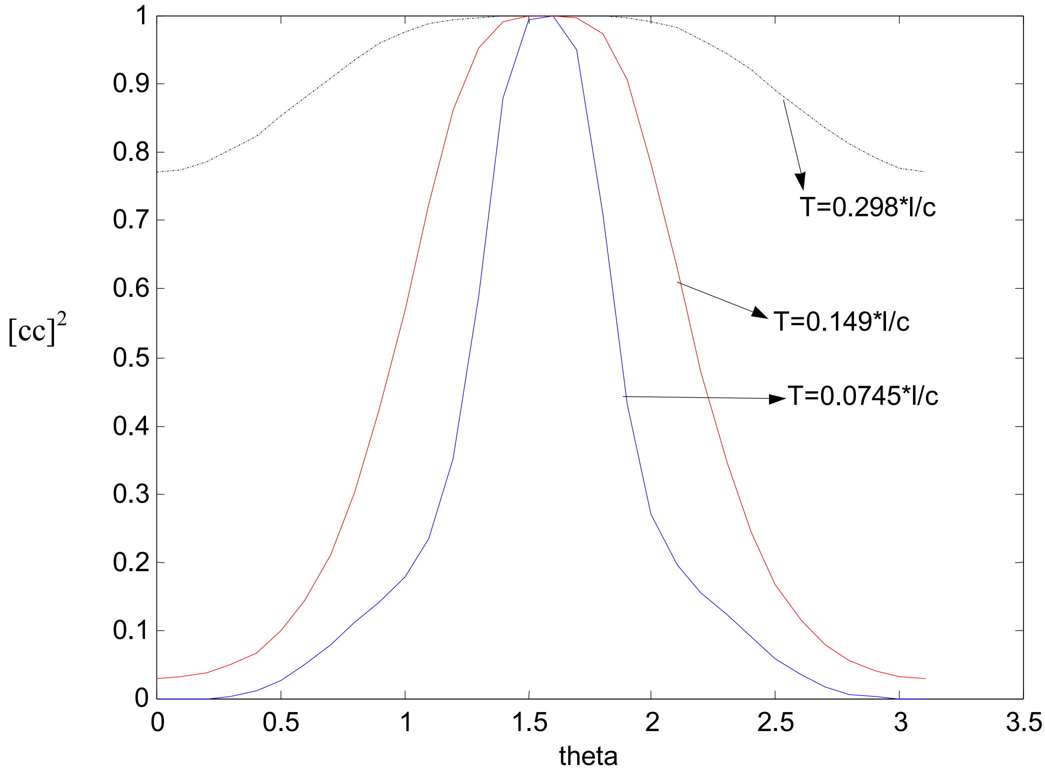

Figure 2.2. Correlation coefficient between **E**(f,θ) and **E**(f,π/2) for one dipole

As noted earlier, the radiation pattern of the antenna is a function of both frequency and direction. Additionally, antenna distorts the pulse and causes change in the shape of the incoming pulse. The pulse waveform arriving at the receiver usually does not look like input pulse at the transmitter. This makes detection process of the applied pulse much more complicated. For this reason, in UWB systems, characterizing radiation patterns are not solely enough to describe the antenna behavior. Therefore, pulse detection at the receiver is another important issue and can be accomplished by choosing the template properly. The characteristic of the pulses at the receiver is important for understanding the overall performance of the antenna system.

To asses this abovementioned detection issue; that is, in order to find out how well the dipole antenna at the receiver side is capable of detecting the applied input signal, correlation coefficient between the load voltage at the receiver and the source voltage at the transmitter should be considered. For this purpose, source voltage V_g and load voltage V_L are correlated and each normalized with their energy to obtain the correlation coefficient as follows

$$CC = \frac{\int_{-\infty}^{\infty} V_g(f)V_L^*(f)df}{\sqrt{\int_{-\infty}^{\infty} |V_g(f)|^2 df}\sqrt{\int_{-\infty}^{\infty} |V_L(f)|^2 df}}. \tag{45}$$

The numerator $\int_{-\infty}^{\infty} V_g(f)V_L^*(f)df$, which is the correlation between $V_g(f)$ and $V_L(f)$ is determined as follows:

$$= \hat{\mathbf{a}}_0\hat{\mathbf{a}}_{\theta r}\int_{-\infty}^{\infty}(2\pi)^{3/2}T^2 fe^{-2(\pi fT)^2}\frac{\zeta_0\sqrt{2\pi}cT^2e^{-(2\pi fT)^2}Z_L[\cos\frac{2\pi fl\cos\theta}{c}-\cos\frac{2\pi fl}{c}][\cos\frac{2\pi fl_r\cos\theta_r}{c}-\cos\frac{2\pi fl_r}{c}]}{\pi r\sin\theta\sin\theta_r Z_0[Z_L+j\frac{\zeta_0}{\pi}\ln(\frac{2l}{a})\cot\frac{2\pi fl_r}{c}]f\sin\frac{2\pi fl_r}{c}}e^{+\frac{j2\pi f}{c}(r+l)}$$

$$=\frac{\zeta_0 c(2\pi)^2T^4}{\pi r Z_0\sin\theta\sin\theta_r}\underbrace{\int_{-\infty}^{\infty}\frac{fe^{-(2\pi fT)^2}}{\sin\frac{2\pi fl_r}{c}}\frac{[\cos\frac{2\pi fl\cos\theta}{c}-\cos\frac{2\pi fl}{c}][\cos\frac{2\pi fl_r\cos\theta_r}{c}-\cos\frac{2\pi fl_r}{c}]Z_L}{[Z_L+j\frac{\zeta_0}{\pi}\ln(\frac{2l}{a})\cot\frac{2\pi fl_r}{c}]}e^{+\frac{j2\pi f}{c}(r+l)}df}_{C_I}$$

The integral, which is denoted by C_I can be manipulated as shown below

$$C_I=\int_{0}^{\infty}\frac{fe^{-(2\pi fT)^2}}{\sin\frac{2\pi fl_r}{c}}\frac{[\cos\frac{2\pi fl\cos\theta}{c}-\cos\frac{2\pi fl}{c}][\cos\frac{2\pi fl_r\cos\theta_r}{c}-\cos\frac{2\pi fl_r}{c}]Z_L}{[Z_L+j\frac{\zeta_0}{\pi}\ln(\frac{2l}{a})\cot\frac{2\pi fl_r}{c}]}e^{+\frac{j2\pi f}{c}(r+l)}df$$
$$+\int_{-\infty}^{0}\frac{fe^{-(2\pi fT)^2}}{\sin\frac{2\pi fl_r}{c}}\frac{[\cos\frac{2\pi fl\cos\theta}{c}-\cos\frac{2\pi fl}{c}][\cos\frac{2\pi fl_r\cos\theta_r}{c}-\cos\frac{2\pi fl_r}{c}]Z_L}{[Z_L+j\frac{\zeta_0}{\pi}\ln(\frac{2l}{a})\cot\frac{2\pi fl_r}{c}]}e^{+\frac{j2\pi f}{c}(r+l)}df$$

$$C_I = \int_0^\infty \frac{fe^{-(2\pi fT)^2}}{\sin\frac{2\pi fl_r}{c}} \frac{[\cos\frac{2\pi fl\cos\theta}{c} - \cos\frac{2\pi fl}{c}][\cos\frac{2\pi fl_r\cos\theta_r}{c} - \cos\frac{2\pi fl_r}{c}]Z_L}{[Z_L + j\frac{\zeta_0}{\pi}\ln(\frac{2l}{a})\cot\frac{2\pi fl_r}{c}]} e^{+\frac{j2\pi f}{c}(r+l)}\,df$$
$$+\int_0^\infty \frac{fe^{-(2\pi fT)^2}}{\sin\frac{2\pi fl_r}{c}} \frac{[\cos\frac{2\pi fl\cos\theta}{c} - \cos\frac{2\pi fl}{c}][\cos\frac{2\pi fl_r\cos\theta_r}{c} - \cos\frac{2\pi fl_r}{c}]Z_L}{[Z_L - j\frac{\zeta_0}{\pi}\ln(\frac{2l}{a})\cot\frac{2\pi fl_r}{c}]} e^{-\frac{j2\pi f}{c}(r+l)}\,df$$

$$C_I = \int_0^\infty \frac{fe^{-(2\pi fT)^2}}{\sin\frac{2\pi fl_r}{c}} [\cos\frac{2\pi fl\cos\theta}{c} - \cos\frac{2\pi fl}{c}][\cos\frac{2\pi fl_r\cos\theta_r}{c} - \cos\frac{2\pi fl_r}{c}]Z_L$$
$$\times\underbrace{\left(\frac{e^{+\frac{j2\pi f}{c}(r+l)}}{[Z_L + j\frac{\zeta_0}{\pi}\ln(\frac{2l}{a})\cot\frac{2\pi fl_r}{c}]} + \frac{e^{-\frac{j2\pi f}{c}(r+l)}}{[Z_L - j\frac{\zeta_0}{\pi}\ln(\frac{2l}{a})\cot\frac{2\pi fl_r}{c}]}\right)}_{Z_A} df$$

The expression in parenthesis, which is denoted as Z_A can be determined in the following manner

$$Z_A = 2\,\mathrm{Re}\{\frac{e^{+\frac{j2\pi f}{c}(r+l)}}{[Z_L + j\frac{\zeta_0}{\pi}\ln(\frac{2l}{a})\cot\frac{2\pi fl_r}{c}]}\} = 2\,\mathrm{Re}\{\frac{\cos\frac{2\pi f}{c}(r+l) + j\sin\frac{2\pi f}{c}(r+l)}{[Z_L + j\frac{\zeta_0}{\pi}\ln(\frac{2l}{a})\cot\frac{2\pi fl_r}{c}]}\}$$

$$= 2\,\mathrm{Re}\{\frac{[Z_L - j\frac{\zeta_0}{\pi}\ln(\frac{2l}{a})\cot\frac{2\pi fl_r}{c}][\cos\frac{2\pi f(r+l)}{c} + j\sin\frac{2\pi f(r+l)}{c}]}{Z_L^2 + [\frac{\zeta_0}{\pi}\ln(\frac{2l}{a})\cot\frac{2\pi\, fl_r}{c}]^2}\}$$

$$= 2\,\mathrm{Re}\{\frac{[Z_L\cos\frac{2\pi f(r+l)}{c} + \frac{\zeta_0}{\pi}\ln(\frac{2l}{a})\cot\frac{2\pi\, fl_r}{c}\sin\frac{2\pi f(r+l)}{c}]}{Z_L^2 + [\frac{\zeta_0}{\pi}\ln(\frac{2l}{a})\cot\frac{2\pi\, fl_r}{c}]^2}$$
$$+\frac{j[Z_L\sin\frac{2\pi f(r+l)}{c} - \frac{\zeta_0}{\pi}\ln(\frac{2l}{a})\cot\frac{2\pi fl_r}{c}\cos\frac{2\pi f(r+l)}{c}]}{Z_L^2 + [\frac{\zeta_0}{\pi}\ln(\frac{2l}{a})\cot\frac{2\pi\, fl_r}{c}]^2}\}$$

Z_A then can then be found as

$$Z_A = 2\frac{[Z_L \cos\frac{2\pi f}{c}(r+l) + \frac{\zeta_0}{\pi}\ln(\frac{2l}{a})\cot\frac{2\pi f l_r}{c}\sin\frac{2\pi f}{c}(r+l)]}{Z_L^2 + [\frac{\zeta_0}{\pi}\ln(\frac{2l}{a})\cot\frac{2\pi f l_r}{c}]^2}. \tag{46}$$

Then C_I reduces to

$$C_I = \int_0^\infty \frac{f e^{-(2\pi f T)^2}}{\sin\frac{2\pi f l_r}{c}}[\cos\frac{2\pi f l\cos\theta}{c} - \cos\frac{2\pi f l}{c}][\cos\frac{2\pi f l_r \cos\theta_r}{c} - \cos\frac{2\pi f l_r}{c}]$$
$$\times \frac{2Z_L}{Z_L^2 + [\frac{\zeta_0}{\pi}\ln(\frac{2l}{a})\cot\frac{2\pi f l_r}{c}]^2}[Z_L \cos\frac{2\pi f}{c}(r+l) + \frac{\zeta_0}{\pi}\ln(\frac{2l}{a})\cot\frac{2\pi f l_r}{c}\sin\frac{2\pi f}{c}(r+l)]df \cdot \tag{47}$$

$\sqrt{\int_{-\infty}^{\infty}|V_g(f)|^2 df}$ in the denominator is determined as follows:

$$\sqrt{\int_{-\infty}^{\infty}\left|(2\pi)^{3/2}T^2 f e^{-2\pi^2T^2f^2}\right| df} = (2\pi)^{3/2}T^2\sqrt{\int_{-\infty}^{\infty} f^2 e^{-4\pi^2T^2f^2}df} = (2\pi)^{3/2}T^2\sqrt{2\int_0^{\infty} f^2 e^{-4\pi^2T^2f^2}df} \tag{48}$$

Again, using the expressions introduced previously (Gradshteyn, 1980)

$$\int_0^\infty x^{2n}e^{-px^2}dx = \frac{(2n-1)!}{2.(2p)^n}\sqrt{\frac{\pi}{p}}, \ \ [p>0, n=0,1,....],$$

And applying this into Eqn. (48), it can be written as

$$\sqrt{\int_{-\infty}^{\infty}\left|V_g(f)\right|^2 df} = (2\pi)^{3/2}T^2\sqrt{2\frac{(2-1)!}{2(2.4\pi^2T^2)}\sqrt{\frac{\pi}{4\pi^2T^2}}} = (2\pi)^{3/2}T^2\sqrt{\frac{1}{(2\pi T)^3}\sqrt{\frac{\pi}{2}}} \tag{49}$$

in which n=1 and $p=4\pi^2T^2$.

Next, $\sqrt{\int_{-\infty}^{\infty}\left|V_L(f)\right|^2 df}$ is evaluated as written below:

$$\sqrt{\int_{-\infty}^{\infty}\left|V_L(f)\right|^2 df} = \sqrt{\int_{-\infty}^{\infty}\left|\frac{\zeta_0\sqrt{2\pi}cT^2e^{-(2\pi fT)^2}Z_L[\cos\frac{2\pi fl\cos\theta}{c}-\cos\frac{2\pi fl}{c}][\cos\frac{2\pi fl_r\cos\theta_r}{c}-\cos\frac{2\pi fl_r}{c}]}{\pi r\sin\theta\sin\theta_r Z_0[Z_L-j\frac{\zeta_0}{\pi}\ln(\frac{2l}{a})\cot\frac{2\pi fl_r}{c}]fs\sin\frac{2\pi fl_r}{c}}e^{-\frac{j2\pi f}{c}(r+l)}\right|^2 df}$$

$$= \frac{(2\pi)^{1/2}cT^2Z_L}{r\ln(\frac{2l}{a})\sin\theta\sin\theta_r}\sqrt{\int_0^{\infty}\frac{e^{-(2\pi Tf)^2}}{\sin^2\left(\frac{2\pi fl_r}{c}\right)}\frac{\left[\cos\frac{2\pi fl\cos\theta}{c}-\cos\frac{2\pi fl}{c}\right]^2\left[\cos\frac{2\pi fl_r\cos\theta_r}{c}-\cos\frac{2\pi fl_r}{c}\right]^2}{Z_L^2+[\frac{\zeta_0}{\pi}\ln(\frac{2l}{a})\cot\frac{2\pi fl_r}{c}]^2}df} \tag{50}$$

Then, substituting these derived numerator and denominator expressions, correlation coefficient is obtained as follows

$$CC = \frac{2(2\pi T)^{3/2}}{\pi^{1/4}}\frac{\int_0^{\infty}\frac{fe^{-(2\pi Tf)^2}}{\sin\frac{2\pi fl_r}{c}}\cdot\frac{[\cos\frac{2\pi fl\cos\theta}{c}-\cos\frac{2\pi fl}{c}][\cos\frac{2\pi fl_r\cos\theta_r}{c}-\cos\frac{2\pi fl_r}{c}]}{Z_L^2+[\frac{\zeta_0}{\pi}\ln(\frac{2l}{a})\cot\frac{2\pi fl_r}{c}]^2}\times\left[Z_L\cos\frac{2\pi f}{c}(r+l)+\frac{\zeta_0}{\pi}\ln(\frac{2l}{a})\cot\frac{2\pi fl_r}{c}\sin\frac{2\pi f}{c}(r+l)\right]df}{\sqrt{\int_0^{\infty}\frac{e^{-(2\pi Tf)^2}}{\sin^2(\frac{2\pi fl_r}{c})}\cdot\frac{[\cos\frac{2\pi fl\cos\theta}{c}-\cos\frac{2\pi fl}{c}]^2[\cos\frac{2\pi fl_r\cos\theta_r}{c}-\cos\frac{2\pi fl_r}{c}]^2}{Z_L^2+[\frac{\zeta_0}{\pi}\ln(\frac{2l}{a})\cot\frac{2\pi fl_r}{c}]^2}df}}. \tag{51}$$

Computer programs are created based on the mathematical manipulations performed here, and obtained results are presented choosing the transmitting and receiving dipole length as $\lambda_c/2$, where λ_c is the wavelength at the center frequency f_c of the 3.1-10.6 GHz UWB range. For all dipoles, length/radius=100 and T=1/f_c.

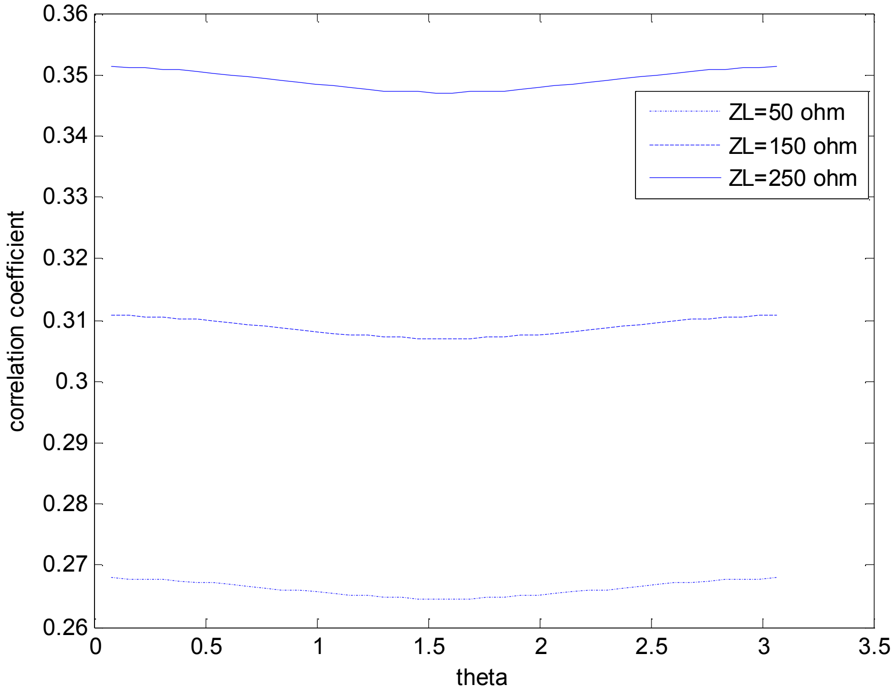

Figure 2.3. Correlation coefficient between $V_L(f)$ and $V_g(f)$ for one dipole antenna with dipole lengths $2l = 2l_r = \lambda_c/2$, $2l/a$=100 , —— Z_L=250 Ω, ------ Z_L=150 Ω, -.-.-.Z_L=50 Ω

Figure 2.3 shows the correlation coefficient between the load voltage and generator voltage for different values of terminal load. As Z_L increases, correlation coefficient also increases. Increasing the load does not affect the shape of the correlation coefficient curve. The correlation coefficient depicts a smooth behavior with respect to direction for each Z_L value.

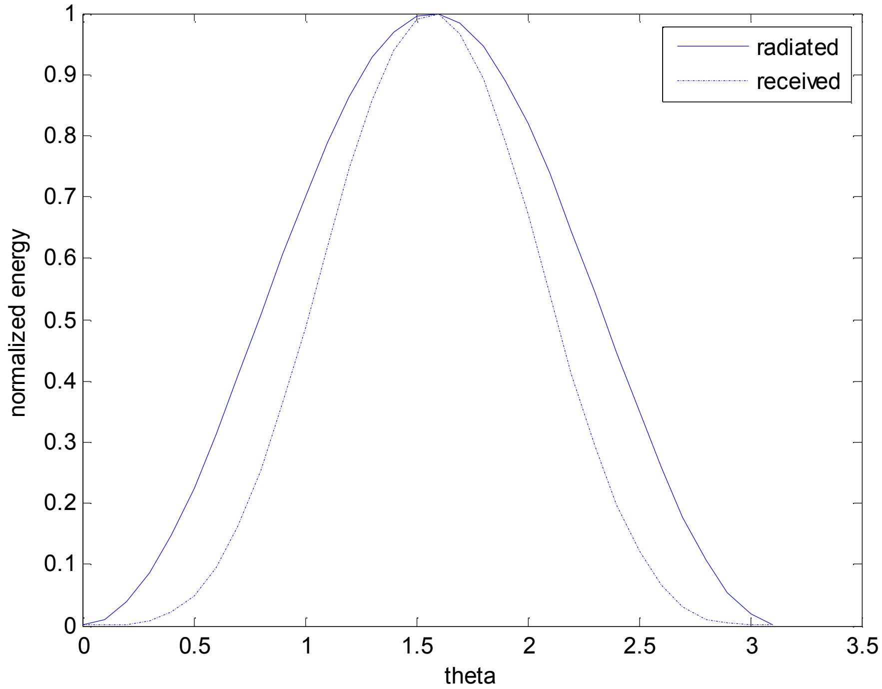

Figure 2.4. —— Radiated and ------ received energies which are normalized by energy at broadside direction with dipole lengths $2l = 2l_r = \lambda_c/2$, $2l/a$=100, T= $1/f_c$, Z_L=150 Ω.

As shown in Figure 2.4 above, the normalized radiated and received energies are also plotted with respect to observation angle. The normalization is performed with respect to the value of energy at broadside direction. The beam width of the received energy is narrower than the beam width of the radiated energy. This shows the filtering effect of the UWB antenna.

3. ULTRA WIDEBAND ANTENNA ARRAYS WITH EQUALLY SPACED SAME LENGTH ELEMENTS

3.1. Introduction

Antenna arrays can be considered as an important option to deal with challenging properties of UWB systems, since array parameters can be adjusted to improve the radiation and detection characteristics.

In this section it is aimed to perform analysis in the frequency domain to evaluate the behavior of dipole arrays with equally spaced same length elements. The analysis is performed in the frequency domain that has already been proved to give accurate results for one single dipole in Section 2. Considering the total spectrum of the UWB signal, radiated and received energy formulas are derived and energy patterns are plotted with respect to angle. Also, for examining detection capability at the receiver, correlation coefficient between the load voltage at the terminals of the receiving antenna and the generator voltage applied to the transmitting antenna is investigated.

Here, UWB signal is applied to the array of thin dipoles again, since examining thin dipole provides the idea about general behavior of arrays.

3.2. Theory of Radiation from an Array of Thin Dipoles

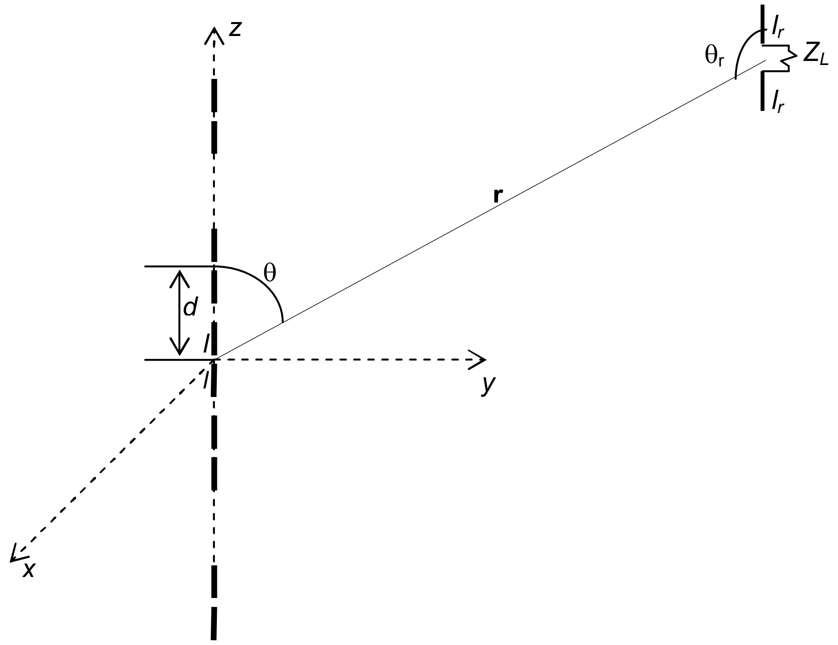

Figure 3.1. Geometry of a linear array of thin dipoles and a receiving thin dipole

The current distribution along each of the dipoles in the array can be regarded as being the distribution along an open-ended transmission line with characteristic impedance $Z=(\zeta_0/\pi)*\ln(2l/a)$ where $2l$ and a are dipole length and radius, respectively, and ζ_0 is the free space impedance. The expression is as follows

$$I(z,f)=\frac{2jVg(f)}{Z_0(1+\alpha)}\frac{\sin\frac{2\pi f}{c}(1-|z|)}{1+\Gamma\exp(-j\frac{2\pi f}{c}l)}\exp(-j\frac{2\pi f}{c}l) \qquad (52)$$

As noted earlier, this current distribution approximation has already been presented by (Franceschietti and Papas, 1974), (Samaddar,1992) when the internal impedance of the generator is equal to $(1-\Gamma)Z_0/(1+\Gamma)$, where Γ is the reflection coefficient from the antenna to the generator, and if the antenna is assumed to be very thin, that is $2l/a>>1$.

The electric field radiated from each dipole is given below

$$\mathbf{E}_0(\mathbf{r},f)=-\vec{\mathbf{a}}_\theta \frac{\zeta_0 V_g(f)}{2\pi r Z_0 \sin\theta\sqrt{2N+1}}\left[\cos(\frac{2\pi f l\cos\theta}{c})-\cos(\frac{2\pi f l}{c})\right]\exp\left(-\frac{j2\pi f(r+l)}{c}\right)$$

$$\mathbf{E}_1(\mathbf{r},f)=-\vec{\mathbf{a}}_\theta \frac{\zeta_0 V_g(f)}{2\pi r Z_0 \sin\theta\sqrt{2N+1}}\left[\cos(\frac{2\pi f l\cos\theta}{c})-\cos(\frac{2\pi f l}{c})\right]\exp\left(-\frac{j2\pi f(r-d\cos\theta+l)}{c}\right)$$

$$\vdots \qquad\qquad \vdots$$

$$\vdots \qquad\qquad \vdots$$

$$\mathbf{E}_n(\mathbf{r},f)=-\vec{\mathbf{a}}_\theta \frac{\zeta_0 V_g(f)}{2\pi r Z_0 \sin\theta\sqrt{2N+1}}\left[\cos(\frac{2\pi f l\cos\theta}{c})-\cos(\frac{2\pi f l}{c})\right]\exp\left(-\frac{j2\pi f(r-nd\cos\theta+l)}{c}\right).$$

The total electric field radiated from the array of dipoles at far field region is obtained as the superposition of electric fields from individual elements, and is obtained as follows

$$\mathbf{E}_T(\mathbf{r},f)=-\vec{\mathbf{a}}_\theta \frac{\zeta_0 V_g(f)}{2\pi r Z_0 \sin\theta\sqrt{2N+1}}\sum_{n=-N}^{N}\left[\cos(\frac{2\pi f l\cos\theta}{c})-\cos(\frac{2\pi f l}{c})\right]\exp\left(-\frac{j2\pi f(r-nd\cos\theta+l)}{c}\right). \tag{53}$$

where the dipoles are matched to the feed network and equally weighted with $\sqrt{2N+1}$. Mutual coupling between the elements is ignored here.

When Gaussian monocycle of duration T is applied as the input, radiated energy of the array at a distance r is derived as follows

$$\int_{-\infty}^{\infty}\left|E_T(r,f)\right|^2 df=\frac{\zeta_0^2}{(2\pi r Z_0\sin\theta)^2(2N+1)}\int_{-\infty}^{\infty}\left|V_g(f)\right|^2[\cos(\frac{2\pi f l\cos\theta}{c})-\cos(\frac{2\pi f l}{c})]^2\left|\sum_{n=-N}^{N}e^{-\frac{j2\pi f(r-nd\cos\theta+l)}{c}}\right|^2 df. \tag{54}$$

Using the identity

$$\left|\sum_{i=1}^{N} Z_i\right|^2 = \sum_{i=1}^{N}|Z_i|^2 + \sum_{i=1}^{N}\sum_{j=1}^{N}\mathrm{Re}(Z_i^* Z_j) = \sum_{i=1}^{N}|Z_i|^2 + 2\sum_{i=1}^{N}\sum_{j=i+1}^{N}\mathrm{Re}(Z_i^* Z_j) \qquad (55)$$

where Z_i is a complex function, the magnitude square expression in Eqn. (54) is determined as follows

$$|\sum_{n=-N}^{N} e^{-\frac{j2\pi f(r-nd\cos\theta+l)}{c}}|^2 = \sum_{n=-N}^{N}|e^{-j\frac{2\pi f(r-nd\cos\theta+l)}{c}}|^2 + \sum_{n=-N}^{N}\sum_{m=-N}^{N}\mathrm{Re}\left\{e^{j\frac{2\pi f(r-nd\cos\theta+l)}{c}}\cdot e^{-j\frac{2\pi f(r-md\cos\theta+l)}{c}}\right\}$$

$$= \sum_{n=-N}^{N}|e^{-\frac{j2\pi f(r-nd\cos\theta+l)}{c}}|^2 + \sum_{n=-N}^{N}\sum_{m=-N}^{N}\mathrm{Re}\left\{e^{\frac{j2\pi f(r-(m-n)d\cos\theta+l)}{c}}\right\} = \sum_{n=-N}^{N}1 + \sum_{n=-N}^{N}\sum_{m=-N}^{N}\cos\frac{2\pi f}{c}[(m-n)d\cos\theta].$$

$$(56)$$

Then, radiated energy becomes

$$W_{rad} = \frac{1}{2[r\sin\theta\,\ln(\frac{2l}{a})]^2(2N+1)}\int_0^{\infty}|V_g(f)|^2[\cos\frac{2\pi fl\cos\theta}{c} - \cos\frac{2\pi fl}{c}]^2$$

$$\times[(2N+1) + \sum_{\substack{n=-N\\ n\neq m}}^{N}\sum_{m=-N}^{N}\cos\frac{2\pi f}{c}[(m-n)d\cos\theta]]df \qquad (57)$$

Substituting $V_g(f) = (2\pi)^{3/2}T^2 f e^{-2\pi^2T^2f^2}$ into Eqn. (57), W_{rad} is derived as follows

$$W_{rad} = \frac{4\pi^3T^4}{[r\sin\theta\,\ln(\frac{2l}{a})]^2(2N+1)}\int_0^{\infty} f^2 e^{-(2\pi Tf)^2}[\cos\frac{2\pi fl\cos\theta}{c} - \cos\frac{2\pi fl}{c}]^2$$

$$\times[(2N+1) + \sum_{\substack{n=-N\\ n\neq m}}^{N}\sum_{m=-N}^{N}\cos\frac{2\pi f}{c}[(m-n)d\cos\theta]]df. \qquad (58)$$

The parenthesis in Eqn. (58) can be expanded to obtain an explicit expression for W_{rad} as follows

$$W_{rad} = \frac{4\pi^3 T^4}{(r\sin\theta \ln(\frac{2l}{a})])^2 (2N+1)} \int_0^\infty f^2 e^{-(2\pi T f)^2}$$

$$\times\{[\cos^2 \frac{2\pi f l\cos\theta}{c} - 2\cos\frac{2\pi f l\cos\theta}{c}\cos\frac{2\pi f l}{c} + \cos^2\frac{2\pi f l}{c}](2N+1)$$

$$+\sum_{\substack{n=-N\\ n\neq m}}^{N}\sum_{m=-N}^{N}\cos\frac{2\pi f}{c}[(m-n)d\cos\theta]\}df\ . \qquad (59)$$

Using the identities which were designated before in equations (17) and (18) (Gradshteyn, 1980), explicit expressions for the radiated energy can be obtained using the following procedure

$$A = \int_0^\infty f^2 e^{-(2\pi T f)^2} \cos^2\frac{2\pi f l_n \cos\theta}{c} df$$

$$A = \int_0^\infty f^2 e^{-(2\pi T f)^2} \frac{1+\cos\frac{4\pi f l\cos\theta}{c}}{2} df = \int_0^\infty \frac{f^2 e^{-(2\pi T f)^2}}{2} df + \int_0^\infty f^2 e^{-(2\pi T f)^2} \frac{\cos\frac{4\pi f l\cos\theta}{c}}{2} df$$

$$A = \frac{1}{2}[\frac{1}{2(2.4\pi^2 T^2)}\sqrt{\frac{\pi}{4\pi^2 T^2}} + \sqrt{\pi}\frac{2(2\pi T)^2 - \left(\frac{4\pi l\cos\theta}{c}\right)^2}{8(2\pi T)^5} e^{-\frac{(4\pi l\cos\theta)^2}{c^2 4(2\pi T)^2}}]$$

$$A = \frac{1}{2}[\frac{\sqrt{\pi}}{4(2\pi T)^3} + \sqrt{\pi}\frac{8(\pi T c)^2 - (4\pi l\cos\theta)^2}{8c^2(2\pi T)^5} e^{-\left(\frac{l\cos\theta}{cT}\right)^2}]$$

$$B = \int_0^\infty f^2 e^{-(2\pi T f)^2} \cos\frac{2\pi f l\cos\theta}{c}.\cos\frac{2\pi f l}{c} df$$

$$B=\int_0^\infty f^2 e^{-(2\pi Tf)^2}\frac{1}{2}[\cos\frac{2\pi fl(\cos\theta+1)}{c}.\cos\frac{2\pi fl(\cos\theta-1)}{c}df$$

$$B=\sqrt{\pi}\frac{1}{2}[\frac{2(2\pi T)^2-\left(\frac{2\pi l(\cos\theta+1)}{c}\right)^2}{8(2\pi T)^5}e^{-\frac{(2\pi l(\cos\theta+1))^2}{c^2 4(2\pi T)^2}}+\frac{2(2\pi T)^2-\left(\frac{2\pi l(\cos\theta-1)}{c}\right)^2}{8(2\pi T)^5}e^{-\frac{(2\pi l(\cos\theta-1))^2}{c^2 4(2\pi T)^2}}]$$

$$B=\sqrt{\pi}\frac{1}{2}[\frac{8(\pi Tc)^2-\left(2\pi l(\cos\theta+1)\right)^2}{8c^2(2\pi T)^5}e^{-\left(\frac{l(\cos\theta+1)}{2cT}\right)^2}+\frac{8(\pi Tc)^2-\left(2\pi l(\cos\theta-1)\right)^2}{8c^2(2\pi T)^5}e^{-\left(\frac{l(\cos\theta-1)}{2cT}\right)^2}]$$

$$C=\int_0^\infty f^2 e^{-(2\pi Tf)^2}\cos^2\frac{2\pi fl}{c}df$$

$$C=\int_0^\infty f^2 e^{-(2\pi Tf)^2}\frac{1+\cos\frac{4\pi fl}{c}}{2}df=\frac{1}{2}[\int_0^\infty f^2 e^{-(2\pi Tf)^2}df+\int_0^\infty f^2 e^{-(2\pi Tf)^2}\cos\frac{4\pi fl}{c}df]$$

$$C=\frac{1}{2}[\frac{1}{2(2.4\pi^2T^2)}\sqrt{\frac{\pi}{4\pi^2T^2}}+\sqrt{\pi}\frac{2(2\pi T)^2-\left(\frac{4\pi l}{c}\right)^2}{8(2\pi T)^5}e^{-\frac{(4\pi l)^2}{c^2 4(2\pi T)^2}}]$$

$$C=\frac{1}{2}[\frac{\sqrt{\pi}}{4(2\pi T)^3}+\sqrt{\pi}\frac{8(\pi Tc)^2-\left(4\pi l\right)^2}{8c^2(2\pi T)^5}e^{-\left(\frac{1}{cT}\right)^2}]$$

$$D=\int_0^\infty f^2 e^{-(2\pi Tf)^2}\cos^2\frac{2\pi fl\cos\theta}{c}.\cos\frac{2\pi f}{c}[(m-n)d\cos\theta]df$$

$$D=\int_0^\infty f^2 e^{-(2\pi Tf)^2}\frac{1}{2}\cos\frac{2\pi f(m-n)d\cos\theta}{c}df$$

$$+\int_0^\infty f^2 e^{-(2\pi Tf)^2}\frac{1}{2}\cos\frac{4\pi fl\cos\theta}{c}\cos\frac{2\pi f(m-n)d\cos\theta}{c}df$$

$$D=\frac{1}{2}\int_0^\infty f^2 e^{-(2\pi Tf)^2}\cos\frac{2\pi f(m-n)d\cos\theta}{c}df$$

$$+\frac{1}{2}\int_0^\infty f^2 e^{-(2\pi Tf)^2}\frac{1}{2}[\cos\frac{2\pi f[2l\cos\theta+(m-n)d\cos\theta]}{c}+\cos\frac{2\pi f[2l\cos\theta-(m-n)d\cos\theta]}{c}]df$$

$$D=\frac{1}{2}\int_0^\infty f^2 e^{-(2\pi Tf)^2}\cos\frac{2\pi f(m-n)d\cos\theta}{c}df$$

$$+\frac{1}{4}\int_0^\infty f^2 e^{-(2\pi Tf)^2}[\cos\frac{2\pi f[2l\cos\theta+(m-n)d\cos\theta]}{c}df$$

$$+\frac{1}{4}\int_0^\infty f^2 e^{-(2\pi Tf)^2}[\cos\frac{2\pi f[2l\cos\theta-(m-n)d\cos\theta]}{c}df$$

$$D=\frac{1}{2}\{\sqrt{\pi}\frac{2(2\pi Tc)^2-\{2\pi(m-n)d\cos\theta\}^2}{8c^2(2\pi T)^5}e^{-\frac{\{2\pi[(m-n)d\cos\theta]\}^2}{c^2 4(2\pi T)^2}}$$

$$+\sqrt{\pi}\frac{2(2\pi Tc)^2-\{2\pi[2l\cos\theta+(m-n)d\cos\theta\}^2}{8c^2(2\pi T)^5}e^{-\frac{\{2\pi[2l\cos\theta+(m-n)d\cos\theta]\}^2}{c^2 4(2\pi T)^2}}$$

$$+\sqrt{\pi}\frac{2(2\pi Tc)^2-\{2\pi[2l\cos\theta-(m-n)d\cos\theta]\}^2}{8c^2(2\pi T)^5}e^{-\frac{\{2\pi[2l\cos\theta-(m-n)d\cos\theta]\}^2}{c^2 4(2\pi T)^2}}$$

$$D=\frac{1}{2}\{\sqrt{\pi}\frac{8\pi^2T^2c^2-\{2\pi[(m-n)d\cos\theta]\}^2}{8c^2(2\pi T)^5}e^{-\left[\frac{(m-n)d\cos\theta)}{2cT}\right]^2}$$

$$+\frac{1}{4}\sqrt{\pi}\frac{8\pi^2T^2c^2-\{2\pi[2l\cos\theta+(m-n)d\cos\theta]\}^2}{8c^2(2\pi T)^5}e^{-\left[\frac{2l\cos\theta+(m-n)d\cos\theta}{2cT}\right]^2}$$

$$+\sqrt{\pi}\frac{8\pi^2T^2c^2-\{2\pi[2l\cos\theta-(m-n)d\cos\theta]\}^2}{8c^2(2\pi T)^5}e^{-\left[\frac{2l\cos\theta-(m-n)d\cos\theta}{2cT}\right]^2}$$

$$E=\int_0^\infty f^2 e^{-(2\pi T f)^2}\cos\frac{2\pi f l\cos\theta}{c}.\cos\frac{2\pi f l}{c}\cos\frac{2\pi f}{c}[(m-n)d\cos\theta]df$$

$$E=\frac{1}{4}\{\sqrt{\pi}\frac{8\pi^2T^2c^2-\left\{2\pi[l\cos\theta+l+(m-n)d\cos\theta]\right\}^2}{8c^2(2\pi T)^5}e^{-\left[\frac{l\cos\theta+l+(m-n)d\cos\theta}{2cT}\right]^2}$$

$$+\sqrt{\pi}\frac{8\pi^2T^2c^2-\left\{2\pi[l\cos\theta+l-(m-n)d\cos\theta]\right\}^2}{8c^2(2\pi T)^5}e^{-\left[\frac{l\cos\theta+l-(m-n)d\cos\theta}{2cT}\right]^2}$$

$$+\sqrt{\pi}\frac{8\pi^2T^2c^2-\left\{2\pi[l\cos\theta-l+(m-n)d\cos\theta]\right\}^2}{8c^2(2\pi T)^5}e^{-\left[\frac{l\cos\theta-l+(m-n)d\cos\theta}{2cT}\right]^2}$$

$$+\sqrt{\pi}\frac{8\pi^2T^2c^2-\left\{2\pi[l\cos\theta-l-(m-n)d\cos\theta]\right\}^2}{8c^2(2\pi T)^5}e^{-\left[\frac{l\cos\theta-l-(m-n)d\cos\theta}{2cT}\right]^2}$$

$$F=\int_0^\infty f^2 e^{-(2\pi T f)^2}\cos^2\frac{2\pi f l}{c}.\cos\frac{2\pi f}{c}[(m-n)d\cos\theta]df$$

$$F=\int_0^\infty f^2 e^{-(2\pi T f)^2}\frac{1}{2}\cos\frac{2\pi f(m-n)d\cos\theta}{c}df$$

$$+\int_0^\infty f^2 e^{-(2\pi T f)^2}\frac{1}{2}\cos\frac{4\pi f l}{c}\cos\frac{2\pi f(m-n)d\cos\theta}{c}df$$

$$F=\frac{1}{2}\int_0^\infty f^2 e^{-(2\pi T f)^2}\cos\frac{2\pi f(m-n)d\cos\theta}{c}df$$

$$+\frac{1}{2}\int_0^\infty f^2 e^{-(2\pi T f)^2}\frac{1}{2}[\cos\frac{2\pi f[2l+(m-n)d\cos\theta]}{c}+\cos\frac{2\pi f[2l-(m-n)d\cos\theta]}{c}]df$$

$$F=\frac{1}{2}\int_0^\infty f^2 e^{-(2\pi T f)^2}\cos\frac{2\pi f(m-n)d\cos\theta}{c}df$$

$$+\frac{1}{4}\int_0^\infty f^2 e^{-(2\pi T f)^2}[\cos\frac{2\pi f[2l+(m-n)d\cos\theta]}{c}df$$

$$+\frac{1}{4}\int_0^\infty f^2 e^{-(2\pi T f)^2}[\cos\frac{2\pi f[2l-(m-n)d\cos\theta]}{c}df$$

$$F=\frac{1}{2}\{\sqrt{\pi}\frac{2(2\pi Tc)^2-\{2\pi(m-n)d\cos\theta\}^2}{8c^2(2\pi T)^5}e^{-\frac{\{2\pi[(m-n)d\cos\theta]\}^2}{c^2 4(2\pi T)^2}}$$
$$+\sqrt{\pi}\frac{2(2\pi Tc)^2-\{2\pi[2l+(m-n)d\cos\theta\}^2}{8c^2(2\pi T)^5}e^{-\frac{\{2\pi[2l+(m-n)d\cos\theta]\}^2}{c^2 4(2\pi T)^2}}$$
$$+\sqrt{\pi}\frac{2(2\pi Tc)^2-\{2\pi[2l-(m-n)d\cos\theta]\}^2}{8c^2(2\pi T)^5}e^{-\frac{\{2\pi[2l\cos\theta-(m-n)d\cos\theta]\}^2}{c^2 4(2\pi T)^2}}$$

$$F=\frac{1}{2}\{\sqrt{\pi}\frac{8\pi^2T^2c^2-\{2\pi[(m-n)d\cos\theta]\}^2}{8c^2(2\pi T)^5}e^{-\left[\frac{(m-n)d\cos\theta)}{2cT}\right]^2}$$
$$+\frac{1}{4}\sqrt{\pi}\frac{8\pi^2T^2c^2-\{2\pi[2l+(m-n)d\cos\theta]\}^2}{8c^2(2\pi T)^5}e^{-\left[\frac{2l+(m-n)d\cos\theta}{2cT}\right]^2}$$
$$+\sqrt{\pi}\frac{8\pi^2T^2c^2-\{2\pi[2l-(m-n)d\cos\theta]\}^2}{8c^2(2\pi T)^5}e^{-\left[\frac{2l-(m-n)d\cos\theta}{2cT}\right]^2}$$

Then the explicit form of the radiated energy can be expressed as follows

$$W_{rad}=\frac{4\pi^3T^4}{(r\sin\theta\ln(\frac{2l}{a}))^2(2N+1)}[(2N+1)[A-2B+C]+\sum_{\substack{n,m\\ n\neq m}}^{N}\sum_{=-N}^{N}[D-2E+F]] \tag{60}$$

3.3. Analysis at the Receiver Side

At the receiver side, the voltage produced on the load impedance Z_L across the terminals of the antenna is calculated from $V_L(f)=\mathbf{E_T}(r,f).\mathbf{h}_{\text{eff}}(f).Z_L/(Z_L+Z_{in,r})$, where $\mathbf{h}_{eff}$ and Z_r are the effective length and input impedance of the receiving dipole, respectively (Samaddar,1993). They are calculated according to the same current distribution approximation and transmission line approach made for the dipole elements in the transmitter. Therefore, $V_L(f)$ is derived as

$$V_L(f)=\frac{\zeta_0 Z_L V_g(f)}{\pi r Z\sqrt{2N+1}}\frac{(\cos\frac{2\pi fl\cos\theta}{c}-\cos\frac{2\pi fl}{c})(\cos\frac{2\pi fl_r\cos\theta_r}{c}-\cos\frac{2\pi fl_r}{c})\sum_{n=-N}^{N}\exp\left(-j\frac{2\pi f}{c}(r-nd\cos\theta+l)\right)}{\sin\theta\sin\theta_r(\frac{2\pi f}{c})\sin\frac{2\pi fl_r}{c}(Z_L-j\frac{\zeta_0}{\pi}\ln(\frac{2l_r}{b})\cot\frac{2\pi fl_r}{c})} \tag{61}$$

where $2l_r$ and b are the length and radius of the receiving dipole, respectively. Substituting Gaussian monocycle expression in $V_g(f)$, $V_L(f)$ becomes

$$V_L(f)=\frac{(2\pi)^{1/2}T^2 cZ_L e^{-2\pi^2T^2f^2}}{r\ln(\frac{2l}{a})\sin\theta\sin\theta_r\sqrt{2N+1}}\frac{(\cos\frac{2\pi fl\cos\theta}{c}-\cos\frac{2\pi fl}{c})(\cos\frac{2\pi fl_r\cos\theta_r}{c}-\cos\frac{2\pi fl_r}{c})}{\sin\frac{2\pi fl_r}{c}(Z_L-j\frac{\zeta_0}{\pi}\ln(\frac{2l_r}{b})\cot\frac{2\pi fl_r}{c})}$$
$$\times\sum_{n=-N}^{N}e^{-j\frac{2\pi f}{c}(r-nd\cos\theta+l)} \tag{62}$$

The received energy by the load Z_L at the receiving antenna is calculated as shown below

$$W_{rec}=\int_{-\infty}^{\infty}\frac{|V_L(f)|^2}{Z_L}df=\frac{2\pi T^4c^2Z_L^2}{Z_L[r\ln(\frac{2l}{a})\sin\theta\sin\theta_r]^2(2N+1)}2\int_0^{\infty}\frac{e^{-(2\pi Tf)^2}}{\sin^2(\frac{2\pi fl_r}{c})}$$
$$\times\frac{[\cos\frac{2\pi fl\cos\theta}{c}-\cos\frac{2\pi fl}{c}]^2[\cos\frac{2\pi fl_r\cos\theta_r}{c}-\cos\frac{2\pi fl_r}{c}]^2}{Z_L^2+[\frac{\zeta_0}{\pi}\ln(\frac{2l_r}{b})\cot\frac{2\pi fl_r}{c}]^2}\left|\sum_{n=-N}^{N}e^{-\frac{j2\pi f(r-nd\cos\theta+l)}{c}}\right|^2 df$$
$$\tag{63}$$

And using the expression obtained in Eqn. (56) for $\left|\sum_{n=-N}^{N}e^{-\frac{j2\pi f(r-nd\cos\theta+l)}{c}}\right|^2$, W_{rec} reduces to

$$W_{rec} = \frac{4\pi T^4 c^2 Z_L}{[r\sin\theta\sin\theta_r \ln(\frac{2l}{a})]^2 (2N+1)} \int_0^\infty \frac{e^{-(2\pi Tf)^2}}{\sin^2\left(\frac{2\pi\, fl_r}{c}\right)} \frac{[\cos\frac{2\pi fl\cos\theta}{c} - \cos\frac{2\pi fl}{c}]^2 [\cos\frac{2\pi fl_r\cos\theta}{c} - \cos\frac{2\pi fl_r}{c}]^2}{Z_L^2 + [\frac{\zeta_0}{\pi}\ln(\frac{2l_r}{b})\cot\frac{2\pi fl_r}{c}]^2}$$

$$\times[(2N+1) + \sum_{\substack{n=-N \\ n\neq m}}^{N} \sum_{m=-N}^{N} \cos\frac{2\pi f[(m-n)d\cos\theta]}{c}]df\,. \qquad (64)$$

which can easily be solved numerically by using computer programs.

3.4. Correlation Coefficient

In order to figure out the detection mechanism of the receiver, the load voltage V_L at the receiver and the source voltage are correlated and each normalized with their energy to obtain the correlation coefficient.

The numerator $\int_{-\infty}^{\infty} V_g(f)V_L^*(f)df$, which is the correlation between $V_g(f)$ and $V_L(f)$ is determined as follows:

$$C = \hat{\mathbf{a}}_\theta \hat{\mathbf{a}}_{\theta r} \int_{-\infty}^{\infty} (2\pi)^{3/2} T^2 f e^{-2(\pi f T)^2} \frac{\zeta_0\sqrt{2\pi} c T^2 e^{-(2\pi f T)^2} Z_L [\cos\frac{2\pi fl\cos\theta}{c} - \cos\frac{2\pi fl}{c}][\cos\frac{2\pi fl_r\cos\theta_r}{c} - \cos\frac{2\pi fl_r}{c}]}{\pi r\sqrt{2N+1}\sin\theta\sin\theta_r Z_0 f \sin\frac{2\pi fl_r}{c}}$$

$$\times \frac{1}{[Z_L + j\frac{\zeta_0}{\pi}\ln(\frac{2l}{a})\cot\frac{2\pi fl_r}{c}]} \sum_{n=-N}^{N} e^{+\frac{j2\pi f}{c}(r - nd\cos\theta + l)} df \qquad (65)$$

$$= \frac{c(2\pi)^2 T^4 Z_L}{r\ln(\frac{2l}{a})\sin\theta\sin\theta_r} \int_{-\infty}^{\infty} \frac{fe^{-(2\pi f T)^2}}{\sin\frac{2\pi fl_r}{c}} \frac{[\cos\frac{2\pi fl\cos\theta}{c} - \cos\frac{2\pi fl}{c}][\cos\frac{2\pi fl_r\cos\theta_r}{c} - \cos\frac{2\pi fl_r}{c}]}{[Z_L + j\frac{\zeta_0}{\pi}\ln(\frac{2l}{a})\cot\frac{2\pi fl_r}{c}]}$$

$$\times \sum_{n=-N}^{N} e^{+\frac{j2\pi f}{c}(r - nd\cos\theta + l)} df$$

$$C_I = \int_0^{\infty} \frac{fe^{-(2\pi fT)^2}}{\sin\frac{2\pi fl_r}{c}} \frac{[\cos\frac{2\pi fl\cos\theta}{c} - \cos\frac{2\pi fl}{c}][\cos\frac{2\pi fl_r\cos\theta_r}{c} - \cos\frac{2\pi fl_r}{c}]Z_L}{[Z_L + j\frac{\zeta_0}{\pi}\ln(\frac{2l}{a})\cot\frac{2\pi fl_r}{c}]} \times \sum_{n=-N}^{N} e^{+\frac{j2\pi f}{c}(r-nd\cos\theta+l)} df$$

$$+\int_{-\infty}^{0} \frac{fe^{-(2\pi fT)^2}}{\sin\frac{2\pi fl_r}{c}} \frac{[\cos\frac{2\pi fl\cos\theta}{c} - \cos\frac{2\pi fl}{c}][\cos\frac{2\pi fl_r\cos\theta_r}{c} - \cos\frac{2\pi fl_r}{c}]Z_L}{[Z_L + j\frac{\zeta_0}{\pi}\ln(\frac{2l}{a})\cot\frac{2\pi fl_r}{c}]} \times \sum_{n=-N}^{N} e^{+\frac{j2\pi f}{c}(r-nd\cos\theta+l)} df$$

$$C_I = \int_0^{\infty} \frac{fe^{-(2\pi fT)^2}}{\sin\frac{2\pi fl_r}{c}} \frac{[\cos\frac{2\pi fl\cos\theta}{c} - \cos\frac{2\pi fl}{c}][\cos\frac{2\pi fl_r\cos\theta_r}{c} - \cos\frac{2\pi fl_r}{c}]Z_L}{[Z_L + j\frac{\zeta_0}{\pi}\ln(\frac{2l}{a})\cot\frac{2\pi fl_r}{c}]} \times \sum_{n=-N}^{N} e^{+\frac{j2\pi f}{c}(r-nd\cos\theta+l)} df$$

$$+\int_0^{\infty} \frac{fe^{-(2\pi fT)^2}}{\sin\frac{2\pi fl_r}{c}} \frac{[\cos\frac{2\pi fl\cos\theta}{c} - \cos\frac{2\pi fl}{c}][\cos\frac{2\pi fl_r\cos\theta_r}{c} - \cos\frac{2\pi fl_r}{c}]Z_L}{[Z_L - j\frac{\zeta_0}{\pi}\ln(\frac{2l}{a})\cot\frac{2\pi fl_r}{c}]} \times \sum_{n=-N}^{N} e^{-\frac{j2\pi f}{c}(r-nd\cos\theta+l)} df$$

$$C_I = \int_0^{\infty} \frac{fe^{-(2\pi fT)^2}}{\sin\frac{2\pi fl_r}{c}} [\cos\frac{2\pi fl\cos\theta}{c} - \cos\frac{2\pi fl}{c}][\cos\frac{2\pi fl_r\cos\theta_r}{c} - \cos\frac{2\pi fl_r}{c}]Z_L$$

$$\times \underbrace{\left(\frac{\sum_{n=-N}^{N} e^{+\frac{j2\pi f}{c}(r-nd\cos\theta+l)}}{[Z_L + j\frac{\zeta_0}{\pi}\ln(\frac{2l}{a})\cot\frac{2\pi fl_r}{c}]} + \frac{\sum_{n=-N}^{N} e^{-\frac{j2\pi f}{c}(r-nd\cos\theta+l)}}{[Z_L - j\frac{\zeta_0}{\pi}\ln(\frac{2l}{a})\cot\frac{2\pi fl_r}{c}]} \right)}_{Z_A} df$$

$$Z_A = 2\,\mathrm{Re}\{\sum_{n=-N}^{N} \frac{e^{+\frac{j2\pi f}{c}(r - nd\cos\theta + l)}}{[Z_L + j\frac{\zeta_0}{\pi}\ln(\frac{2l}{a})\cot\frac{2\pi f l_r}{c}]}\}$$

$$= 2\,\mathrm{Re}\{\sum_{n=-N}^{N} \frac{\cos\frac{2\pi f}{c}(r - nd\cos\theta + l) + j\sin\frac{2\pi f}{c}(r - nd\cos\theta + l)}{[Z_L + j\frac{\zeta_0}{\pi}\ln(\frac{2l}{a})\cot\frac{2\pi f l_r}{c}]}\}$$

$$= 2\,\mathrm{Re}\{\sum_{n=-N}^{N} \frac{[Z_L - j\frac{\zeta_0}{\pi}\ln(\frac{2l}{a})\cot\frac{2\pi f l_r}{c}][\cos\frac{2\pi f(r - nd\cos\theta + l)}{c} + j\sin\frac{2\pi f(r - nd\cos\theta + l)}{c}]}{Z_L^2 + [\frac{\zeta_0}{\pi}\ln(\frac{2l}{a})\cot\frac{2\pi\, f l_r}{c}]^2}\}$$

$$= 2\,\mathrm{Re}\{\sum_{n=-N}^{N} \frac{[Z_L\cos\frac{2\pi f(r - nd\cos\theta + l)}{c} + \frac{\zeta_0}{\pi}\ln(\frac{2l}{a})\cot\frac{2\pi\, f l_r}{c}\sin\frac{2\pi f(r - nd\cos\theta + l)}{c}]}{Z_L^2 + [\frac{\zeta_0}{\pi}\ln(\frac{2l}{a})\cot\frac{2\pi\, f l_r}{c}]^2}$$

$$+ \sum_{n=-N}^{N} \frac{j[Z_L\sin\frac{2\pi f(r - nd\cos\theta + l)}{c} - \frac{\zeta_0}{\pi}\ln(\frac{2l}{a})\cot\frac{2\pi f l_r}{c}\cos\frac{2\pi f(r - nd\cos\theta + l)}{c}]}{Z_L^2 + [\frac{\zeta_0}{\pi}\ln(\frac{2l}{a})\cot\frac{2\pi\, f l_r}{c}]^2}\}$$

$$Z_A = 2\sum_{n=-N}^{N} \frac{[Z_L\cos\frac{2\pi f}{c}(r - nd\cos\theta + l) + \frac{\zeta_0}{\pi}\ln(\frac{2l}{a})\cot\frac{2\pi f l_r}{c}\sin\frac{2\pi f}{c}(r - nd\cos\theta + l)]}{Z_L^2 + [\frac{\zeta_0}{\pi}\ln(\frac{2l}{a})\cot\frac{2\pi f l_r}{c}]^2}\,. \tag{66}$$

Then C_I reduces to

$$C_I = \int_0^\infty \frac{fe^{-(2\pi fT)^2}}{\sin\frac{2\pi fl_r}{c}} \frac{2Z_L[\cos\frac{2\pi fl\cos\theta}{c} - \cos\frac{2\pi fl}{c}][\cos\frac{2\pi fl_r\cos\theta_r}{c} - \cos\frac{2\pi fl_r}{c}]}{Z_L^2 + [\frac{\zeta_0}{\pi}\ln(\frac{2l}{a})\cot\frac{2\pi fl_r}{c}]^2}$$
$$\times \sum_{n=-N}^{N} [Z_L \cos\frac{2\pi f}{c}(r - nd\cos\theta + l) + \frac{\zeta_0}{\pi}\ln(\frac{2l}{a})\cot\frac{2\pi fl_r}{c}\sin\frac{2\pi f}{c}(r - nd\cos\theta + l)]df \tag{67}$$

$\sqrt{\int_{-\infty}^{\infty} |V_g(f)|^2\, df}$ in the denominator has already been determined in Section 2, Eqn. (49) as follows:

$$\sqrt{\int_{-\infty}^{\infty} \left|(2\pi)^{3/2} T^2 fe^{-2\pi^2 T^2 f^2}\right| df} = (2\pi)^{3/2} T^2 \sqrt{\int_{-\infty}^{\infty} f^2 e^{-4\pi^2 T^2 f^2} df} = (2\pi)^{3/2} T^2 \sqrt{2\int_0^{\infty} f^2 e^{-4\pi^2 T^2 f^2} df} \tag{68}$$

Using the identity

$$\int_0^\infty x^{2n} e^{-px^2} dx = \frac{(2n-1)!}{2.(2p)^n}\sqrt{\frac{\pi}{p}}, \ [p>0, n=0,1,....],$$

It becomes

$$\sqrt{\int_{-\infty}^{\infty} |V_g(f)|^2\, df} = (2\pi)^{3/2} T^2 \sqrt{2\frac{(2-1)!}{2(2.4\pi^2 T^2)}\sqrt{\frac{\pi}{4\pi^2 T^2}}} = (2\pi)^{3/2} T^2 \sqrt{\frac{1}{(2\pi T)^3}\sqrt{\frac{\pi}{2}}}$$

$\sqrt{\int_{-\infty}^{\infty} |V_L(f)|^2\, df}$ is derived in the same manner as shown below:

$$\sqrt{\int_{-\infty}^{\infty}|V_L(f)|^2\,df}=\sqrt{\int_{-\infty}^{\infty}\left|\frac{(2\pi)^{1/2}T^2cZ_Le^{-2\pi^2T^2f^2}}{r\ln(\frac{2l}{a})\sin\theta\sin\theta_r\sqrt{2N+1}}\frac{(\cos\frac{2\pi fl\cos\theta}{c}-\cos\frac{2\pi fl}{c})(\cos\frac{2\pi fl_r\cos\theta_r}{c}-\cos\frac{2\pi fl_r}{c})}{\sin\frac{2\pi fl_r}{c}(Z_L-j\frac{\zeta_0}{\pi}\ln(\frac{2l_r}{b})\cot\frac{2\pi fl_r}{c})}\sum_{n=-N}^{N}e^{-j\frac{2\pi f}{c}(r-nd\cos\theta+l)}\right|^2df}$$

$$=\sqrt{\frac{2\pi T^4c^2Z_L^2}{[r\sin\theta\sin\theta_r\ln(\frac{2l}{a})]^2(2N+1)}2\int_0^{\infty}\frac{e^{-(2\pi Tf)^2}}{\sin^2\left(\frac{2\pi fl_r}{c}\right)}\frac{[\cos\frac{2\pi fl\cos\theta}{c}-\cos\frac{2\pi fl}{c}]^2[\cos\frac{2\pi fl_r\cos\theta}{c}-\cos\frac{2\pi fl_r}{c}]^2\times|\sum_{n=-N}^{N}e^{-j\frac{2\pi f}{c}(r-nd\cos\theta+l)}|^2}{Z_L^2+[\frac{\zeta_0}{\pi}\ln(\frac{2l_r}{b})\cot\frac{2\pi fl_r}{c}]^2}\times|\sum_{n=-N}^{N}e^{-j\frac{2\pi f}{c}(r-nd\cos\theta+l)}|^2df}$$

It reduces to

$$\sqrt{\int_{-\infty}^{\infty}|V_L(f)|^2\,df}=\sqrt{\frac{4\pi T^4c^2Z_L^2}{[r\sin\theta\sin\theta_r\ln(\frac{2l}{a})]^2(2N+1)}\int_0^{\infty}\frac{e^{-(2\pi Tf)^2}}{\sin^2\left(\frac{2\pi fl_r}{c}\right)}\frac{[\cos\frac{2\pi fl\cos\theta}{c}-\cos\frac{2\pi fl}{c}]^2[\cos\frac{2\pi fl_r\cos\theta}{c}-\cos\frac{2\pi fl_r}{c}]^2}{Z_L^2+[\frac{\xi_0}{\pi}\ln(\frac{2l_r}{b})\cot\frac{2\pi fl_r}{c}]^2}\times[(2N+1)+\sum_{\substack{n=-N\\n\neq m}}^{N}\sum_{m=-N}^{N}\cos\frac{2\pi f[(m-n)d\cos\theta]}{c}]df} \tag{69}$$

After substituting derived results into Eqn. (45), correlation coefficient expression becomes

$$CC=\frac{\frac{2(2\pi T)^{3/2}}{\pi^{1/4}}\int_0^{\infty}\frac{fe^{-(2\pi Tf)^2}}{\sin\frac{2\pi fl_r}{c}}\frac{[\cos\frac{2\pi fl\cos\theta}{c}-\cos\frac{2\pi fl}{c}][[\cos\frac{2\pi fl_r\cos\theta_r}{c}-\cos\frac{2\pi fl_r}{c}]}{Z_L^2+[\frac{\zeta_0}{\pi}\ln(\frac{2l_r}{b})\cot\frac{2\pi fl_r}{c}]^2}\times\sum_{n=-N}^{N}[Z_L\cos\frac{2\pi f}{c}(r-nd\cos\theta+1)+\frac{\zeta_0}{\pi}\ln(\frac{2l_r}{b})\cot\frac{2\pi fl_r}{c}\sin\frac{2\pi f}{c}(r-nd\cos\theta+1)]df}{\sqrt{\int_0^{\infty}\frac{e^{-(2\pi Tf)^2}}{\sin^2\frac{2\pi fl_r}{c}}\frac{[\cos\frac{2\pi fl\cos\theta}{c}-\cos\frac{2\pi fl}{c}]^2[\cos\frac{2\pi fl_r\cos\theta_r}{c}-\cos\frac{2\pi fl_r}{c}]^2}{Z_L^2+[\frac{\zeta_0}{\pi}\ln(\frac{2l_r}{b})\cot\frac{2\pi fl_r}{c}]^2}\times[(2N+1)+\sum_{\substack{n=-N\\n\neq m}}^{N}\sum_{m=-N}^{N}\cos\frac{2\pi f((m-n)d\cos\theta)}{c}]df}} \tag{70}$$

3.5. Numerical Results

Computer programs are built up based on the mathematical manipulations performed here for M=(2N+1) dipoles and computed results are presented by choosing the dipole length as $\lambda_c/2$, where λ_c is the wavelength at the center frequency f_c of the 3.1-10.6 GHz UWB range. For all dipoles, length/radius=100 and T=1/f_c.

Figures 3.2, 3.3, and 3.4 illustrate the correlation coefficient, normalized radiated and received energy patterns with respect to angle θ, respectively. In these figures, for a fixed element spacing, d=0.6c/f_c, plots for different number of elements (M=2N+1=7, 9, 11) are shown.

As seen from Figure 3.2, if the element number M increases, correlation coefficient curve tends to become narrower, thus resulting in a narrower beam width for the pattern. If the number of elements is smaller, the correlation coefficient varies in a smaller range with direction. If the number of elements increases, as moved away from the broadside, the variation of the correlation coefficient with direction increases.

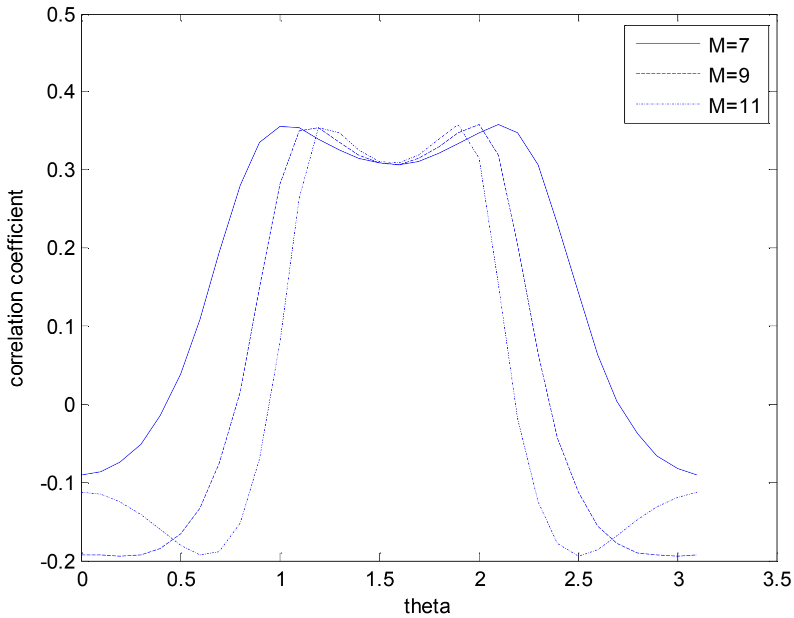

Figure 3.2. Correlation coefficient for different element numbers M = 7, 9, 11; Receiver dipole length = $\lambda_c/2$; $2l_n/a_n$ = 100; d = 0.6λ_c, Z_L = 150 Ω.

In Figures 3.3 and 3.4, when element number M increases, radiated and received energy curves tend to be narrower just as the correlation coefficient curve. This again results in a narrower beam width for the patterns. It is also seen from figures that the maximum energy is achieved in neighborhood of the broadside direction as expected.

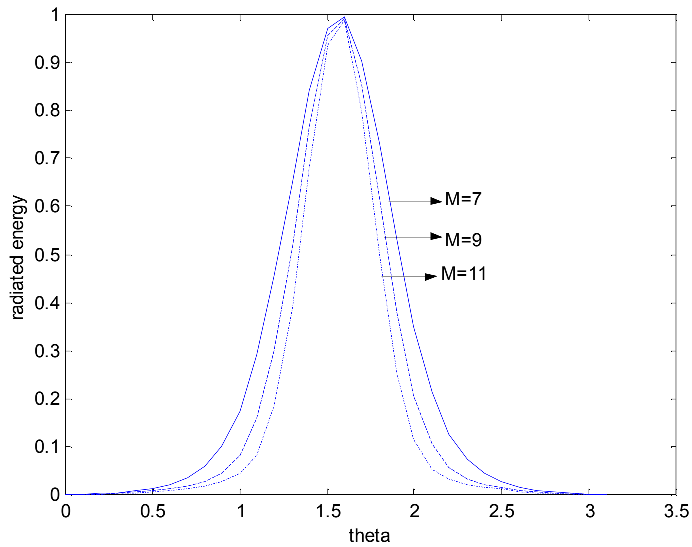

Figure 3.3. Normalized radiated energy for different element numbers M = 7, 9, 11; Receiver dipole length = $\lambda_c/2$; $2l_n/a_n$ = 100; $d = 0.6\lambda_c$, Z_L = 150 Ω.

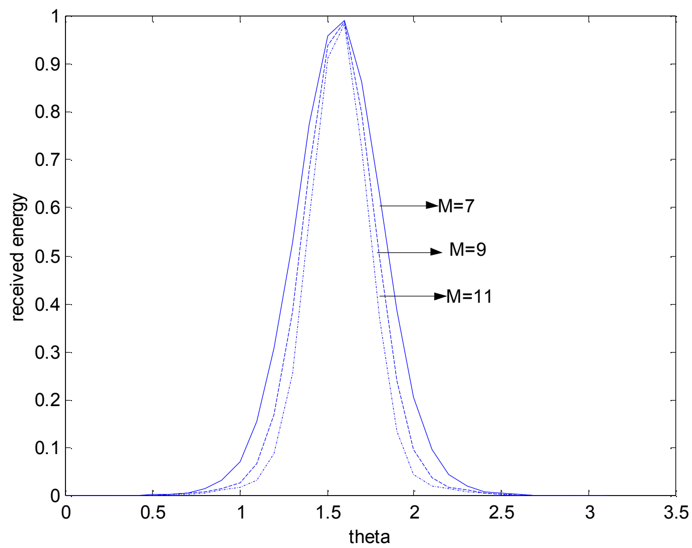

Figure 3.4. Normalized received energy for different element numbers M = 7, 9, 11; Receiver dipole length = $\lambda_c/2$; $2l_n/a_n$ = 100; $d = 0.6\lambda_c$, Z_L = 150Ω.

The characteristic obtained for the radiation pattern using this approach is in agreement with studies that have been performed in time domain by various authors (Mokole, 1996), (Sörgel et.al., 2005).

In Figure 3.5, the graph for the correlation coefficient with respect to angle θ for element spacing d=0.7λ_c and for different number of elements (M = 2N+1=7, 9, 11) is illustrated. As shown in the figure, the variation of correlation coefficient with direction increases as d increases from 0.6λ_c to 0.7λ_c. Towards the end fire, this variation can be observed more clearly.

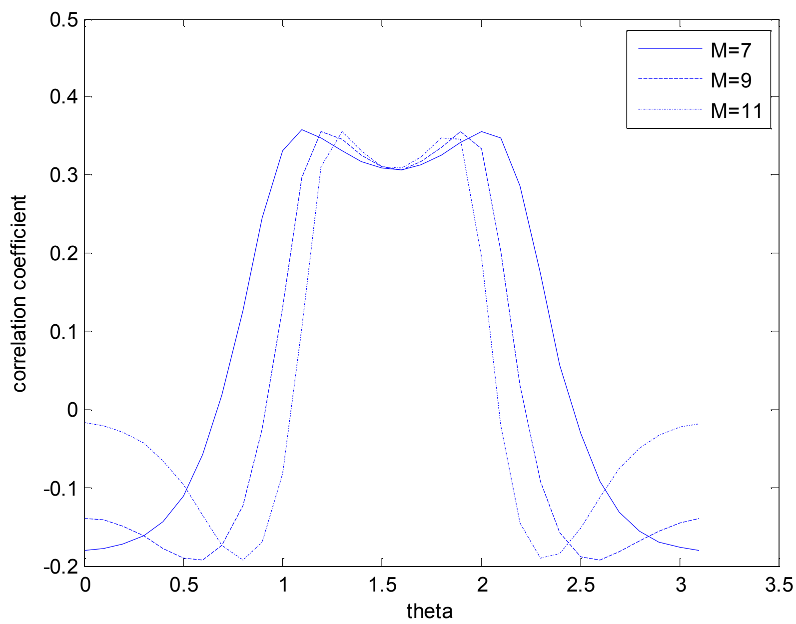

Figure 3.5. Correlation coefficient for different element numbers M = 7, 9, 11; Receiver dipole length = $\lambda_c/2$; $2l_n/a_n$ = 100; d = 0.7λ_c, Z_L = 150 Ω.

In Figures 3.6 and 3.7 the graphs for the normalized radiated and received energy patterns with respect to angle θ for element spacing d=0.7λ_c and for different number of elements (M=2N+1=7, 9, 11) are illustrated. The behavior of energy patterns is the same as in the case of element spacing d=0.7λ_c. The only difference is that the beamwidth is narrower with larger element spacing.

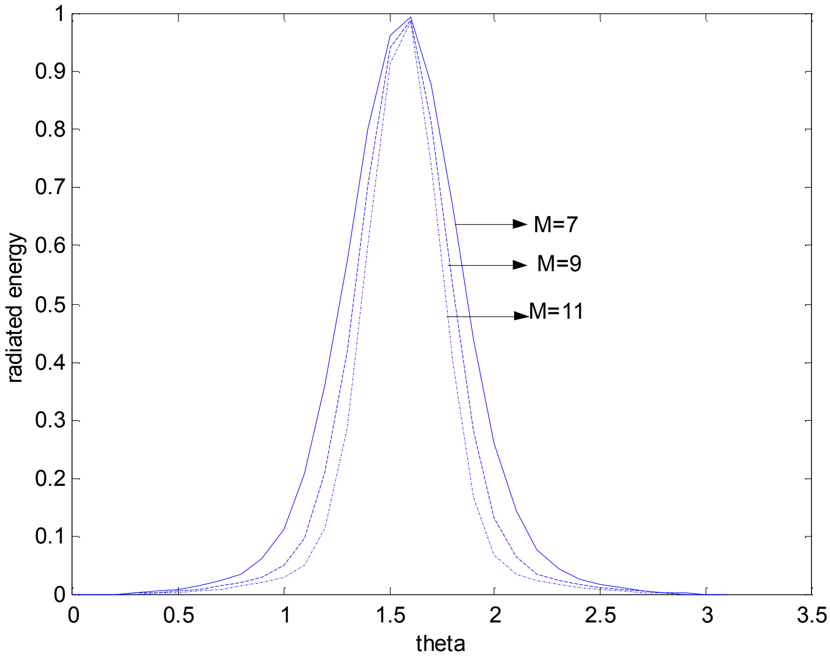

Figure 3.6. Normalized radiated energy for different element numbers M = 7, 9, 11; Receiver dipole length = $\lambda_c/2$; $2l_n/a_n = 100$; $d = 0.7\lambda_c$, $Z_L = 150\Omega$.

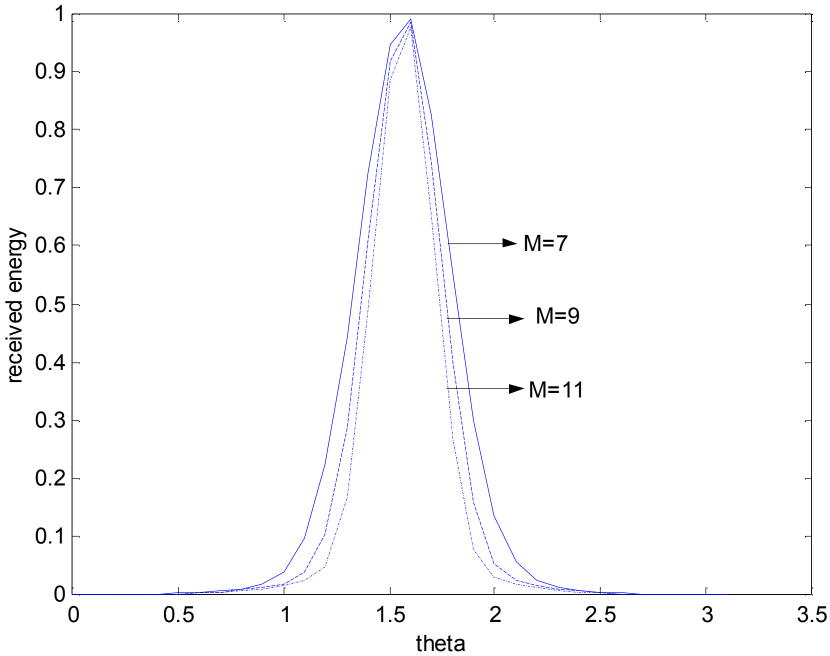

Figure 3.7. Normalized received energy for different element numbers M = 7, 9, 11; Receiver dipole length = $\lambda_c/2$; $2l_n/a_n = 100$; $d = 0.7\lambda_c$, $Z_L = 150\Omega$.

In Figure 3.8, the correlation coefficient versus θ is plotted for various element spacing (d=0.6λ_c, d=0.7λ_c, d=0.8λ_c) with a fixed number of elements M=9.

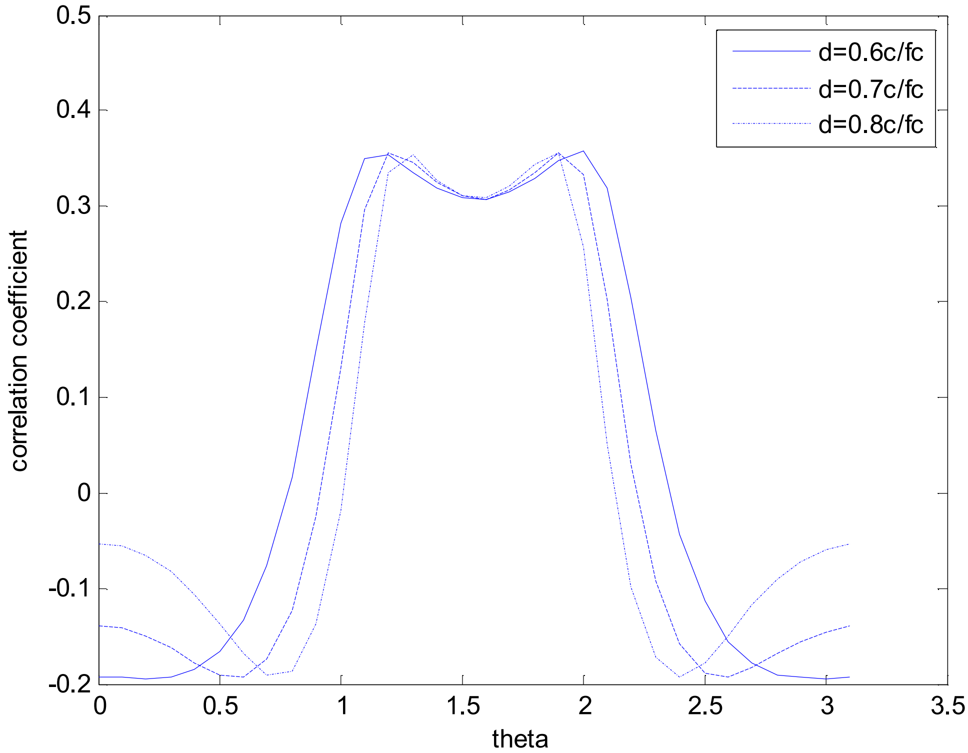

Figure 3.8. Correlation coefficient of V_L with Vg for different element spacing with M=9 Receiver dipole length = $\lambda_c/2$; $2l_n/a_n$ = 100; d=0.6λ_c, d=0.7λ_c, and d=0.8λ_c, Z_L = 150 Ω.

As it is illustrated in the figure, if d increases, patterns show similar behavior to the ones in figures 3.2, and 3.5 with increasing M. That is, when element spacing d increases, correlation coefficient curve becomes narrower. And similarly, the correlation coefficient varies in a smaller range with direction when the element spacing smaller. If element spacing increases, as moved away from the broadside, the variation of the correlation coefficient with direction increases.

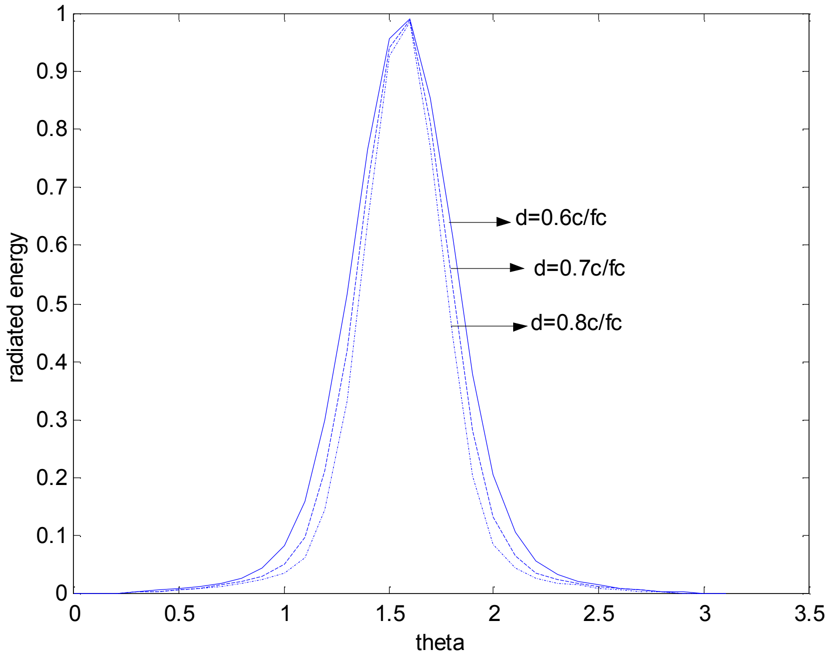

Figure 3.9. Normalized radiated energy with M=9 Receiver dipole length = $\lambda_c/2$; $2l_n/a_n$ = 100; d=0.6λ_c, d=0.7λ_c and d=0.8λ_c, Z_L = 150 Ω.

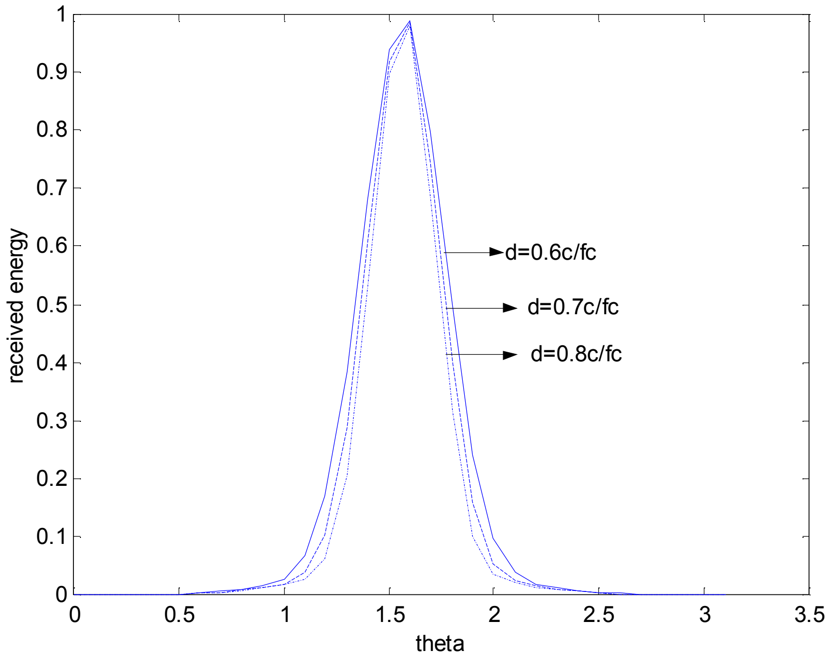

Figure 3.10. Normalized received energy with M=9 Receiver dipole length = $\lambda_c/2$; $2l_n/a_n$ = 100 d=0.6λ_c, d=0.7λ_c, and d=0.8λ_c, Z_L = 150 Ω.

In Figures 3.9 and 3.10, radiated energy and received energy are plotted with respect to θ for various element spacings (d=0.6λ_c, d=0.7λ_c, d=0.8λ_c) and a fixed number of elements M=9. In the figures, when element spacing d increases, both radiated and received energy curves tend to become narrower resulting in a narrower beam width for the patterns.

From the illustrated results it can be concluded that, the beam width of the main lobe for each pattern will be narrowed by increasing the number of antenna elements, or the element spacing. A narrower beam width is achieved by increasing the array size, either by increasing the number of elements or the element spacing.

4. ULTRA WIDEBAND ANTENNA ARRAYS WITH EQUALLY SPACED DIFFERENT LENGTH ELEMENTS

4.1. Introduction

In this section, the analysis which is performed in the frequency domain is expanded to an array of different length elements. The radiation of an UWB signal from the array and reception of the radiated pulse by a receiving dipole is investigated. The array elements are considered to have different lengths such that each element works at a specific frequency and the combination of all elements' bandwidths forms the frequency range of the array. This makes the array effective over a wider range of frequencies (Ni and Grebel, 2005).

The chapter includes derivation of radiated energy from the array and received energy at the terminals of the receiving antenna. As noted earlier, detection process at the receiver also needs special consideration to capture the incoming signal effectively. For this purpose, correlation coefficient is investigated to examine the correlation detection behavior of the receiving dipole. Frequency domain correlation coefficient between the generator voltage applied to the transmitting antenna and load voltage at the terminals of the receiving antenna are determined.

4.2. Theory of Radiation from an Array of Thin Dipoles with Different Lengths

Consider a linear array of (2N+1) equally spaced center-fed thin dipoles with lengths $2l_n$ and radii a_n is positioned symmetrically with respect to the origin along the *z*-axis with each dipole also being oriented along the *z*-axis (Fig. 4.1). The spacing between the elements is *d* and a receiving dipole orienting along the *z*-axis is located at a distance *r* in the far field region of the array.

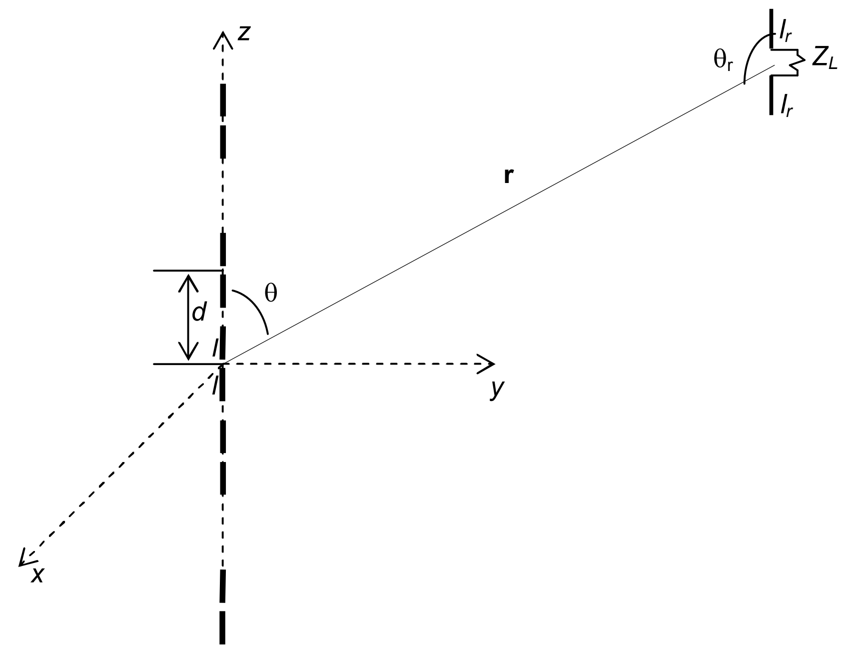

Figure 4.1. Geometry of a linear array of (2N+1) different length dipoles and a receiver at a far distance.

The electric field radiated from each dipole is given below

$$\mathbf{E}_0(\mathbf{r},f)=-\vec{\mathbf{a}}_\theta \frac{\zeta_0 V_g(f)}{2\pi r Z_0 \sin\theta\sqrt{2N+1}}\left[\cos(\frac{2\pi f l_0\cos\theta}{c})-\cos(\frac{2\pi f l_0}{c})\right]\exp\left(-\frac{j2\pi f(r+l_0)}{c}\right)$$

$$\mathbf{E}_1(\mathbf{r},f)=-\vec{\mathbf{a}}_\theta \frac{\zeta_0 V_g(f)}{2\pi r Z_1 \sin\theta\sqrt{2N+1}}\left[\cos(\frac{2\pi f l_1\cos\theta}{c})-\cos(\frac{2\pi f l_1}{c})\right]\exp\left(-\frac{j2\pi f(r-d\cos\theta+l_1)}{c}\right)$$

$$\vdots \qquad\qquad\qquad \vdots$$

$$\mathbf{E}_n(\mathbf{r},f)=-\vec{\mathbf{a}}_\theta \frac{\zeta_0 V_g(f)}{2\pi r Z_n \sin\theta\sqrt{2N+1}}\left[\cos(\frac{2\pi f l_n\cos\theta}{c})-\cos(\frac{2\pi f l_n}{c})\right]\exp\left(-\frac{j2\pi f(r-nd\cos\theta+l_n)}{c}\right).$$

Radiated total electric far field at a distance *r* is found as the superposition of electric fields from individual elements and given by

$$\mathbf{E}_T(\mathbf{r},f) = -\vec{\mathbf{a}}_\theta \frac{\zeta_0 V_g(f)}{2\pi r\sqrt{2N+1}\sin\theta} \sum_{n=-N}^{N} \frac{1}{Z_n}[\cos\frac{2\pi f l_n \cos\theta}{c} - \cos\frac{2\pi f l_n}{c}]\exp(-j\frac{2\pi f}{c}(r - nd\cos\theta + l_n)) \tag{71}$$

Here, the current distribution approximation along each of the dipoles is being represented by the distribution along an open-ended transmission line with characteristic impedance $Z_n=(\zeta_0/\pi)\ln(2l_n/a_n)$ as in previous studies (Franceschietti and Papas, 1974), (Samaddar,1992). Each dipole is assumed to be matched to the feed network. Mutual coupling between the elements is ignored here.

When the source pulse applied as an input to the dipoles in the array is the Gaussian monocycle of duration T, the energy radiated from the array of dipoles at a distance r is derived as follows

$$\int_{-\infty}^{\infty} |\mathbf{E}_T(\mathbf{r},f)|^2 df = \int_{-\infty}^{\infty} \frac{\zeta_0^2 |V_g(f)|^2}{(2\pi r\sin\theta)^2(2N+1)} \underbrace{\left| \sum_{n=-N}^{N} \frac{[\cos\frac{2\pi f l_n \cos\theta}{c} - \cos\frac{2\pi f l_n}{c}]\exp(-j\frac{2\pi f}{c}(r - nd\cos\theta + l_n))}{Z_n} \right|^2}_{Z_B} df. \tag{72}$$

$$Z_B = \sum_{n=-N}^{N} \frac{1}{|Z_n|^2}\left[\cos\frac{2\pi\, f l_n \cos\theta}{c} - \cos\frac{2\pi\, f l_n}{c}\right]^2$$
$$+ \sum_{\substack{n=-N \\ n\neq m}}^{N} \sum_{m=-N}^{N} \frac{\left[\cos\frac{2\pi\, f l_n \cos\theta}{c} - \cos\frac{2\pi\, f l_n}{c}\right]\left[\cos\frac{2\pi\, f l_m \cos\theta}{c} - \cos\frac{2\pi\, f l_m}{c}\right]}{Z_n Z_m}$$
$$.\cos\frac{2\pi f}{c}[(m-n)d\cos\theta + l_n - l_m]\}df \tag{73}$$

Substituting Z_B and Gaussian monocycle expression into Eqn. (72), W_{rad} becomes

$$W_{rad} = \int_{-\infty}^{\infty} \frac{\zeta_0^2 (2\pi)^3 T^4}{4\pi^2 r^2 \sin^2\theta (2N+1)} f^2 e^{-(2\pi Tf)^2} \{ \sum_{n=-N}^{N} \frac{\left[\cos\frac{2\pi\, fl_n \cos\theta}{c} - \cos\frac{2\pi\, fl_n}{c} \right]^2}{[Z_n]^2}$$

$$+ \sum_{\substack{n=-N \\ n\neq m}}^{N} \sum_{m=-N}^{N} \frac{\left[\cos\frac{2\pi\, fl_n \cos\theta}{c} - \cos\frac{2\pi\, fl_n}{c} \right]\left[\cos\frac{2\pi\, fl_m \cos\theta}{c} - \cos\frac{2\pi\, fl_m}{c} \right]}{Z_n Z_m}$$

$$. \cos\frac{2\pi f}{c}[(m-n)d\cos\theta + l_n - l_m]\} df \,. \quad (74)$$

Finally, W_{rad} is obtained as shown below

$$W_{rad} = \frac{4\pi^3 T^4}{(r\sin\theta)^2 (2N+1)} \int_0^{\infty} f^2 e^{-(2\pi Tf)^2} \{ \sum_{n=-N}^{N} \frac{\left[\cos\frac{2\pi\, fl_n \cos\theta}{c} - \cos\frac{2\pi\, fl_n}{c} \right]^2}{[\ln(\frac{2l_n}{a_n})]^2}$$

$$+ \sum_{\substack{n=-N \\ n\neq m}}^{N} \sum_{m=-N}^{N} \frac{\left[\cos\frac{2\pi\, fl_n \cos\theta}{c} - \cos\frac{2\pi\, fl_n}{c} \right]\left[\cos\frac{2\pi\, fl_m \cos\theta}{c} - \cos\frac{2\pi\, fl_m}{c} \right]}{\ln(\frac{2l_n}{a_n})\ln(\frac{2l_m}{a_m})} \cos\frac{2\pi f}{c}[(m-n)d\cos\theta + l_n - l_m]\} df.$$

$$(75)$$

The parenthesis in Eqn. (75) can be expanded to obtain an explicit expression for W_{rad} as follows

$$W_{rad} = \frac{4\pi^3 T^4}{(r\sin\theta)^2 (2N+1)} \int_0^{\infty} f^2 e^{-(2\pi Tf)^2} \{ \sum_{n=-N}^{N} \frac{\left[\cos^2\frac{2\pi fl_n \cos\theta}{c} - 2\cos\frac{2\pi fl_n \cos\theta}{c}\cos\frac{2\pi fl_n}{c} + \cos^2\frac{2\pi fl_n}{c} \right]}{[\ln(\frac{2l_n}{a_n})]^2}$$

$$+ \sum_{\substack{n=-N \\ n\neq m}}^{N} \sum_{m=-N}^{N} \frac{1}{\ln(\frac{2l_n}{a_n})\ln(\frac{2l_m}{a_m})} \cos\frac{2\pi f}{c}[(m-n)d\cos\theta + l_n - l_m]$$

$$\times[\cos\frac{2\pi fl_n \cos\theta}{c}\cos\frac{2\pi fl_m \cos\theta}{c} - \cos\frac{2\pi fl_n \cos\theta}{c}\cos\frac{2\pi fl_m}{c}$$

$$-\cos\frac{2\pi\, fl_n}{c}\cos\frac{2\pi fl_m \cos\theta}{c} + \cos\frac{2\pi\, fl_n}{c}\cos\frac{2\pi fl_m}{c}]\} df$$

Using the identities which were designated before in equations (17) and (18) (Gradshteyn, 1980), each integral is evaluated as follows

$$A=\int_0^\infty f^2 e^{-(2\pi Tf)^2}\cos^2\frac{2\pi f l_n\cos\theta}{c}df$$

$$A=\int_0^\infty f^2 e^{-(2\pi Tf)^2}\frac{1+\cos\frac{4\pi f l_n\cos\theta}{c}}{2}df=\int_0^\infty\frac{f^2 e^{-(2\pi Tf)^2}}{2}df+\int_0^\infty f^2 e^{-(2\pi Tf)^2}\frac{\cos\frac{4\pi f l_n\cos\theta}{c}}{2}df$$

$$A=\frac{1}{2}[\frac{1}{2(2.4\pi^2T^2)}\sqrt{\frac{\pi}{4\pi^2T^2}}+\sqrt{\pi}\frac{2(2\pi T)^2-\left(\frac{4\pi l_n\cos\theta}{c}\right)^2}{8(2\pi T)^5}e^{-\frac{(4\pi l_n\cos\theta)^2}{c^2 4(2\pi T)^2}}]$$

$$A=\frac{1}{2}[\frac{\sqrt{\pi}}{4(2\pi T)^3}+\sqrt{\pi}\frac{8(\pi Tc)^2-(4\pi l_n\cos\theta)^2}{8c^2(2\pi T)^5}e^{-\left(\frac{l_n\cos\theta}{cT}\right)^2}]$$

$$B=\int_0^\infty f^2 e^{-(2\pi Tf)^2}\cos\frac{2\pi f l_n\cos\theta}{c}.\cos\frac{2\pi f l_n}{c}df$$

$$B=\int_0^\infty f^2 e^{-(2\pi Tf)^2}\frac{1}{2}[\cos\frac{2\pi f l_n(\cos\theta+1)}{c}.\cos\frac{2\pi f l_n(\cos\theta-1)}{c}df$$

$$B=\sqrt{\pi}\frac{1}{2}[\frac{2(2\pi T)^2-\left(\frac{2\pi l_n(\cos\theta+1)}{c}\right)^2}{8(2\pi T)^5}e^{-\frac{(2\pi l_n(\cos\theta+1))^2}{c^2 4(2\pi T)^2}}+\frac{2(2\pi T)^2-\left(\frac{2\pi l_n(\cos\theta-1)}{c}\right)^2}{8(2\pi T)^5}e^{-\frac{(2\pi l_n(\cos\theta-1))^2}{c^2 4(2\pi T)^2}}]$$

$$B=\sqrt{\pi}\frac{1}{2}[\frac{8(\pi Tc)^2-(2\pi l_n(\cos\theta+1))^2}{8c^2(2\pi T)^5}e^{-\left(\frac{l_n(\cos\theta+1)}{2cT}\right)^2}+\frac{8(\pi Tc)^2-(2\pi l_n(\cos\theta-1))^2}{8c^2(2\pi T)^5}e^{-\left(\frac{l_n(\cos\theta-1)}{2cT}\right)^2}]$$

$$C=\int_0^\infty f^2 e^{-(2\pi Tf)^2}\cos^2\frac{2\pi f l_n}{c}df$$

$$C=\int_0^\infty f^2 e^{-(2\pi Tf)^2}\frac{1+\cos\frac{4\pi f l_n}{c}}{2}df=\frac{1}{2}[\int_0^\infty f^2 e^{-(2\pi Tf)^2}df+\int_0^\infty f^2 e^{-(2\pi Tf)^2}\cos\frac{4\pi f l_n}{c}df]$$

$$C=\frac{1}{2}[\frac{1}{2(2.4\pi^2T^2)}\sqrt{\frac{\pi}{4\pi^2T^2}}+\sqrt{\pi}\frac{2(2\pi T)^2-\left(\frac{4\pi l_n}{c}\right)^2}{8(2\pi T)^5}e^{-\frac{(4\pi l_n)^2}{c^2 4(2\pi T)^2}}]$$

$$C=\frac{1}{2}[\frac{\sqrt{\pi}}{4(2\pi T)^3}+\sqrt{\pi}\frac{8(\pi Tc)^2-\left(4\pi l_n\right)^2}{8c^2(2\pi T)^5}e^{-\left(\frac{l_n}{cT}\right)^2}]$$

$$D=\int_0^\infty f^2 e^{-(2\pi Tf)^2}\cos\frac{2\pi f l_n\cos\theta}{c}.\cos\frac{2\pi f l_m\cos\theta}{c}\cos\frac{2\pi f}{c}[(m-n)d\cos\theta+l_n-l_m]df$$

$$D=\int_0^\infty f^2 e^{-(2\pi Tf)^2}\frac{1}{2}[\cos\frac{2\pi f(l_n+l_m)\cos\theta}{c}+\cos\frac{2\pi f(l_n-l_m)\cos\theta}{c}]$$
$$.\cos\frac{2\pi f}{c}[(m-n)d\cos\theta+l_n-l_m]df$$

$$D=\frac{1}{2}\int_0^\infty f^2 e^{-(2\pi Tf)^2}\{\cos\frac{2\pi f(l_n+l_m)\cos\theta}{c}.\cos\frac{2\pi f}{c}[(m-n)d\cos\theta+l_n-l_m]df$$
$$+\cos\frac{2\pi f(l_n-l_m)\cos\theta}{c}.\cos\frac{2\pi f}{c}[(m-n)d\cos\theta+l_n-l_m]df\}$$

$$D=\frac{1}{2}\int_0^\infty f^2 e^{-(2\pi Tf)^2}\frac{1}{2}\{\cos\frac{2\pi f}{c}[(l_n+l_m)\cos\theta+(m-n)d\cos\theta+(l_n-l_m)]$$
$$+\cos\frac{2\pi f}{c}[(l_n+l_m)\cos\theta-(m-n)d\cos\theta-(l_n-l_m)]$$
$$+\cos\frac{2\pi f}{c}[(l_n-l_m)\cos\theta+(m-n)d\cos\theta+(l_n-l_m)]$$
$$+\cos\frac{2\pi f}{c}[(l_n-l_m)\cos\theta-(m-n)d\cos\theta-(l_n-l_m)]\}df$$

$$D=\frac{1}{4}\{\sqrt{\pi}\,\frac{2(2\pi Tc)^2-\{2\pi[(l_n+l_m)\cos\theta+(m-n)d\cos\theta+(l_n-l_m)]\}^2}{8c^2(2\pi T)^5}e^{-\frac{\{2\pi[(l_n+l_m)\cos\theta+(m-n)d\cos\theta+(l_n-l_m)]\}^2}{c^2 4(2\pi T)^2}}$$

$$+\sqrt{\pi}\,\frac{2(2\pi Tc)^2-\{2\pi[(l_n+l_m)\cos\theta-(m-n)d\cos\theta-(l_n-l_m)]\}^2}{8c^2(2\pi T)^5}e^{-\frac{\{2\pi[(l_n+l_m)\cos\theta-(m-n)d\cos\theta-(l_n-l_m)]\}^2}{c^2 4(2\pi T)^2}}$$

$$+\sqrt{\pi}\,\frac{2(2\pi Tc)^2-\{2\pi[(l_n-l_m)\cos\theta+(m-n)d\cos\theta+(l_n-l_m)]\}^2}{8c^2(2\pi T)^5}e^{-\frac{\{2\pi[(l_n-l_m)\cos\theta+(m-n)d\cos\theta+(l_n-l_m)]\}^2}{c^2 4(2\pi T)^2}}$$

$$+\sqrt{\pi}\,\frac{2(2\pi Tc)^2-\{2\pi[(l_n-l_m)\cos\theta-(m-n)d\cos\theta-(l_n-l_m)]\}^2}{8c^2(2\pi T)^5}e^{-\frac{\{2\pi[(l_n-l_m)\cos\theta-(m-n)d\cos\theta-(l_n-l_m)]\}^2}{c^2 4(2\pi T)^2}}$$

$$D=\frac{1}{4}\{\sqrt{\pi}\,\frac{8\pi^2T^2c^2-\{2\pi[(l_n+l_m)\cos\theta+(m-n)d\cos\theta+(l_n-l_m)]\}^2}{8c^2(2\pi T)^5}e^{-\left[\frac{(l_n+l_m)\cos\theta+(m-n)d\cos\theta+(l_n-l_m)}{2cT}\right]^2}$$

$$+\sqrt{\pi}\,\frac{8\pi^2T^2c^2-\{2\pi[(l_n+l_m)\cos\theta-(m-n)d\cos\theta-(l_n-l_m)]\}^2}{8c^2(2\pi T)^5}e^{-\left[\frac{(l_n+l_m)\cos\theta-(m-n)d\cos\theta-(l_n-l_m)}{2cT}\right]^2}$$

$$+\sqrt{\pi}\,\frac{8\pi^2T^2c^2-\{2\pi[(l_n-l_m)\cos\theta+(m-n)d\cos\theta+(l_n-l_m)]\}^2}{8c^2(2\pi T)^5}e^{-\left[\frac{(l_n-l_m)\cos\theta+(m-n)d\cos\theta+(l_n-l_m)}{2cT}\right]^2}$$

$$+\sqrt{\pi}\,\frac{8\pi^2T^2c^2-\{2\pi[(l_n-l_m)\cos\theta-(m-n)d\cos\theta-(l_n-l_m)]\}^2}{8c^2(2\pi T)^5}e^{-\left[\frac{(l_n-l_m)\cos\theta-(m-n)d\cos\theta-(l_n-l_m)}{2cT}\right]^2}$$

$$E=\int_0^\infty f^2e^{-(2\pi Tf)^2}\cos\frac{2\pi fl_n\cos\theta}{c}.\cos\frac{2\pi fl_m}{c}\cos\frac{2\pi f}{c}[(m-n)d\cos\theta+l_n-l_m]df$$

$$E=\frac{1}{4}\{\sqrt{\pi}\,\frac{8\pi^2T^2c^2-\{2\pi[l_n\cos\theta+l_m+(m-n)d\cos\theta+(l_n-l_m)]\}^2}{8c^2(2\pi T)^5}e^{-\left[\frac{l_n\cos\theta+l_m+(m-n)d\cos\theta+(l_n-l_m)}{2cT}\right]^2}$$

$$+\sqrt{\pi}\,\frac{8\pi^2T^2c^2-\{2\pi[l_n\cos\theta+l_m-(m-n)d\cos\theta-(l_n-l_m)]\}^2}{8c^2(2\pi T)^5}e^{-\left[\frac{l_n\cos\theta+l_m-(m-n)d\cos\theta-(l_n-l_m)}{2cT}\right]^2}$$

$$+\sqrt{\pi}\,\frac{8\pi^2T^2c^2-\{2\pi[l_n\cos\theta-l_m+(m-n)d\cos\theta+(l_n-l_m)]\}^2}{8c^2(2\pi T)^5}e^{-\left[\frac{l_n\cos\theta-l_m+(m-n)d\cos\theta+(l_n-l_m)}{2cT}\right]^2}$$

$$+\sqrt{\pi}\,\frac{8\pi^2T^2c^2-\{2\pi[l_n\cos\theta-l_m-(m-n)d\cos\theta-(l_n-l_m)]\}^2}{8c^2(2\pi T)^5}e^{-\left[\frac{l_n\cos\theta-l_m-(m-n)d\cos\theta-(l_n-l_m)}{2cT}\right]^2}$$

$$F=\int_0^\infty f^2 e^{-(2\pi Tf)^2}\cos\frac{2\pi f l_n}{c}.\cos\frac{2\pi f l_m\cos\theta}{c}\cos\frac{2\pi f}{c}[(m-n)d\cos\theta+l_n-l_m]df$$

$$F=\frac{1}{4}\{\sqrt{\pi}\frac{8\pi^2T^2c^2-\{2\pi[l_n+l_m\cos\theta+(m-n)d\cos\theta+(l_n-l_m)]\}^2}{8c^2(2\pi T)^5}e^{-\left[\frac{l_n+l_m\cos\theta+(m-n)d\cos\theta+(l_n-l_m)}{2cT}\right]^2}$$
$$+\sqrt{\pi}\frac{8\pi^2T^2c^2-\{2\pi[l_n+l_m\cos\theta-(m-n)d\cos\theta-(l_n-l_m)]\}^2}{8c^2(2\pi T)^5}e^{-\left[\frac{l_n+l_m\cos\theta-(m-n)d\cos\theta-(l_n-l_m)}{2cT}\right]^2}$$
$$+\sqrt{\pi}\frac{8\pi^2T^2c^2-\{2\pi[l_n-l_m\cos\theta+(m-n)d\cos\theta+(l_n-l_m)]\}^2}{8c^2(2\pi T)^5}e^{-\left[\frac{l_n-l_m\cos\theta+(m-n)d\cos\theta+(l_n-l_m)}{2cT}\right]^2}$$
$$+\sqrt{\pi}\frac{8\pi^2T^2c^2-\{2\pi[l_n-l_m\cos\theta-(m-n)d\cos\theta-(l_n-l_m)]\}^2}{8c^2(2\pi T)^5}e^{-\left[\frac{l_n-l_m\cos\theta-(m-n)d\cos\theta-(l_n-l_m)}{2cT}\right]^2}$$

$$G=\int_0^\infty f^2 e^{-(2\pi Tf)^2}\cos\frac{2\pi f l_n}{c}.\cos\frac{2\pi f l_m}{c}\cos\frac{2\pi f}{c}[(m-n)d\cos\theta+l_n-l_m]df$$

$$G=\frac{1}{4}\{\sqrt{\pi}\frac{8\pi^2T^2c^2-\{2\pi[l_n+l_m+(m-n)d\cos\theta+(l_n-l_m)]\}^2}{8c^2(2\pi T)^5}e^{-\left[\frac{l_n+l_m+(m-n)d\cos\theta+(l_n-l_m)}{2cT}\right]^2}$$
$$+\sqrt{\pi}\frac{8\pi^2T^2c^2-\{2\pi[l_n+l_m-(m-n)d\cos\theta-(l_n-l_m)]\}^2}{8c^2(2\pi T)^5}e^{-\left[\frac{l_n+l_m-(m-n)d\cos\theta-(l_n-l_m)}{2cT}\right]^2}$$
$$+\sqrt{\pi}\frac{8\pi^2T^2c^2-\{2\pi[l_n-l_m+(m-n)d\cos\theta+(l_n-l_m)]\}^2}{8c^2(2\pi T)^5}e^{-\left[\frac{l_n-l_m+(m-n)d\cos\theta+(l_n-l_m)}{2cT}\right]^2}$$
$$+\sqrt{\pi}\frac{8\pi^2T^2c^2-\{2\pi[l_n-l_m-(m-n)d\cos\theta-(l_n-l_m)]\}^2}{8c^2(2\pi T)^5}e^{-\left[\frac{l_n-l_m-(m-n)d\cos\theta-(l_n-l_m)}{2cT}\right]^2}$$

Then the explicit form of the radiated energy can be expressed as

$$W_{rad}=\frac{4\pi^3T^4}{(r\sin\theta)^2(2N+1)}\left[\sum_{n=-N}^{N}\frac{A-2B-C}{[\ln(\frac{2l_n}{a_n})]^2}+\sum_{\substack{n,m\\n\neq m}}^{N}\sum_{=-N}^{N}\frac{D-E-F+G}{\ln(\frac{2l_n}{a_n})\ln(\frac{2l_m}{a_m})}\right]. \qquad (76)$$

4.3. Analysis at the Receiving Dipole

When the radiated field from the transmitting antenna is incident on a receiving dipole of length $2l_r$ and radius b, in the far field region of the transmitting antenna (Figure 4.1), load voltage across the terminals of the receiving dipole is calculated using the relation (Samaddar,1993)

$$V_L(f) = \frac{\mathbf{E}_T(\mathbf{r},f)\cdot\mathbf{h}_{eff}(f)Z_L}{Z_L + Z_r} \tag{77}$$

again, where $\mathbf{h}_{eff}$, Z_r, and Z_L are the effective length, input and load impedance of the receiving dipole, respectively. They are calculated according to the same current distribution approximation and transmission line approach made for the dipole elements on the transmitter side again. Therefore, after certain mathematical operations, $V_L(f)$ can be derived as follows

$$V_L(f) = \frac{\zeta_0 Z_L c V_g(f)}{2\pi^2 r\sqrt{2N+1}\sin\theta\sin\theta_r}\frac{(\cos\frac{2\pi f l_r\cos\theta_r}{c} - \cos\frac{2\pi f l_r}{c})}{f\sin\frac{2\pi f l_r}{c}(Z_L - j\frac{\zeta_0}{\pi}\ln(\frac{2l_r}{b})\cot\frac{2\pi f l_r}{c})}$$
$$\times\sum_{n=-N}^{N}\frac{\left[\cos\frac{2\pi f l_n\cos\theta}{c} - \cos\frac{2\pi f l_n}{c}\right]}{Z_n}\exp(-\frac{j2\pi f(r - nd\cos\theta + l_n)}{c}). \tag{78}$$

Using Gaussian monocycle as the input, $V_L(f)$ then becomes

$$V_L(f) = \frac{(2\pi)^{1/2} cT^2 Z_L e^{-2\pi^2 f^2 T^2}}{r\sqrt{2N+1}\sin\theta\sin\theta_r}\frac{[\cos\frac{2\pi f l_r\cos\theta_r}{c} - \cos\frac{2\pi f l_r}{c}]}{\sin\frac{2\pi f l_r}{c}(Z_L - j\frac{\zeta_0}{\pi}\ln(\frac{2l_r}{b})\cot\frac{2\pi f l_r}{c})}$$
$$\times\sum_{n=-N}^{N}\frac{\left[\cos\frac{2\pi f l_n\cos\theta}{c} - \cos\frac{2\pi f l_n}{c}\right]}{\ln(\frac{2l_n}{a_n})}\exp(-\frac{j2\pi f(r - nd\cos\theta + l_n)}{c}) \tag{79}$$

The energy received by the load at the terminals of the receiving dipole can be obtained as follows:

$$
\begin{aligned}
W_{rec} &= \int_{-\infty}^{\infty} \frac{|V_L(f)|^2}{Z_L} df = \frac{4\pi c^2 T^4 Z_L}{(r\sin\theta\sin\theta_r)^2(2N+1)} \int_0^{\infty} \frac{e^{-(2\pi f T)^2}}{\sin^2\frac{2\pi f l_r}{c}} \frac{[\cos\frac{2\pi f l_r\cos\theta_r}{c} - \cos\frac{2\pi f l_r}{c}]^2}{Z_L^2 + (\frac{\zeta_0}{\pi}\ln(\frac{2l_r}{b})\cot\frac{2\pi f l_r}{c})^2} \\
&\times [\sum_{n=-N}^{N} \frac{\left[\cos\frac{2\pi f l_n\cos\theta}{c} - \cos\frac{2\pi f l_n}{c}\right]^2}{[\ln(\frac{2l_n}{a_n})]^2} + \sum_{\substack{n=-N \\ n\neq m}}^{N}\sum_{m=-N}^{N} \frac{\left[\cos\frac{2\pi f l_n\cos\theta}{c} - \cos\frac{2\pi f l_n}{c}\right]\left[\cos\frac{2\pi f l_m\cos\theta}{c} - \cos\frac{2\pi f l_m}{c}\right]}{\ln(\frac{2l_n}{a_n})\ln(\frac{2l_m}{a_m})} \\
&\quad .\cos\frac{2\pi f}{c}[(m-n)d\cos\theta + l_n - l_m]]df \qquad (80)
\end{aligned}
$$

The correlation coefficient between the load voltage V_L at the receiver and the source voltage V_g at the transmitter is derived as

$$
CC = \frac{2(2\pi T)^{3/2}}{\pi^{1/4}} \frac{\begin{aligned}&\int_0^{\infty} \frac{f e^{-(2\pi f T)^2}}{\sin\frac{2\pi f l_r}{c}} \frac{[\cos\frac{2\pi f l_r\cos\theta_r}{c} - \cos\frac{2\pi f l_r}{c}]}{Z_L^2 + [\frac{\zeta_0}{\pi}\ln(\frac{2l_r}{b})\cot\frac{2\pi f l_r}{c}]^2} \sum_{n=-N}^{N} \frac{[\cos\frac{2\pi f l_n\cos\theta}{c} - \cos\frac{2\pi f l_n}{c}]}{\ln(\frac{2l_n}{a_n})} \\ &\times[Z_L\cos\frac{2\pi f}{c}(r - nd\cos\theta + l_n) + \frac{\zeta_0}{\pi}\ln(\frac{2l_r}{b})\cot\frac{2\pi f l_r}{c}\sin\frac{2\pi f}{c}(r - nd\cos\theta + l_n)]df\end{aligned}}{\sqrt{\begin{aligned}&\int_0^{\infty} \frac{e^{-(2\pi f T)^2}}{\sin^2(\frac{2\pi f l_r}{c})} \cdot \frac{[\cos\frac{2\pi f l_r\cos\theta_r}{c} - \cos\frac{2\pi f l_r}{c}]^2}{Z_L^2 + [\frac{\zeta_0}{\pi}\ln(\frac{2l_r}{b})\cot\frac{2\pi f l_r}{c}]^2} \{\sum_{n=-N}^{N} \frac{[\cos\frac{2\pi f l_n\cos\theta}{c} - \cos\frac{2\pi f l_n}{c}]^2}{[\ln(\frac{2l_n}{a_n})]^2} \\ &+ \sum_{\substack{n=-N \\ n\neq m}}^{N}\sum_{m=-N}^{N} \frac{\left[\cos\frac{2\pi f l_n\cos\theta}{c} - \cos\frac{2\pi f l_n}{c}\right]\left[\cos\frac{2\pi f l_m\cos\theta}{c} - \cos\frac{2\pi f l_m}{c}\right]}{\ln(\frac{2l_n}{a_n})\ln(\frac{2l_m}{a_m})} \cos\frac{2\pi f}{c}[(m-n)d\cos\theta + l_n - l_m]\}df\end{aligned}}}
$$

(81)

4.4. Numerical Results

The shortest dipole is half wavelength at 10.6 GHz, and the longest dipole is half wavelength at 3.1 GHz. Each of the other elements in the array is active at a specific frequency between these frequencies.

The figures 4.2 through 4.8 show correlation coefficient and radiated & received energies with respect to θ for various parameters. For these figures, the following common parameters are used: **e**lement spacing $d = \lambda_1/2 = 9.68/2 = 4.84$, receiver dipole length = $\lambda_c/2$, dipole length/radius $(2l_n/a_n) = 100$, $l_1 = \lambda_1/2 = 4.84$ cm (outermost dipoles' length), $l_2 = \lambda_2/2 = 1.41$cm (dipole at the center), $Z_L = 150\ \Omega$,.

Figures 4.2 and 4.3 show the correlation coefficient and radiated & received energies for the element number $M = 7$, respectively. For element number $M = 9$, the results are plotted in Figures 4.4, and 4.5. Figure 4.6 compares the correlation coefficient graphs for element numbers $M = 7$, 9 and 11. Similarly a comparison between the radiated and received energies for different element numbers ($M = 7$, 9, 11) is presented in Figures 4.7 and 7.8, respectively.

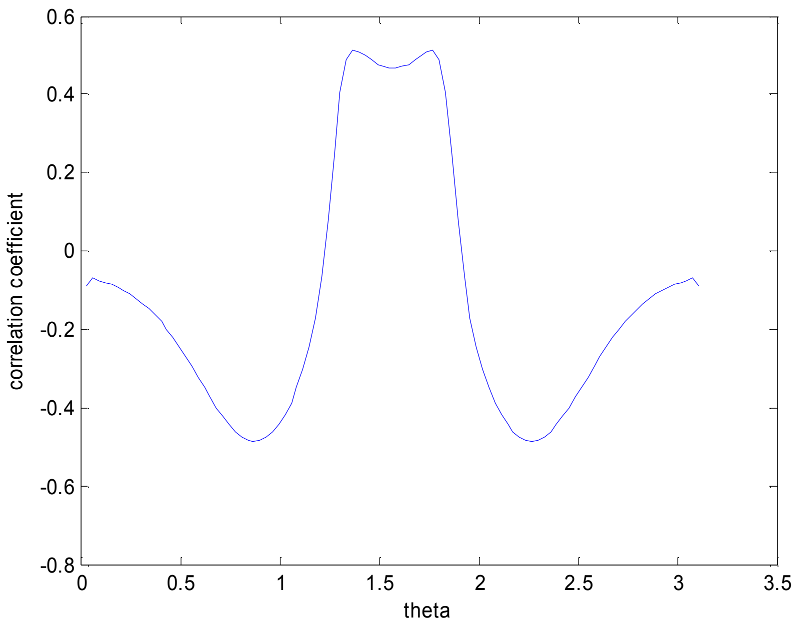

Figure 4.2. Correlation coefficient of V_g and V_L for element number M = 7; receiver dipole length = $\lambda_c/2$; $2l_n/a_n = 100$; $d = \lambda_1/2$, $Z_L = 150\ \Omega$.

As seen in Figure 4.2, correlation coefficient takes maximum values in the neighborhood of the broadside direction. As moved away from broadside to endfire, correlation coefficient decreases and becomes negative and then approaches zero.

It should be noted that, when compared to the array of same size elements, the correlation coefficient curve becomes narrower and its variation with angle becomes more evident.

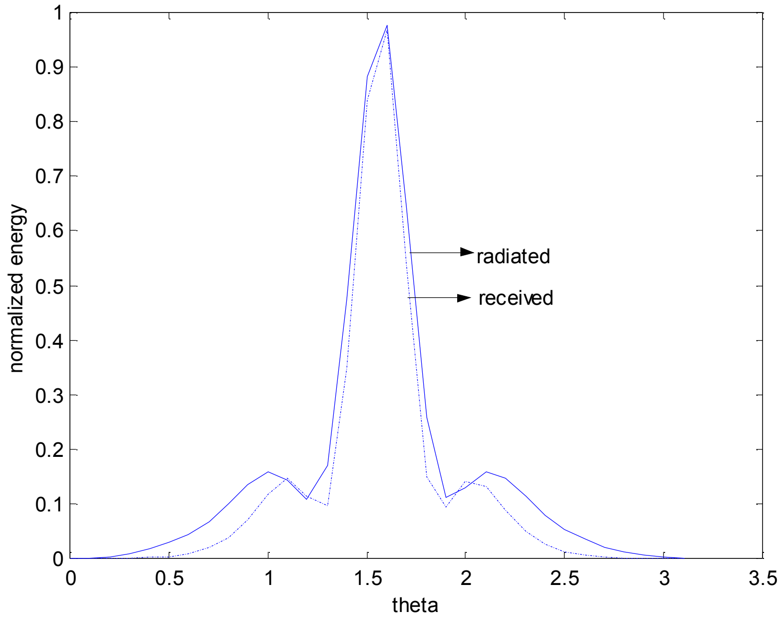

Figure 4.3. Normalized radiated and received energies for element number M = 7; receiver dipole length = $\lambda_c/2$; $2l_n/a_n$ = 100; $d = \lambda_1/2$, Z_L = 150 Ω.

As illustrated in Figure 4.3, received energy has a narrower beam width than the radiated energy as in the one dipole and same-length element case. This shows filtering effect of the ultra wideband antennas. On the other hand, side lobes start to appear in the neighborhood of the main lobe which means a different characteristic when compared to the one-dipole and same length graphs.

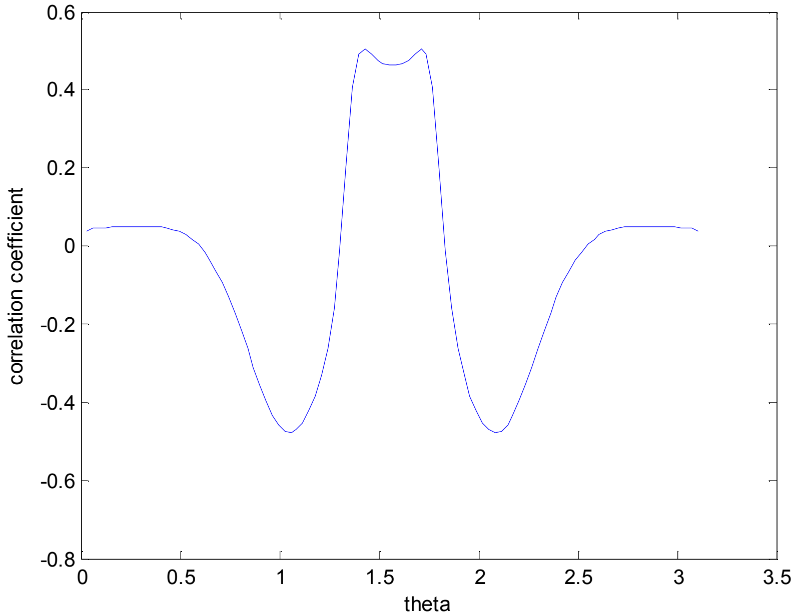

Figure 4.4. Correlation coefficient of V_g and V_L for element number $M = 9$; receiver dipole length = $\lambda_c/2$; $2l_n/a_n = 100$; $d = \lambda_l/2$, $Z_L = 150\ \Omega$.

When element number increases to $M = 9$ as in Figure 4.4, correlation coefficient curve gets narrower and a sharper transition occurs in the values while moving from broadside to end fire direction. Also the range over which higher correlation coefficient is obtained becomes smaller.

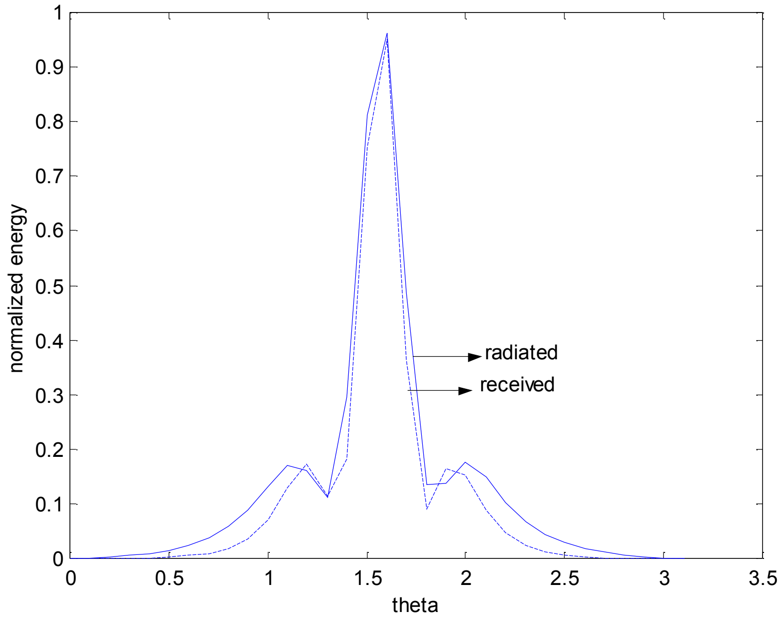

Figure 4.5. Normalized radiated and received energies for element number M = 9; receiver dipole length = $\lambda_c/2$; $2l_n/a_n$ = 100; $d = \lambda_1/2$, Z_L = 150 Ω.

In Figure 4.5, both radiated and received normalized energies are illustrated for element number M = 9. It could be deduced from the graph that, if element number increases form M = 7 to M = 9, small increase in side lobe levels can be observed while the beam width decreases.

Figure 4.6 compares the correlation coefficients for different M values. As it is seen in this figure, when the number of elements in the array increases, correlation coefficient curve tends to become narrower. While θ approaches from broadside to endfire ($\theta \to 0$ or $\theta \to \pi$), as the number of elements increases, deformation occurs in the similarity of two waveform shapes.

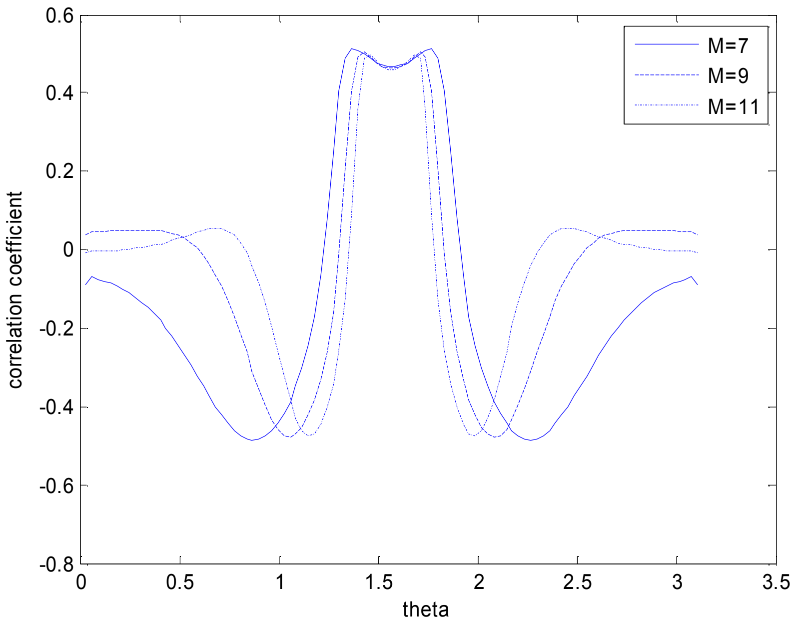

Figure 4.6. Correlation coefficient of V_g and V_L for element number M = 7, 9, 11; receiver dipole length = $\lambda_c/2$; $2l_n/a_n = 100$; $d = \lambda_1/2$, $Z_L = 150\ \Omega$.

Figure 4.7 illustrates the radiated energy patterns which are normalized with respect to the value at broadside direction for different element number. As seen in the figure, for a fixed element spacing *d*, radiated energy beam width decreases. This behavior agrees with the general behavior of arrays in other published papers about UWB antenna arrays (Mokole, 1996), (Sörgel et.al., 2005). On the other hand, side lobe level increases with increasing *M*.

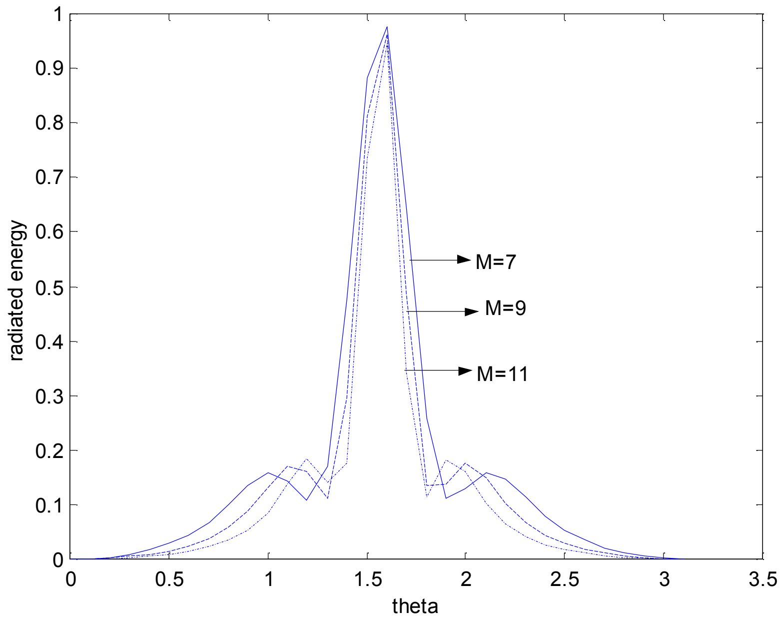

Figure 4.7. Normalized radiated energies for element numbers M = 7, 9, 11; receiver dipole length = $\lambda_c/2$; $2l_n/a_n = 100$; $d = \lambda_1/2$, $Z_L = 150\ \Omega$.

Figure 4.8 illustrates the received energy patterns normalized with respect to the value at broadside direction for different *M* values. Received energy pattern shows the same behavior as the radiated energy pattern except that the beam width is smaller.

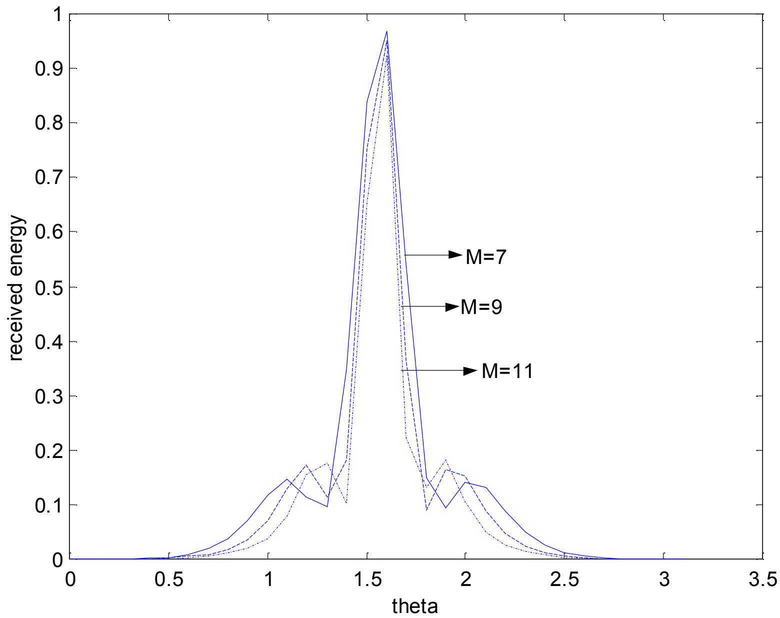

Figure 4.8. Received energies for element numbers M = 7, 9, 11; receiver dipole length = $\lambda_c/2$; $2l_n/a_n = 100$; $d = \lambda_l/2$, $Z_L = 150\ \Omega$.

Although the behavior of the different length dipole elements (Figure 4.6 to 4.8) and the same length dipole elements (Figure 3.5 to 3.7) show similarities as *M* increases, using different length dipoles provides higher correlation coefficient values over the entire pattern. Additionally, when energy patterns are considered, side lobes are developed if different length elements are used in the array.

In order to demonstrate this situation, correlation coefficients are plotted for one dipole, same length dipole array and different length dipole array in a single graph.

Figure 4.9 illustrates the correlation coefficients for one dipole, same-length element array and different-length element array with element number M = 7. It is clearly seen that, a higher correlation coefficient is obtained when different length elements are used in the array.

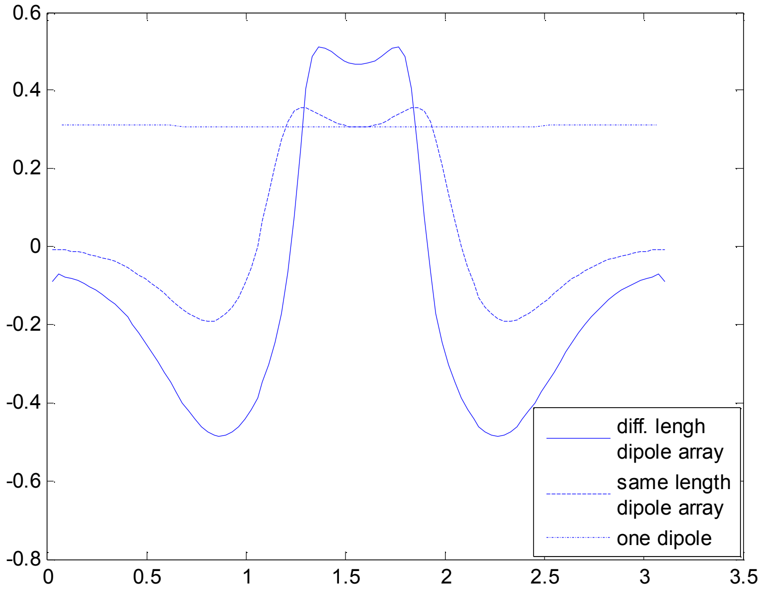

Figure 4.9. Correlation coefficients of V_g and V_L for one-dipole, same-length element array and different length element array for M = 7. Receiver dipole length = $\lambda_c/2$; $2l_n/a_n = 100$; $d = \lambda_l/2$, $Z_L = 150\ \Omega$.

Figures 4.10 and 4.11 illustrate the normalized energies for one dipole, same-length element array and different-length element array with element number M = 7. As seen in the figures, side lobes appear when different length elements are used in the array while no side lobe is observed in the pattern of same length element array.

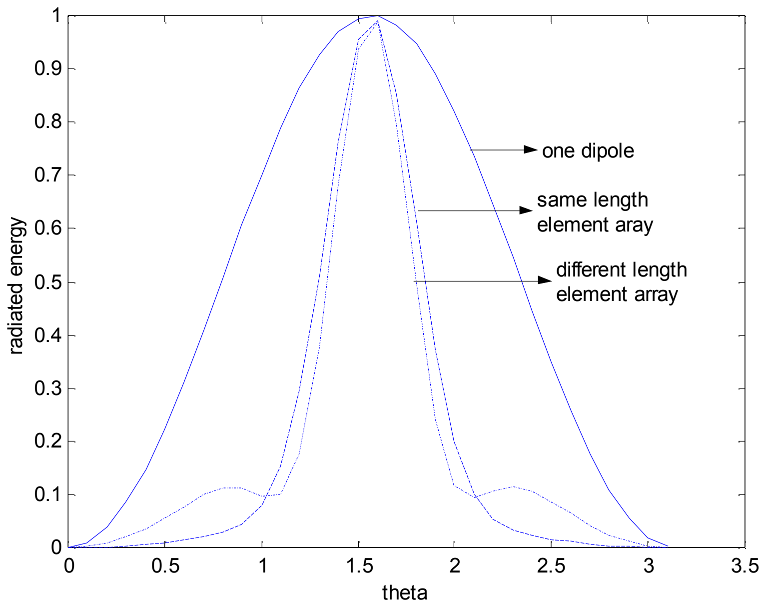

Figure 4.10. Normalized radiated energies for one-dipole, same-length element array and different length element array for M = 7. Receiver dipole length = $\lambda_c/2$; $d = \lambda_1/2$, $Z_L = 150\ \Omega$.

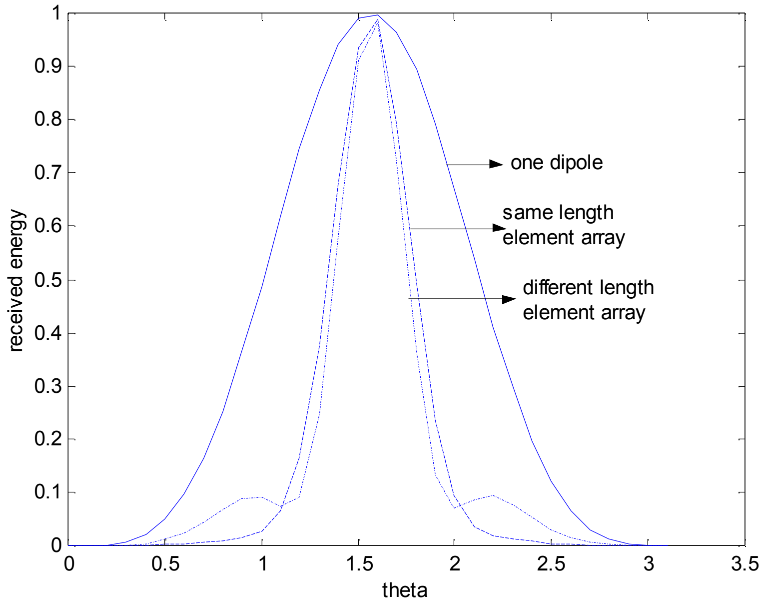

Figure 4.11. Normalized received energies for one-dipole, same-length element array and different length element array for M = 7. Receiver dipole length = $\lambda_c/2$; $2l_n/a_n = 100$; $d = \lambda_1/2$, $Z_L = 150\ \Omega$.

In Figure 4.12, a comparison of correlation coefficients for element number $M = 7$ and for various element spacings ($d = 0.5\lambda_l$, $d = 0.6\lambda_l$ and $d = 0.7\lambda_l$) is shown. For a fixed element number, as the spacing d between the elements of the array increases, correlation coefficient curve tends to become narrower.

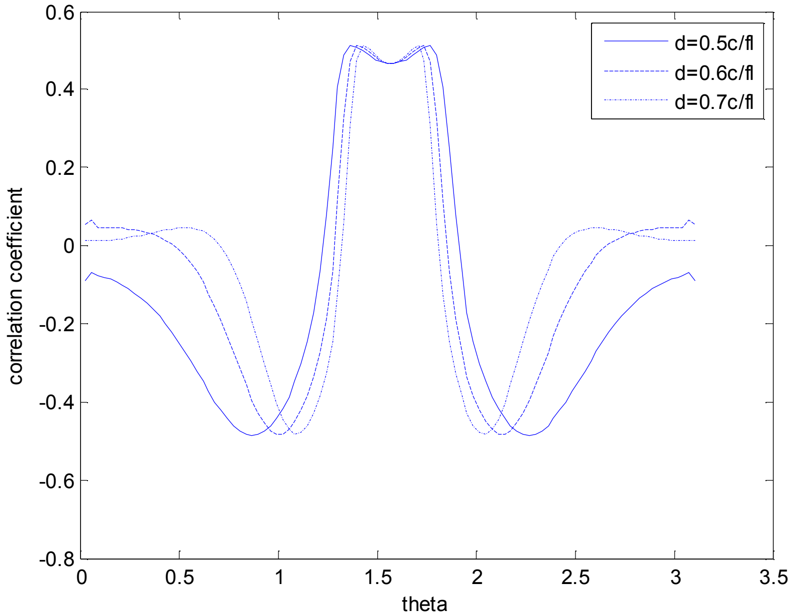

Figure 4.12. Correlation coefficients of V_g and V_L for $M = 7$ and $d = 0.5\lambda_l$, $d = 0.6\lambda_l$ and $d = 0.7\lambda_l$. Receiver dipole length = $\lambda_c/2$; $2l_n/a_n = 100$; $Z_L = 150\ \Omega$.

The following figures, that is, Figure 4.13 and Figure 4.14 illustrate the normalized radiated and received energies, respectively for different element spacing. As it is seen from the figures, the beam width for both radiated and received energies decreases. This behavior agrees with the behavior of ultra wideband arrays presented in other published papers (Mokole, 1996), (Sörgel, 2005). Side lobes are clearly seen also in this pattern as different from conventional same length element array, and peak of the side lobe increases with increasing d.

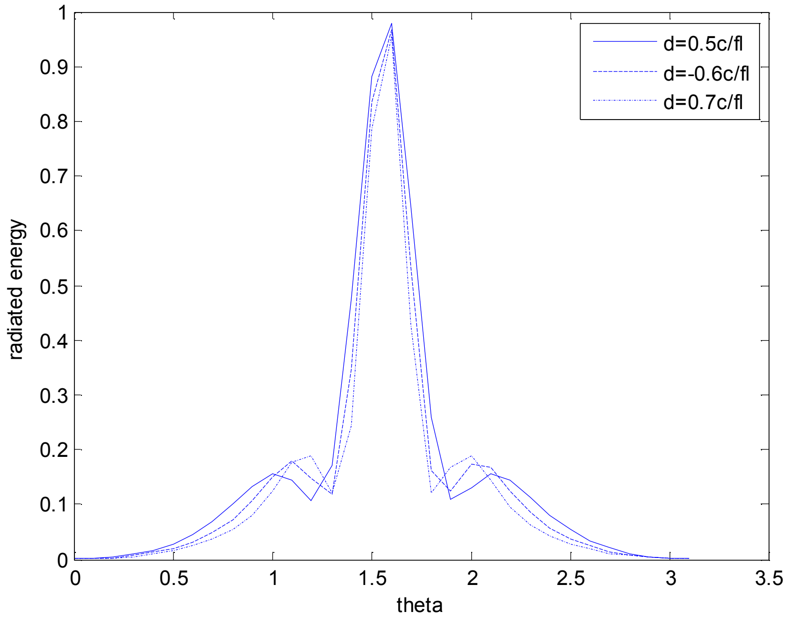

Figure 4.13. Normalized radiated energies for $M = 7$ and $d = 0.5\lambda_1$, $d = 0.6\lambda_1$ and $d = 0.7\lambda_1$. Receiver dipole length = $\lambda_c/2$; $2l_n/a_n = 100$; $Z_L = 150\ \Omega$.

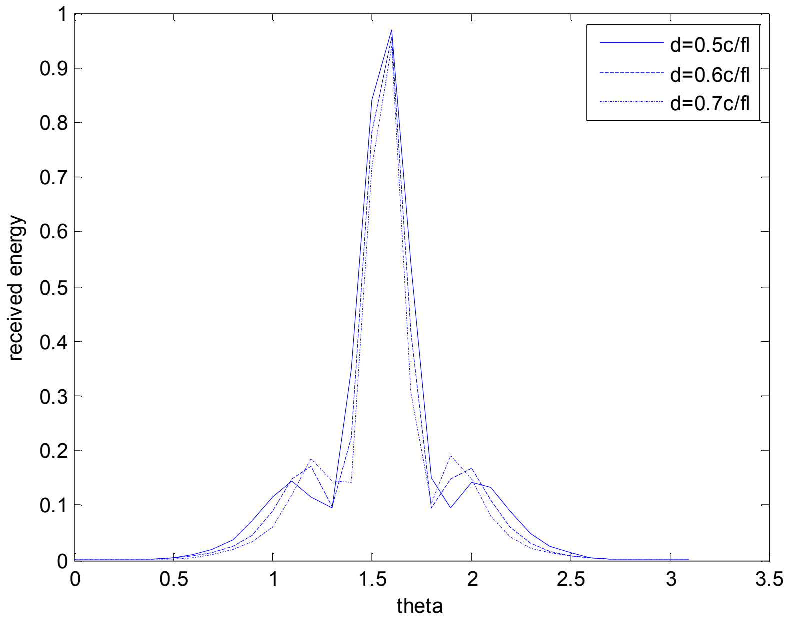

Figure 4.14. Normalized received energies for $M = 7$ and $d = 0.5\lambda_1$, $d = 0.6\lambda_1$ and $d = 0.7\lambda_1$. Receiver dipole length = $\lambda_c/2$; $2l_n/a_n = 100$; $Z_L = 150\ \Omega$.

In Figure 4.15, a comparison of correlation coefficients is shown for element number M = 9 and for various element spacing (d =0.5λ_1, d = 0.6λ_1 and d = 0.7λ_1). Figures 4.16 and 4.17 show normalized radiated and received energies for element number M = 7, respectively.

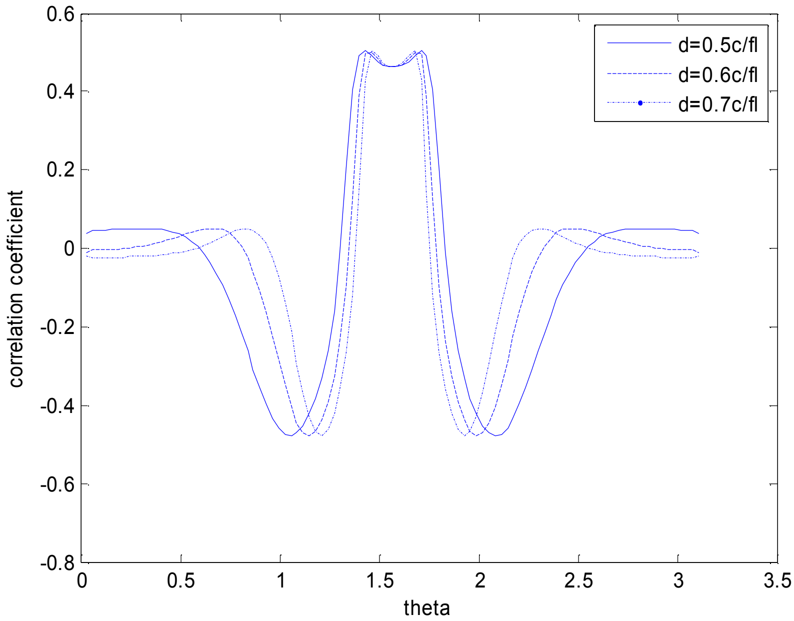

Figure 4.15. Correlation coefficients of V_g and V_L for M = 9 and d = 0.5λ_1, d = 0.6λ_1, and d = 0.7λ_1. Receiver dipole length = $\lambda_c/2$; $2l_n/a_n$ = 100; Z_L = 150 Ω.

As observed from the figure, with increasing element number, the behavior with respect to element spacing is the same, except that the correlation coefficient curve gets narrower and sharper. This means that a good correlation coefficient is achieved in a smaller interval over the entire pattern.

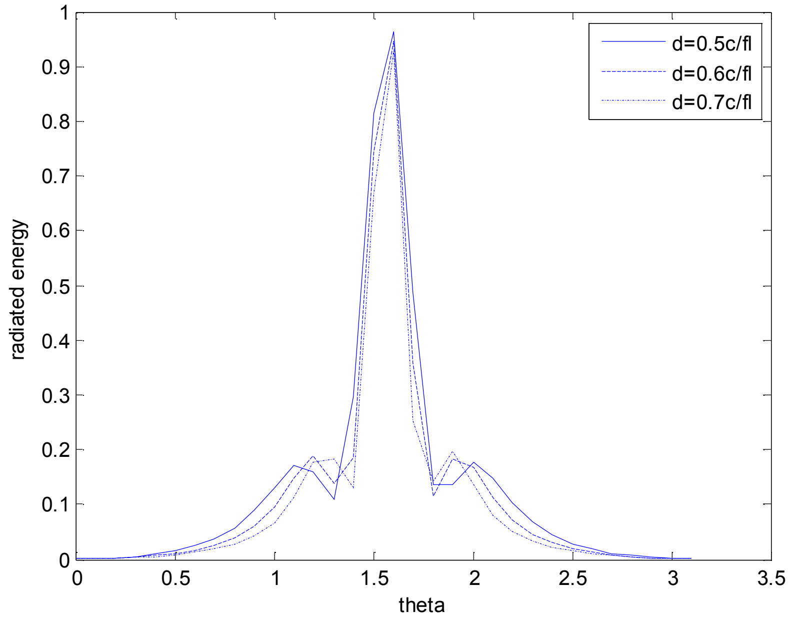

Figure 4.16. Normalized radiated energies for $M = 9$ and $d = 0.5\lambda_1$, $d = 0.6\lambda_1$ and $d = 0.7\lambda_1$. Receiver dipole length = $\lambda_c/2$; $2l_n/a_n = 100$; $Z_L = 150\ \Omega$.

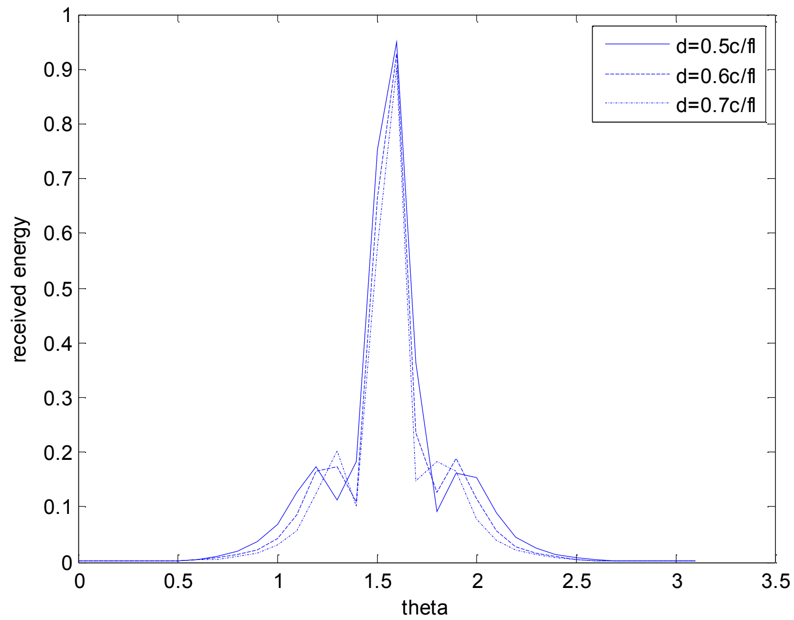

Figure 4.17. Normalized received energies for $M = 9$ and $d = 0.5\lambda_1$, $d = 0.6\lambda_1$ and $d = 0.7\lambda_1$. Receiver dipole length = $\lambda_c/2$; $2l_n/a_n = 100$; $Z_L = 150\ \Omega$.

As observed from energy pattern figures (Figures 4.16-4.17), with increasing element number, the energy curves get narrower and sharper, and side lobes also become sharper with increasing level.

Figure 4.18 compares the correlation coefficients of arrays with different length elements for various load impedances (Element number $M = 7$). It is seen that load impedance does not affect the behavior of the correlation coefficient significantly (shapes are quite similar) but a variation is observed in correlation coefficient values at broadside and end fire directions by varying Z_L.

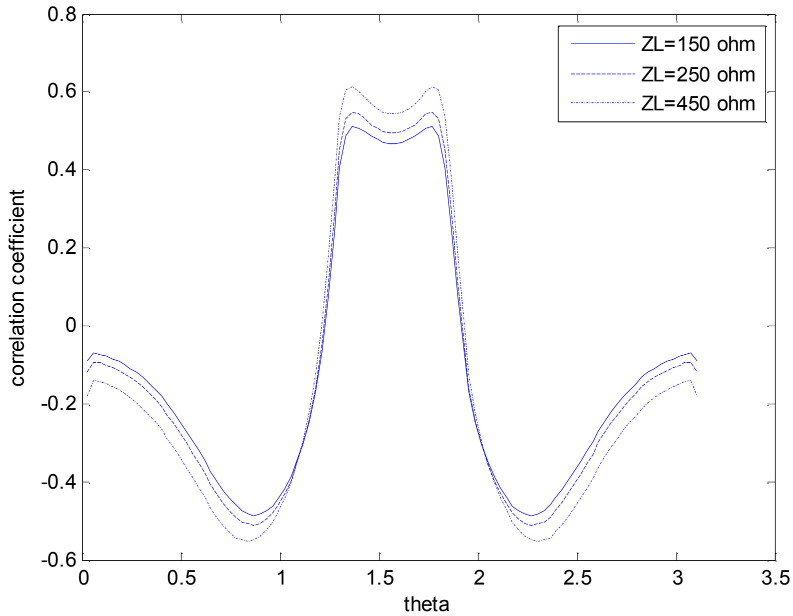

Figure 4.18. Correlation coefficients for Z_L = 150, 250, 450 Ω with $M = 7$ and $d = \lambda_1/2$. Receiver dipole length = $\lambda_c/2$; $2l_n/a_n = 100$.

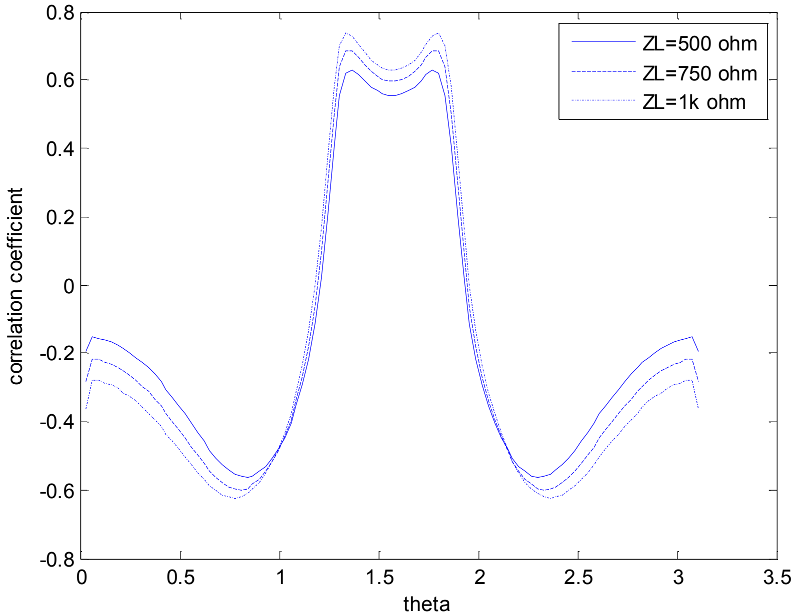

Figure 4.19. Correlation coefficients for Z_L = 500, 750, 1k Ω for element number M = 7 and element spacing $d = \lambda_1/2$. Receiver dipole length = $\lambda_c/2$; $2l_n/a_n$ = 100.

If Z_L is increased even more as in Figure 4.19, correlation coefficient value increases too.

In order to find the optimum parameters for achieving maximum correlation coefficient, a program is coded in MATLAB. This program is run for different ranges of Z_L, M, and d. After many runs, the maximum value of the correlation coefficient is obtained as 0.8260. The parameters that give this optimum value are found as follows

Correlation Coefficient	:	$CC_{max} = 0.8260$
Load Impedance	:	$Z_{Lopt} = 1.9512.10^3\Omega$
Element Number	:	$M_{opt} = 5$
Element Spacing	:	$d_{opt} = 0.0433$m

5. BEAM SCANNING FOR ULTRA WIDEBAND ANTENNA ARRAYS

5.1. Introduction

In this section, it is aimed to examine beam scanning concept for UWB dipole arrays. Radiated energy expression is derived and energy patterns are obtained with respect to observation angle for different scan directions. As in previous sections, the analysis is carried out in the frequency domain. The scanning is achieved by applying a time delay τ between consecutive elements. This means phase shift in the electric field expression (Sörgel et.al., 2005). Therefore, the scanning is accomplished by applying weights that has phase $n\tau$ for the nth element (Mokole, 1996).

5.2. Analysis of the Problem

Consider a linear array of (2N+1) equally spaced center-fed thin dipoles with lengths $2l_n$ and radii a_n which is positioned symmetrically with respect to the origin along the z-axis with each dipole also being oriented along the z-axis (Fig.5.1). The spacing between the elements is d. Radiated electric field for dipole n is as follows:

$$\mathbf{E}_n(\mathbf{r},f) = -\vec{\mathbf{a}}_\theta \frac{\zeta_0 V(f)}{2\pi r Z_n \sqrt{2N+1}\sin\theta}\left[\cos\frac{2\pi f l_n\cos\theta}{c} - \cos\frac{2\pi f l_n}{c}\right]\exp\left(-j\frac{2\pi f}{c}(r - nd\cos\theta + l_n + nc\tau)\right) \qquad (82)$$

which includes $n\tau$ term as being different from the previous array structure. Here, $\tau = d^*\cos(\theta_s)/c$ is the delay parameter which is applied between the consecutive elements. According to this, the maximum amplitude occurs at θ_s and is independent of frequency (Mokole, 1996). Here, the current distribution approximation along each of the dipoles is being represented by the distribution along an open-ended transmission line with characteristic impedance $Z_n = (\zeta_0/\pi)\ln(2l_n/a_n)$ as in previous sections. Each dipole is assumed to be matched to the feed network.

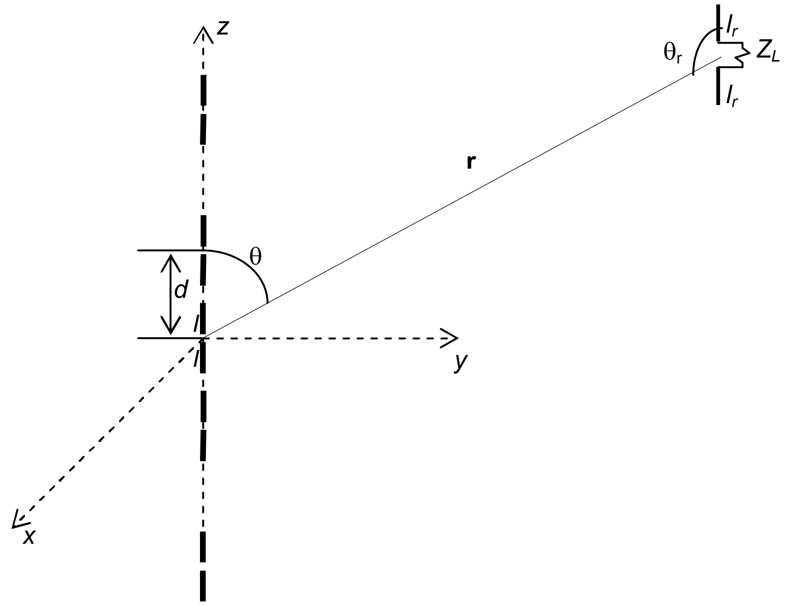

Figure. 5.1. Geometry of a linear array of (2N+1) dipoles

Radiated total electric far field at a distance *r* is found as the superposition of electric fields from individual elements and given by

$$\mathbf{E}_T(\mathbf{r}, f, \theta, \theta_s) = -\vec{\mathbf{a}}_\theta \sum_{n=-N}^{N} \frac{\zeta_0 V(f)}{2\pi r Z_n \sqrt{2N+1}\sin\theta} \left[\cos\frac{2\pi f l_n \cos\theta}{c} - \cos\frac{2\pi f l_n}{c}\right] \exp\left(-j\frac{2\pi f}{c}(r - nd\cos\theta + l_n + nc\tau)\right) \tag{83}$$

The expression for the radiated far field energy is given by (Mokole, 1996)

$$W(\theta, \theta_s) = \frac{1}{\zeta_0} \int_{-\infty}^{\infty} \left|\mathbf{E}_T(\mathbf{r}, f, \theta, \theta_s)\right|^2 df \tag{84}$$

Then radiated energy of the array is derived from

$$W_{rad} = \int_{-\infty}^{\infty} |-\vec{\mathbf{a}}_\theta \sum_{n=-N}^{N} \frac{\xi_0 V_g(f)}{2\pi r Z_n \sqrt{2N+1}\sin\theta}[\cos\frac{2\pi f l_n \cos\theta}{c} - \cos\frac{2\pi f l_n}{c}]$$

$$\exp(-j\frac{2\pi f}{c}(r - nd\cos\theta + l_n + nc\tau))|^2 \, df \qquad (85)$$

If the source voltage is Gaussian monocycle, then the radiated energy becomes

$$W_{rad} = \frac{4\pi^3 T^4}{(r\sin\theta)^2(2N+1)}\int_0^{\infty} f^2 e^{-(2\pi T f)^2}\{\sum_{n=-N}^{N}\frac{\left[\cos\frac{2\pi\, f l_n \cos\theta}{c} - \cos\frac{2\pi\, f l_n}{c}\right]^2}{[\ln(\frac{2l_n}{a_n})]^2}$$

$$+\sum_{\substack{n=-N\\n\neq m}}^{N}\sum_{m=-N}^{N}\frac{\left[\cos\frac{2\pi\, f l_n\cos\theta}{c} - \cos\frac{2\pi\, f l_n}{c}\right]\left[\cos\frac{2\pi\, f l_m\cos\theta}{c} - \cos\frac{2\pi\, f l_m}{c}\right]}{\ln(\frac{2l_n}{a_n})\ln(\frac{2l_m}{a_m})}$$

$$.\cos\frac{2\pi f}{c}[(m-n)(d\cos\theta - c\tau) + l_n - l_m]\}df \qquad (86)$$

which has the same form as in Section 4 except the $c\tau$ term.

The energy pattern is described as the normalized energy (Mokole, 1996)

$$W_n = \frac{W(\theta,\theta_s)}{W(\pi/2,\pi/2)} \qquad (87)$$

which is normalized relative to the energy at broadside observation and broadside scan angles.

Parenthesis in Eqn. (86) can be expanded to obtain an explicit expression for W_{rad} as follows

$$W_{rad} = \frac{4\pi^3 T^4}{(r\sin\theta)^2(2N+1)} \int_0^\infty f^2 e^{-(2\pi T f)^2}$$

$$\times\{\sum_{n=-N}^{N} \frac{\left[\cos^2 \frac{2\pi f l_n \cos\theta}{c} - 2\cos\frac{2\pi f l_n \cos\theta}{c}\cos\frac{2\pi f l_n}{c} + \cos^2\frac{2\pi f l_n}{c}\right]}{[\ln(\frac{2l_n}{a_n})]^2}$$

$$+\sum_{\substack{n=-N\\ n\neq m}}^{N}\sum_{m=-N}^{N}\frac{1}{\ln(\frac{2l_n}{a_n})\ln(\frac{2l_m}{a_m})}\cos\frac{2\pi f}{c}[(m-n)(d\cos\theta - c\tau) + l_n - l_m]$$

$$\times[\cos\frac{2\pi f l_n \cos\theta}{c}\cos\frac{2\pi f l_m \cos\theta}{c} - \cos\frac{2\pi f l_n \cos\theta}{c}\cos\frac{2\pi f l_m}{c}$$

$$-\cos\frac{2\pi f l_n}{c}\cos\frac{2\pi f l_m \cos\theta}{c} + \cos\frac{2\pi f l_n}{c}\cos\frac{2\pi f l_m}{c}]\}df$$

Then, each integral can be evaluated similarly using the identities used in previous sections designated before in equations (17) and (18) (Gradshteyn, 1980). Including the $c\tau$ term, the expressions are evaluated as listed below

$$A = \frac{1}{2}[\frac{\sqrt{\pi}}{4(2\pi T)^3} + \sqrt{\pi}\frac{8(\pi T c)^2 - \left(4\pi l_n \cos\theta\right)^2}{8c^2(2\pi T)^5} e^{-\left(\frac{l_n\cos\theta}{cT}\right)^2}]$$

$$B = \sqrt{\pi}\frac{1}{2}[\frac{8(\pi T c)^2 - \left(2\pi l_n(\cos\theta+1)\right)^2}{8c^2(2\pi T)^5} e^{-\left(\frac{l_n(\cos\theta+1)}{2cT}\right)^2}$$

$$+\frac{8(\pi T c)^2 - \left(2\pi l_n(\cos\theta-1)\right)^2}{8c^2(2\pi T)^5} e^{-\left(\frac{l_n(\cos\theta-1)}{2cT}\right)^2}]$$

$$C = \frac{1}{2}[\frac{\sqrt{\pi}}{4(2\pi T)^3} + \sqrt{\pi}\frac{8(\pi T c)^2 - \left(4\pi l_n\right)^2}{8c^2(2\pi T)^5} e^{-\left(\frac{l_n}{cT}\right)^2}]$$

$$D=\frac{1}{4}\{\sqrt{\pi}\,\frac{8\pi^2T^2c^2-\left\{2\pi[(l_n+l_m)\cos\theta+(m-n)(d\cos\theta-c\tau)+(l_n-l_m)]\right\}^2}{8c^2(2\pi T)^5}$$

$$.\,e^{-\left[\frac{(l_n+l_m)\cos\theta+(m-n)(d\cos\theta-c\tau)+(l_n-l_m)}{2cT}\right]^2}$$

$$+\sqrt{\pi}\,\frac{8\pi^2T^2c^2-\left\{2\pi[(l_n+l_m)\cos\theta-(m-n)(d\cos\theta-c\tau)-(l_n-l_m)]\right\}^2}{8c^2(2\pi T)^5}$$

$$.\,e^{-\left[\frac{(l_n+l_m)\cos\theta-(m-n)(d\cos\theta-c\tau)-(l_n-l_m)}{2cT}\right]^2}$$

$$+\sqrt{\pi}\,\frac{8\pi^2T^2c^2-\left\{2\pi[(l_n-l_m)\cos\theta+(m-n)(d\cos\theta-c\tau)+(l_n-l_m)]\right\}^2}{8c^2(2\pi T)^5}$$

$$.\,e^{-\left[\frac{(l_n-l_m)\cos\theta+(m-n)(d\cos\theta-c\tau)+(l_n-l_m)}{2cT}\right]^2}$$

$$+\sqrt{\pi}\,\frac{8\pi^2T^2c^2-\left\{2\pi[(l_n-l_m)\cos\theta-(m-n)(d\cos\theta-c\tau)-(l_n-l_m)]\right\}^2}{8c^2(2\pi T)^5}$$

$$.\,e^{-\left[\frac{(l_n-l_m)\cos\theta-(m-n)(d\cos\theta-c\tau)-(l_n-l_m)}{2cT}\right]^2}$$

$$E=\frac{1}{4}\{\sqrt{\pi}\,\frac{8\pi^2T^2c^2-\left\{2\pi[l_n\cos\theta+l_m+(m-n)(d\cos\theta-c\tau)+(l_n-l_m)]\right\}^2}{8c^2(2\pi T)^5}$$

$$.\,e^{-\left[\frac{l_n\cos\theta+l_m+(m-n)(d\cos\theta-c\tau)+(l_n-l_m)}{2cT}\right]^2}$$

$$+\sqrt{\pi}\,\frac{8\pi^2T^2c^2-\left\{2\pi[l_n\cos\theta+l_m-(m-n)(d\cos\theta-c\tau)-(l_n-l_m)]\right\}^2}{8c^2(2\pi T)^5}$$

$$.\,e^{-\left[\frac{l_n\cos\theta+l_m-(m-n)(d\cos\theta-c\tau)-(l_n-l_m)}{2cT}\right]^2}$$

$$+\sqrt{\pi}\,\frac{8\pi^2T^2c^2-\left\{2\pi[l_n\cos\theta-l_m+(m-n)(d\cos\theta-c\tau)+(l_n-l_m)]\right\}^2}{8c^2(2\pi T)^5}$$

$$.\,e^{-\left[\frac{l_n\cos\theta-l_m+(m-n)(d\cos\theta-c\tau)+(l_n-l_m)}{2cT}\right]^2}$$

$$+\sqrt{\pi}\,\frac{8\pi^2T^2c^2-\left\{2\pi[l_n\cos\theta-l_m-(m-n)(d\cos\theta-c\tau)-(l_n-l_m)]\right\}^2}{8c^2(2\pi T)^5}$$

$$.\,e^{-\left[\frac{l_n\cos\theta-l_m-(m-n)(d\cos\theta-c\tau)-(l_n-l_m)}{2cT}\right]^2}$$

$$F=\frac{1}{4}\{\sqrt{\pi}\frac{8\pi^2T^2c^2-\{2\pi[l_n+l_m\cos\theta+(m-n)(d\cos\theta-c\tau)+(l_n-l_m)]\}^2}{8c^2(2\pi T)^5}$$

$$.\,e^{-\left[\frac{l_n+l_m\cos\theta+(m-n)(d\cos\theta-c\tau)+(l_n-l_m)}{2cT}\right]^2}$$

$$+\sqrt{\pi}\frac{8\pi^2T^2c^2-\{2\pi[l_n+l_m\cos\theta-(m-n)(d\cos\theta-c\tau)-(l_n-l_m)]\}^2}{8c^2(2\pi T)^5}$$

$$.\,e^{-\left[\frac{l_n+l_m\cos\theta-(m-n)(d\cos\theta-c\tau)-(l_n-l_m)}{2cT}\right]^2}$$

$$+\sqrt{\pi}\frac{8\pi^2T^2c^2-\{2\pi[l_n-l_m\cos\theta+(m-n)(d\cos\theta-c\tau)+(l_n-l_m)]\}^2}{8c^2(2\pi T)^5}$$

$$.\,e^{-\left[\frac{l_n-l_m\cos\theta+(m-n)(d\cos\theta-c\tau)+(l_n-l_m)}{2cT}\right]^2}$$

$$+\sqrt{\pi}\frac{8\pi^2T^2c^2-\{2\pi[l_n-l_m\cos\theta-(m-n)(d\cos\theta-c\tau)-(l_n-l_m)]\}^2}{8c^2(2\pi T)^5}$$

$$.\,e^{-\left[\frac{l_n-l_m\cos\theta-(m-n)(d\cos\theta-c\tau)-(l_n-l_m)}{2cT}\right]^2}$$

$$G=\frac{1}{4}\{\sqrt{\pi}\frac{8\pi^2T^2c^2-\{2\pi[l_n+l_m+(m-n)(d\cos\theta-c\tau)+(l_n-l_m)]\}^2}{8c^2(2\pi T)^5}$$

$$.\,e^{-\left[\frac{l_n+l_m+(m-n)(d\cos\theta-c\tau)+(l_n-l_m)}{2cT}\right]^2}$$

$$+\sqrt{\pi}\frac{8\pi^2T^2c^2-\{2\pi[l_n+l_m-(m-n)(d\cos\theta-c\tau)-(l_n-l_m)]\}^2}{8c^2(2\pi T)^5}$$

$$.\,e^{-\left[\frac{l_n+l_m-(m-n)(d\cos\theta-c\tau)-(l_n-l_m)}{2cT}\right]^2}$$

$$+\sqrt{\pi}\frac{8\pi^2T^2c^2-\{2\pi[l_n-l_m+(m-n)(d\cos\theta-c\tau)+(l_n-l_m)]\}^2}{8c^2(2\pi T)^5}$$

$$.\,e^{-\left[\frac{l_n-l_m+(m-n)(d\cos\theta-c\tau)+(l_n-l_m)}{2cT}\right]^2}$$

$$+\sqrt{\pi}\frac{8\pi^2T^2c^2-\{2\pi[l_n-l_m-(m-n)(d\cos\theta-c\tau)-(l_n-l_m)]\}^2}{8c^2(2\pi T)^5}$$

$$.\,e^{-\left[\frac{l_n-l_m-(m-n)(d\cos\theta-c\tau)-(l_n-l_m)}{2cT}\right]^2}$$

The explicit form of the radiated energy can then be expressed as follows

$$W_{rad} = \frac{4\pi^3 T^4}{(r\sin\theta)^2 (2N+1)} \left[\sum_{n=-N}^{N} \frac{I - 2II - III}{[\ln(\frac{2l_n}{a_n})]^2} + \sum_{\substack{n,m \\ n\neq m}} \sum_{=-N}^{N} \frac{IV - V - VI + VII}{\ln(\frac{2l_n}{a_n})\ln(\frac{2l_m}{a_m})} \right] \quad (88)$$

5.3. Numerical Results for the Same Length Element Array

Based on the mathematical treatments obtained here, computer programs are created for $M = 2N+1$ dipoles and computed results are graphed. Each dipole length is chosen as $\lambda_c/2$, which corresponds the half wavelength at the center frequency f_c=6.85 GHz of the 3.1-10.6 GHz UWB range. Length/radius for all dipoles is 100. Pulse duration is $T=1/f_c$.

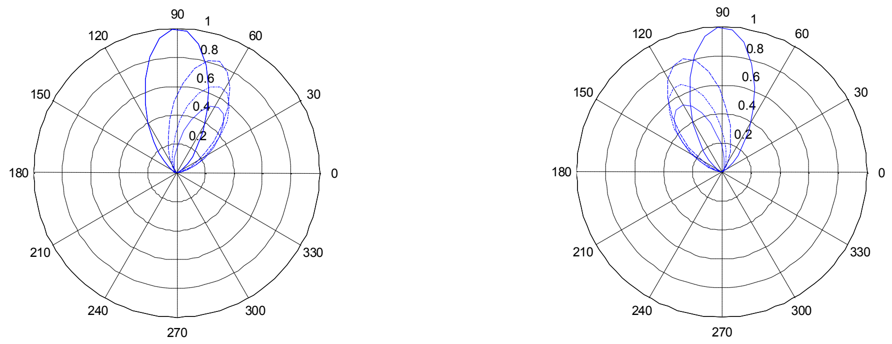

Figure 5.2. Radiation pattern in polar plot for $M = 5$ and $d = 0.6\lambda$, with scan angles a) θ_s=π/2, π/3, π/4, π/6 , b) θ_s=π/2, 2π/3, 3π/4, 5π/6

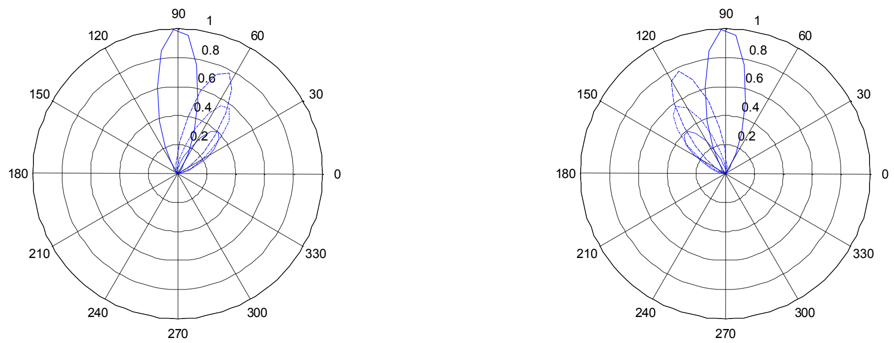

Figure 5.3. Radiation pattern in polar plot for $M = 9$ and $d = 0.6\lambda$, with scan angles a) θ_s=π/2, π/3, π/4, π/6, b) θ_s=π/2, 2π/3, 3π/4, 5π/6

In Figures 5.2 and 5.3, normalized energy patterns are illustrated with respect to observation angle θ for element number $M = 5$ and $M = 9$, respectively. The element spacing is chosen as $d = 0.6c/f_c$. Energy patterns are graphed in a polar plot for various different scan angles a) $\theta_s = 90^o, 60^o, 45^o, 30^o$ and b) $\theta_s = 90^o, 120^o, 135^o, 150^o$, respectively and compared in a single graph for each case.

As it is seen form the figures, maximum energy is achieved when both scan and observation angles are at broadside direction. As scan angle θ_s moves from broadside to end fire the main beam decreases. Additionally, as moved away from broadside towards the end fire, maximum value of the energy is not achieved at the specified scan direction. This situation is improved when the number of elements in the array increases. As expected, this behaviour is similar to the studies made for scanning dipole arrays in time domain (Mokole, 1996).

Note that when the element number is increased from 5 to 11 as in Figure 5.4, maximum energy is obtained almost at scan directions even if the scan direction moves away from broadside. On the other hand, when element number increases, as moved towards the end fire, maximum energy occurred at the scan direction decreases more rapidly.

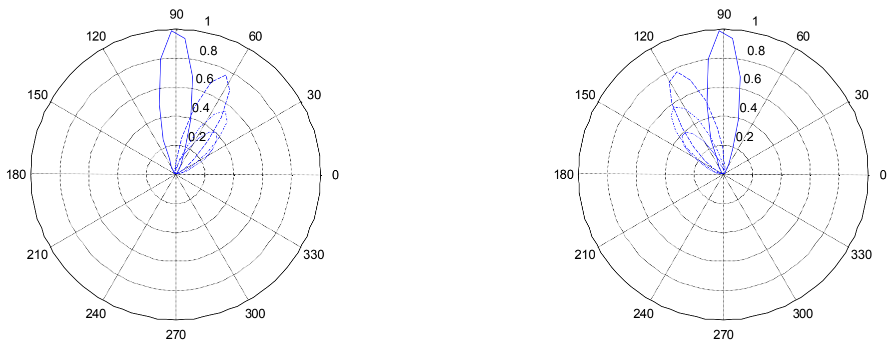

(a) (b)

Figure 5.4. Radiation pattern in polar plot for $M = 11$ and $d = 0.6\lambda$, with scan angles a) θ_s=$\pi/2$, $\pi/3$, $\pi/4$, $\pi/6$, b) θ_s=$\pi/2$, $2\pi/3$, $3\pi/4$, $5\pi/6$

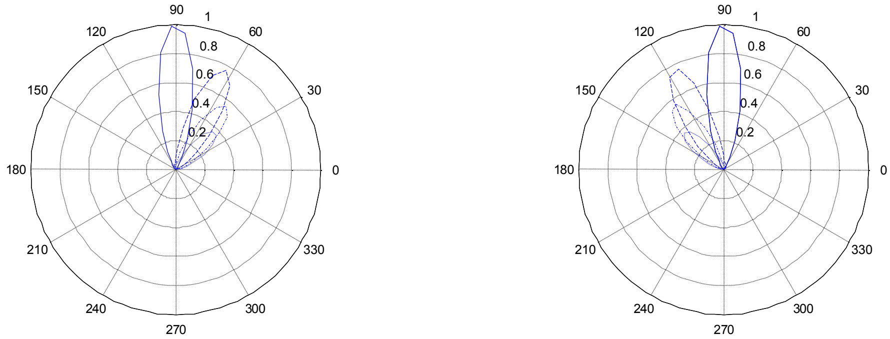

(a) (b)

Figure 5.5. Radiation pattern in polar plot for $M = 9$ and $d = 0.7\lambda$, with scan angles a) $\theta_s=\pi/2, \pi/3, \pi/4, \pi/6$, b) $\theta_s=\pi/2, 2\pi/3, 3\pi/4, 5\pi/6$

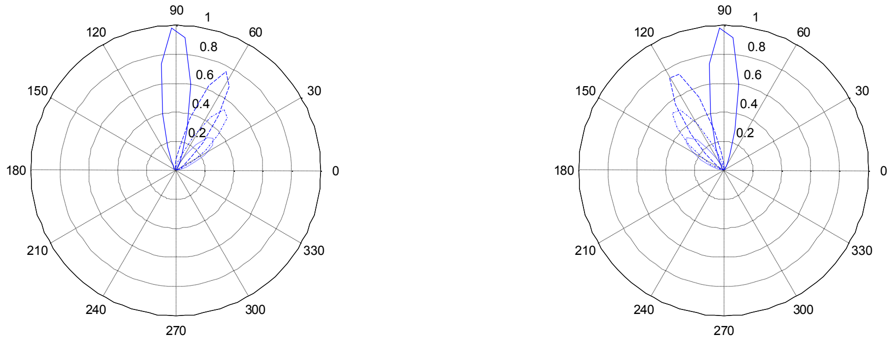

(a) (b)

Figure 5.6. Radiation pattern in polar plot for $M = 11$ and $d = 0.7\lambda$, with scan angles a) $\theta_s=\pi/2, \pi/3, \pi/4, \pi/6$, b) $\theta_s=\pi/2, 2\pi/3, 3\pi/4, 5\pi/6$

Figure 5.5 illustrates the radiation pattern for element number $M = 9$ and element spacing $d= 0.7c/f_c$. If the element spacing increases, maximum energy occurring at the scan direction decreases more rapidly as moved towards the end fire.

In Figure 5.6, the pattern is plotted for $M = 11$ and $d = 0.7c/f_c$. It is pretty clear that when M and d increases, in other words, when the array dimension increases, beam width of the energy decreases.

5.4. Numerical Results for the Different Length Element Array

Beam steering analysis is repeated with the array of different length elements. The elements in the array have different lengths such that each element in the array works at a specific frequency. The shortest dipole is half wavelength at 10.6 GHz, and the longest dipole is half wavelength at 3.1 GHz. Each of the other elements in the array is active at a specific frequency between these frequencies.

To highlight the beam steering phenomenon for this structure and for clarity, both types of plots are illustrated for each scan angle.

As in the case of same-length elements array maximum energy is achieved when both scan and observation angles are at broadside direction. As scan angle θ_s moves from broadside to end fire the main beam decreases. Additionally, as moved away from broadside towards the end fire, maximum value of the energy is not achieved at the specified scan direction, a behaviour which is consistent with the results given in (Mokole, 1996).

Here, a situation different from the same-length elements array case is observed such that side lobes appear as moved away from broadside direction and no symmetry occurs any more. Also, side lobe level and beam width increase when the scan angle approaches end fire.

Additionally, when different length elements are used in the array, radiation pattern has a narrower beam width and a better beam scanning is achieved when compared to same length elements array.

In Figures 5.7 through 5.11, radiation pattern is illustrated for element number M = 7 and for various scan angles.

As it is seen from Figure 5.7, at broadside scan angle ($\theta_s = \pi/2$), there is a symmetry around $\pi/2$. Additionally side lobes appear symmetrically around the main lobe.

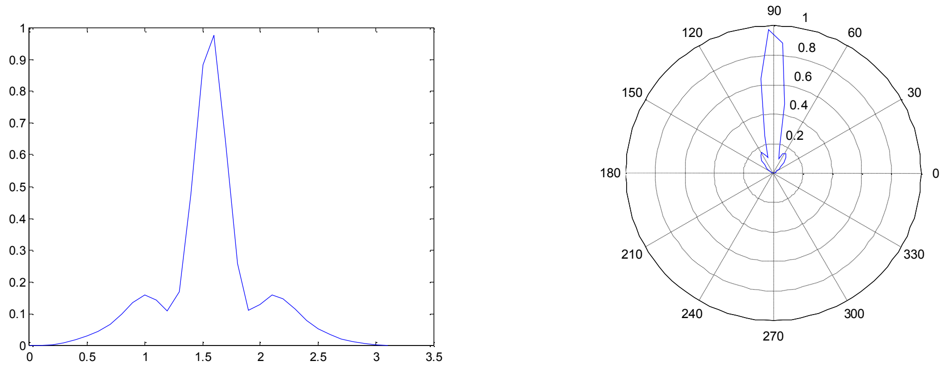

(a) (b)

Figure 5.7. a) Radiation pattern for $M = 7$, scan angle $\theta_s = \pi/2$, b) in polar plot for element spacing $d = \lambda_1/2$.

As shown in Figures 5.8 through 5.11, as moved away from broadside direction, no symmetry occurs any more. Also, side lobe level and beam width increase when the scan angle approaches end fire.

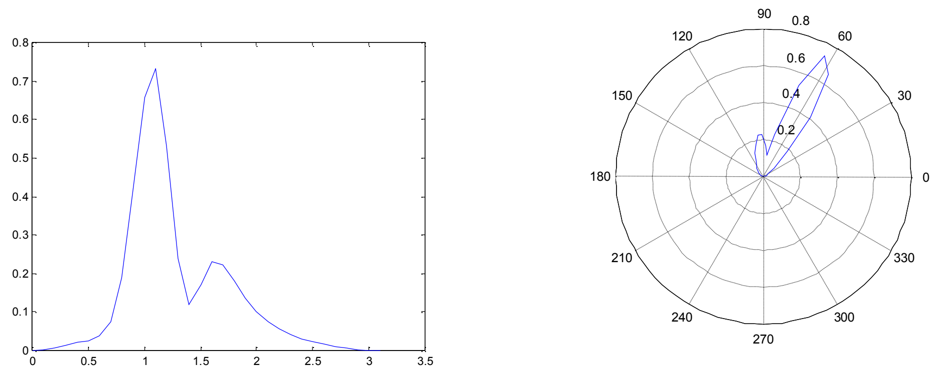

(a) (b)

Figure 5.8. a) Radiation pattern for $M = 7$, scan angle $\theta_s = \pi/3$, b) in polar plot for element spacing $d = \lambda_1/2$.

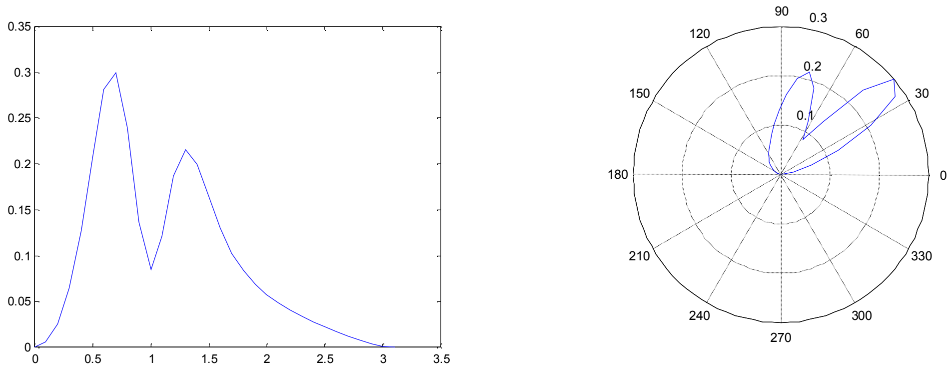

(a) (b)

Figure 5.9. a) Radiation pattern for $M = 7$, scan angle $\theta_s = \pi/6$, b) in polar plot for element spacing $d = \lambda_1/2$.

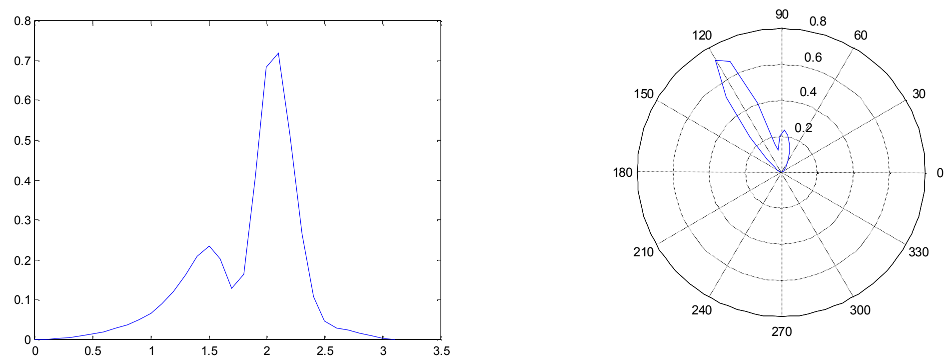

(a) (b)

Figure 5.10. a) Radiation pattern for $M = 7$, scan angle $\theta_s = 2\pi/3$, b) in polar plot for element spacing $d = \lambda_1/2$.

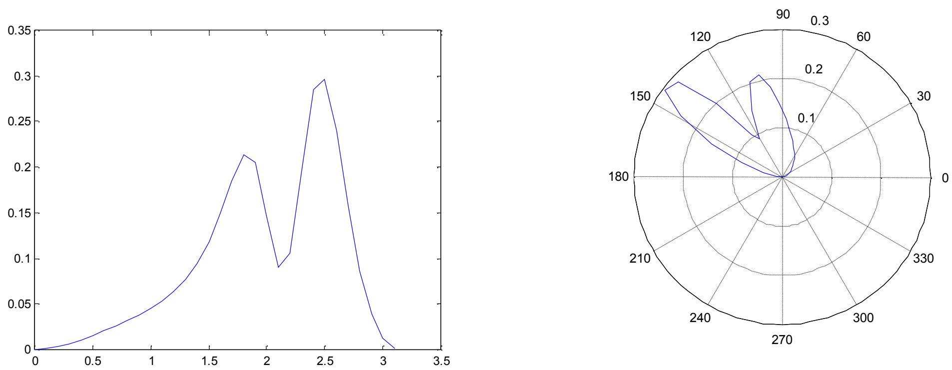

(a) (b)

Figure 5.11. a) Radiation pattern for $M = 7$, scan angle $\theta_s = 5\pi/6$, b) in polar plot for element spacing $d = \lambda_1/2$.

Figures 5.12 through 5.16 shows the results when M = 11. The similar behavior is seen as in the M = 7 case but a better beam scanning is achieved. Also main lobe and side lobe values decreases more rapidly as the scan angle moves towards the end fire.

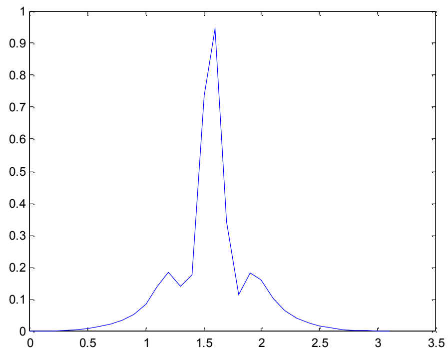

(a)

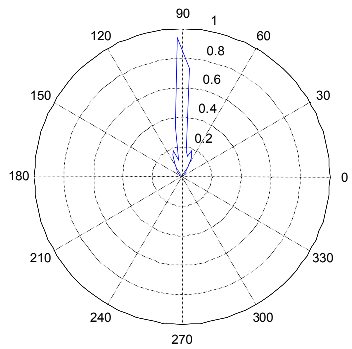

(b)

Figure 5.12. a) Radiation pattern for M = 11, scan angle $\theta_s = \pi/2$, b) in polar plot for element spacing $d = \lambda_1/2$.

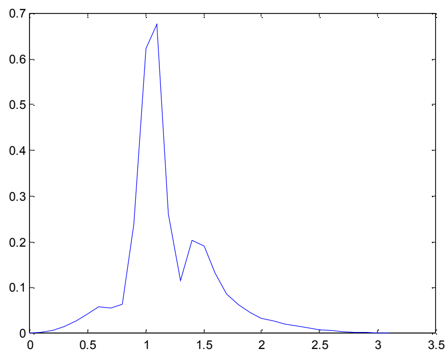

(a)

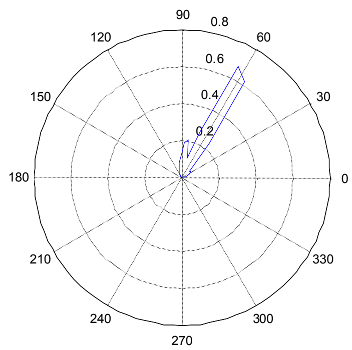

(b)

Figure 5.13. a) Radiation pattern for M = 11, scan angle $\theta_s = \pi/3$, b) in polar plot for element spacing $d = \lambda_1/2$.

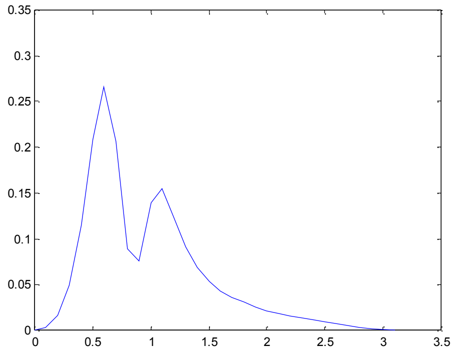

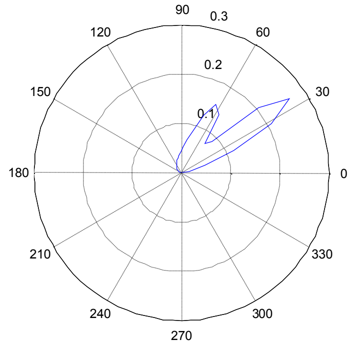

(a) (b)

Figure 5.14. a) Radiation pattern for $M = 11$, scan angle $\theta_s = \pi/6$, b) in polar plot for element spacing $d = \lambda_1/2$.

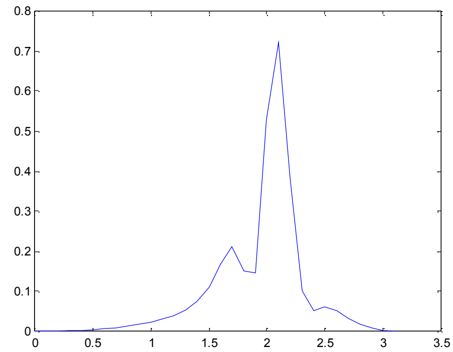

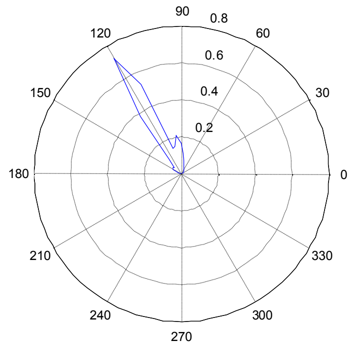

(a) (b)

Figure 5.15. a) Radiation pattern for $M = 11$, scan angle $\theta_s = 2\pi/3$, b) in polar plot for element spacing $d = \lambda_1/2$.

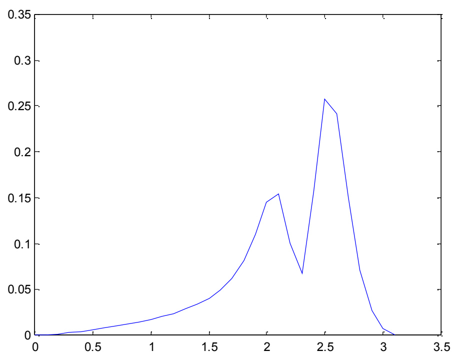

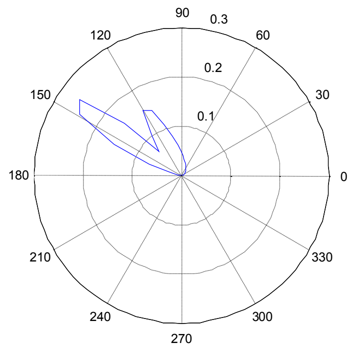

(a) (b)

Figure 5.16. a) Radiation pattern for $M = 11$, scan angle $\theta_s = 5\pi/6$, b) in polar plot for element spacing $d = \lambda_1/2$.

Figures 5.17 through 5.21 show the results when $M = 11$ and $d = 0.6\lambda_1$. When element spacing increases, the main lobe and side lobe values decreases more rapidly as the scan angle moves towards the end fire.

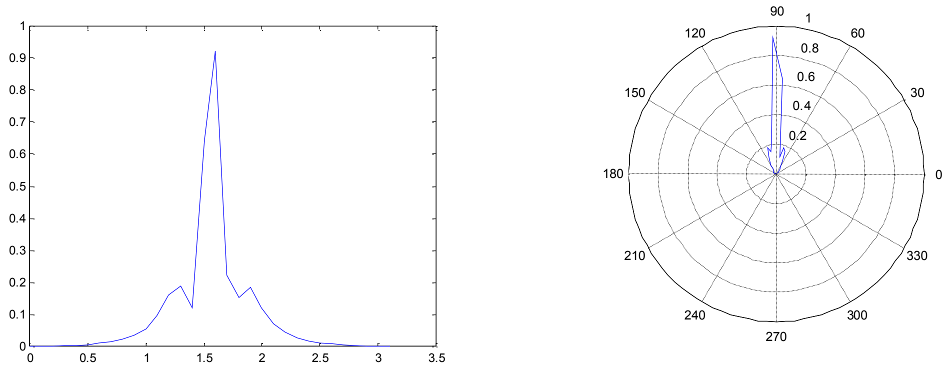

(a) (b)

Figure 5.17. a) Radiation pattern for $M = 11$, scan angle $\theta_s = \pi/2$, b) in polar plot for element spacing $d = 0.6\lambda_1$.

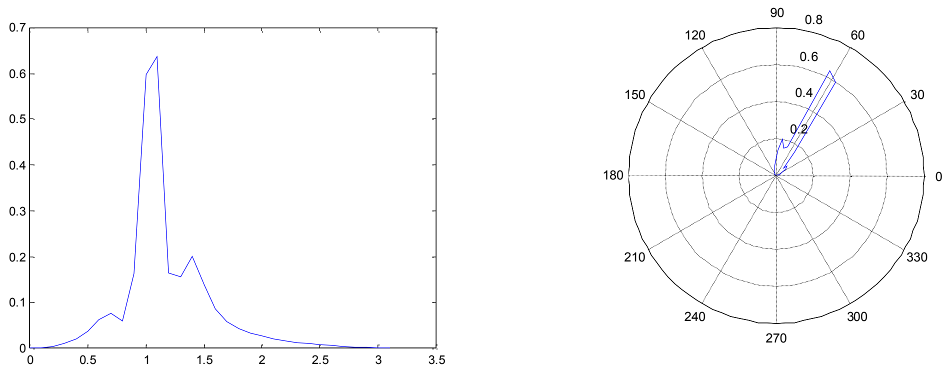

(a) (b)

Figure 5.18. a) Radiation pattern for $M = 11$, scan angle $\theta_s = \pi/3$, b) in polar plot for element spacing $d = 0.6\lambda_1$.

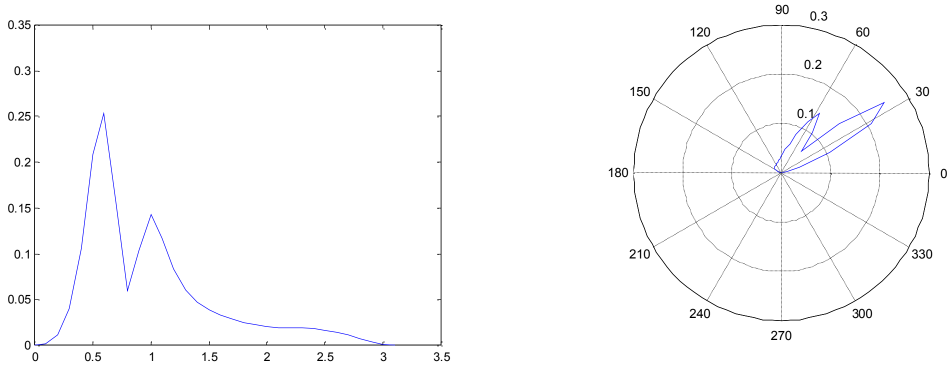

(a) (b)

Figure 5.19. a) Radiation pattern for $M = 11$, scan angle $\theta_s = \pi/6$, b) in polar plot for element spacing $d = 0.6\lambda_1$.

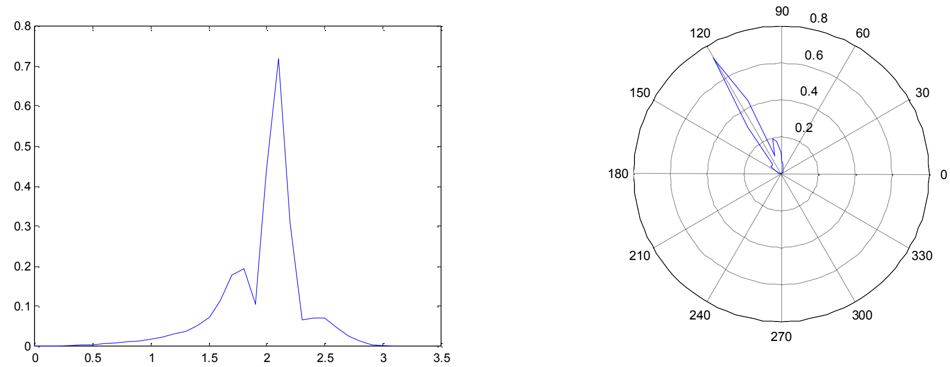

(a) (b)

Figure 5.20. a) Radiation pattern for $M = 11$, scan angle $\theta_s = 2\pi/3$, b) in polar plot for element spacing $d = 0.6\lambda_1$.

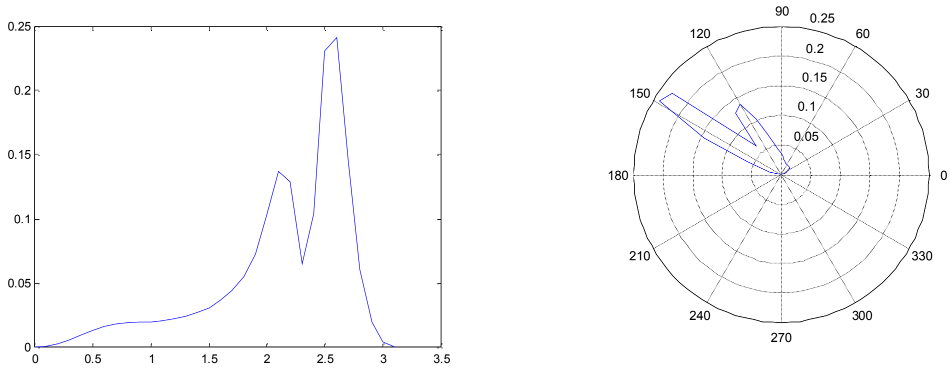

(a) (b)

Figure 5.21. a) Radiation pattern for $M = 11$, scan angle $\theta_s = 5\pi/6$, b) in polar plot for element spacing $d = 0.6\lambda_1$.

6. CONCLUSION

Very short duration pulses are used in ultra wideband (UWB) communications, in which the signal spectrum occupies an extremely large bandwidth causing the design of antennas to be a challenging issue for researchers.

In the literature, there are studies made with dipole for UWB pulse radiation and reception. In these studies various time domain approaches have been proposed and numerical techniques such as FDTD and MoM have generally been used to examine the antenna behavior (Boryssenko, 1999), (Chen et.al., 2003, 2004), (Lu et. al., 2003, 2004), (Mclean et.al., 2005). Although time-domain numerical techniques are mostly used for considering UWB systems, there are also some recent studies using frequency domain techniques (Dissanayake, 2006).

In this study, the radiation and reception characteristics of UWB antennas are investigated in terms of the energy and correlation coefficient concepts. The study obtains results in frequency domain rather than using numerical techniques in time domain providing a new perspective for UWB antenna design concept. The frequency domain analysis is numerically simple and in many cases, explicit expressions can be obtained easily. This is important because the frequency domain analysis presented here can also be applied to other antenna structures.

Although the aim is to analyze various type of dipole arrays as UWB antennas, the approach is first applied to a single dipole considering that it is the fundamental element of the array and mathematically simple (Mokole, 1996).

Dipole is chosen as the antenna element both at the transmitting and the receiving sides, and the radiated energy from the transmitting dipole and the received energy at the terminals of the receiving dipole are calculated. The plots of the radiated and received energy patterns with respect to observation angle show that the behaviors of the radiated and received energies are consistent as expected.

The investigation of the correlation coefficient is accomplished for two different cases. In the first case, in order to determine antenna capability in keeping the waveform shape as a function of direction for a given pulse (Mclean et. al., 2005), the correlation coefficient expression of the radiated electric field and the electric field radiated in the maximum field direction is derived. The correlation coefficient plots obtained in this study are compared with the results given by Mclean et. al. (2005). It is shown that these two results are in agreement and this can be considered as a verification of the analysis presented in this study.

As noted earlier, the characteristic of a received pulse is also useful in improving the overall performance of the transmitting-receiving antenna system; and detection process at the receiver needs special consideration to capture the incoming signal effectively. For this purpose, in the second case, it is aimed to observe detection characteristics in the receiver. Therefore, correlation coefficient is investigated to examine the correlation detection behavior of the receiving dipole. Frequency domain correlation coefficient between the generator voltage applied to the transmitting antenna and load voltage at the terminals of the receiving antenna are determined and correlation coefficient graphs are illustrated with respect to the observation angle.

As known, antenna arrays can be considered as an important option to deal with challenging properties of UWB systems, since array parameters can be adjusted to improve the radiation and detection characteristics. Therefore, in this study, it is additionally aimed to perform analysis to evaluate the behavior of dipole arrays with equally spaced same size elements in the frequency domain. Radiated energy from the array and received energy by the load at the terminals of the receiving antenna are derived and energy patterns which are normalized by the energy at broadside direction are plotted with respect to angle. Also, correlation coefficient between the load voltage at the terminals of the receiving antenna and the generator voltage applied to the transmitting antenna is investigated.

Based on the mathematical manipulations performed, computer programs are developed and computed results are presented. The results imply that, if element number or element spacing increases then beam widths for correlation coefficient, radiated and received energy patterns decrease. If the number of elements and the element spacing is smaller, the correlation coefficient varies in a smaller range with direction. If any of these increases, as moved away from the broadside, the variation of the correlation coefficient with direction increases. The maximum energy is achieved in neighborhood of the broadside direction as expected. Additionally, the characteristic obtained for the radiation pattern using this approach is in agreement with studies that have been performed in time domain by various authors (Mokole, 1996), (Heidary, 2001), (Sorgel et. al., 2005).

The analysis is then extended for an array of dipoles with different length elements. This way, each element works at a specific frequency and the combination of all elements' bandwidths form the frequency range of the array. Therefore, the operational frequency range of the antenna is expanded due to the different length elements corresponding to different frequency components (Ni, and Grebel, 2005).

The array with different length elements depicts similar behavior as the same length element array such that as the element number or element spacing increases, beam widths for correlation coefficient, radiated and received energy patterns decrease. Additionally, variation of correlation coefficient increases as moved away from broadside direction with increasing element number and element spacing. However the beam widths of the patterns for different length element array are narrower than the ones for same length element array. Since received pulse is depended on both the frequency and angle, variation of the correlation coefficient increases when moved away from broadside direction to the end fire.

Also, the results for a single dipole, array of equal length elements and different length elements are also illustrated in the same graph for comparison purposes. It can be concluded that, when different length elements are used in the array, a better correlation coefficient is achieved compared to one dipole and the array with equal length elements.

Finally, beam steering characteristics of UWB dipole arrays is also investigated in the study. Normalized energy patterns are illustrated with respect to observation angle.

In the case of same length element array, energy patterns are graphed in a polar plot for different scan angles. It is observed that, maximum energy is achieved when both scan and observation angles are at broadside direction. As scan angle θ_s moves from broadside to end fire the main beam decreases. Additionally, as moved away from broadside towards the end fire, maximum value of the energy is not achieved at the specified scan direction (this behaviour agrees with the results obtained in time domain by Mokole, 1996). This situation is improved when the number of elements in the array increases.

If different length elements are used in the array, a different situation is observed. As moved away from broadside direction, side lobes start to appear and the symmetry around $\pi/2$ which is seen at broadside scan is not observed any more. Also, radiation pattern has a narrower beam width and a better beam scanning is achieved when compared to same length elements array. When the scan angle approaches end fire, main lobe decreases, while side lobes and beam widths increase.

It should also be noted that, the reason for investigating the correlation coefficient and energy pattern concepts from a different point of view by taking into account both transmitting and receiving antennas, is to achieve a new perspective for the design consideration of UWB antennas.

REFERENCES

BORYSSENKO, A., 1999. Time Domain Studies of Ultra-Wide Band Antennas, Proceedings of the 1999 IEEE Canadian Conference on Electrical and Computer Engineering, 95-100.

BORYSSENKO, A., and TARASUK, V., 1999. Approximated Tedchnique to Simulate Impulse Antennas by Computing in Time Domain, Proceedings of the ICCEA`99 International Conference on Computational Electromagnetics and its Applications, 102-105.

CHEN, Z.N., WU, X.H., LI, H.F., YANG, N., and CHIA, M.Y.W., 2004. Consideretaions for Source Pulses and Antennas in UWB Radio Systems, IEEE Transactions on Antennas and Propagation, vol. 52(7): 1739-1748.

CHEN, Z.N., WU, X.H., YANG, N., and CHIA, M.Y.W., 2003. Design Considerations for Antennas in UWB Wireless Communication Systems, Proceedings of the 2003 IEEE International Symposium on Antennas and Propagation, 822-825.

COLLIN, R.E, 1985. Antennas and Radiowave Propagation. McGraw-Hill International Editions, Electrical Engineering Series, Singapore.

DISSANAYAKE, T., and ESSELLE, K.P., 2006. Correlation-Based Pattern Stabiltiy Analysis and a Figure of Merit for UWB Antennas, IEEE Transactions on Antennas and Propagation, vol. 54(11): 3184-3191.

FEDERAL COMMUNICATIONS COMMISSION (FCC), First Report and Order 02-48, 2002.

FRANCESCHETTI, G., and PAPAS, C. H., 1974. Pulsed Antennas, IEEE Transactions on Antennas and Propagation, vol. 22(5): 651-661.

GHAVAMI, M., MICHAEL, L.B., and KOHNO, R. 2004. Ultra Wideband Signals and Systems in Communication Engineering, John Wiley & Sons, England.

GRADSHTEYN, I.S.,1980. Table of Integrals, Series and Products. Academic New York.

HARMUTH, H.F., 1981. Nonsinusoidal Waves for Radar and Radio Communication, Academic Press, New York.

HEIDARY, K., 2001. Ultra-Wideband Antenna Arrays, Proceedings of the 2001 IEEE International Symposium on Antennas and Propagation, 472-475.

KANG Y.W., POZAR, D.M., 1986. Optimization of Pulse Radiation from Dipole Arrays for Maximum Energy in a Specified Time Interval, IEEE Transactions on Antennas and Propagation, vol. 34: 1383-1390.

LAMENSDORF, D., and SUSMAN, L., 1994. Baseband-Pulse-Antenna Techniques, IEEE Antennas and Propagation Magazine, vol. 36(1): 20-30.

LI, X., KONG, W., and WANG, G., 2006. On the Selection of Template Pulse Waveform in UWB Impulse Communications, Proceedings of the 2006 IEEE International Symposium on Antennas and Propagation, 1311-1314.

LU, G., SPASOJEVIC, P., and GREENSTEIN, L., 2003. Antenna and Pulse Design for Meeting UWB Spectrum Density Requirements, Proceedings of the 2003 IEEE Conference on Ultra Wideband Systems and Technologies, 162-166.

LU, G., KORISCH, I., GREENSTEIN, L., and SPASOJEVIC, P., 2004. Antenna Modeling Using Linear Elements with Applications to UWB, Proceedings of the 2004 IEEE International Symposium on Antennas and Propagation,. 2544-2547.

MALIK W.Q., EDWARDS, D.J., and STEVENS, C.J., 2006. Angular-spectral Antenna Effects in Ultrawideband Communications Links, IEE Proceedings on Communications, vol. 153(1): 99-106.

MCLEAN, J. S., FOLTZ, H., and SUTTON, R., 2004. The Effect of Frequency-Dependent Radiation Pattern on UWB Antenna Performance, Proceedings of the 2004 IEEE Antennas and Propagation Society Symposium, 2540-2543.

MCLEAN, J. S., FOLTZ, H., and SUTTON, R., 2005. Pattern Descriptors for UWB Antennas, IEEE Transactions on Antennas and Propagation, vol. 53(1): 553-559.

MCLEAN, J. S., SUTTON, R., and FOLTZ, H., 2004. The Effect of Source Pulse Shape on the Energy and Correlation Patterns of UWB Antennas, Proceedings of the European Conference on Wireless Technology, 113-116.

MOKOLE, E.L., 1996. Behavior of Ultrawideband-Radar Array Antennas, IEEE International Symposium on Phased Array Systems and Technology, 113-118.

MOLISCH, A.F., 2006. Introduction to UWB Signals and Systems, B. Allen, M. Dohler, E. Okon, W. Malik, A.Brown, D. Edwards, Ultra Wideband Antennas and Propagation for Communications, Radar and Imaging, John Wiley & Sons, 1-17.

NI, N., and GREBEL, H., 2005. Indepentently Center-Fed Dipole Array, Microwave and Optical Technology Letters, Vol. 45(6): 545-548.

NI, N., and GREBEL, H., 2006. Two-Element Indepentently Center-Fed Dipole Array for Ultrawideband and Ultrashort Pulse Applications, IEEE Antennas and Wireless Propogation Letters, Vol.5: 127-129.

POZAR, D.M., MCINTOS, R.E., and WALKER, S.G., 1983. The Optimum Feed Voltage for a Dipole Antenna for Pulse Radiation, IEEE Transactions on Antennas and Propagation, vol. 31:, 563-569.

POZAR, D.M., KANG, Y.W., SCHAUBERT, D.H., and MCINTOS, R. E., 1985. Optimization of the Transient Radiation from a Dipole Array, IEEE Transaction on. Antennas and Propagation, vol. 33: 69-75.

PulsON Technology Overview, http://www.timedomain.com, July 2000.

QUI, R.C., 1998. A Theoretical Study Of The Ultra Wideband Wireless Propagation Channel Based On The Scattering Centers, Proceedings of the IEEE Vehicular Technologies Conference, 308-312.

QUI, R.C. and Lu, I.T., 1999. Multipath Resolving With Frequency Dependence For Wideband Wireless Channel Modeling, IEEE Transactions On Vehicular Technologies, vol. 48(1): 273–285.

QUI, R., 2005. Propagation Effects, M.G.Di Benedetto et al., (ed.). UWB Communications Systems: A Comprehensive Overview, EURASIP publishing.

REED, J. H., 2005, Introduction to Ultra Wideband Communication Systems, www.informit.com.

SAMADDAR, S.N., 1992. Transient Radiation of a Single-Cycle Sinusoidal Pulse from a Thin Dipole, Journal of the Franklin Institute, Vol. 329(2): 259-272. .

SAMADDAR, S.N., 1993. Behavior of a Received Pulse Radiated by Half-Wave Dipole Excited by a Single-Cycle Sinusoidal Voltage, Journal of the Franklin Institute, Vol. 330(1): 17-28.

SCHANTZ, H.G., 2003. Introduction to Ultra-Wideband Antennas, Proceedings of the 2003 IEEE Conference on Ultra Wideband Systems and Technologies, 1-9.

SCHOLTZ, R.A., 1993. Multiple Access with Time Hopping Impulse Modulation, Proceedings of the IEEE MILCOM, 447-450.

SCHOLTZ, R.A., POZAR, D.M., NAMGOONG, W., 2005. Ultra-Wideband Radio, EUROSIP Journal on Applied Signal Processing, vol. 3: 252-272.

SHAN, D.M., CHEN, Z.N., and WU, X.H., 2005, Signal Optimization for UWB Radio Systems, IEEE Transactions on Antennas and Propagation, vol. 53(7): 2178-2184.

SÖRGEL, W., STURM, C., and WIESBECK, W., 2005. Impulse Responses of Linear UWB Antenna Arrays and the Application to Beam Steering, Proceedings of the 2005 IEEE International Conference on Ultra Wideband, 275-280.

TAHA, A., and CHUGG, K.M., 2002. On Designing the Optimal Template Waveform for UWB Impulse Radio In The Presence of Multipath, Proceedings of the 2002 IEEE Conference on Ultra Wideband Systems and Technologies, 41-46

WEIGHTMAN, G., 2003. Signor Marconi’s Magic Box: The Most Remarkable Invention of the 19th Century and the Amateur Inventor Whose Genius Sparked a Revolution”, da Capo Press.

WIN, M.Z., and SCHOLTZ, R.A., 1998. Impulse Radio: How It Works, IEEE Communucations Letters 2: 36-38.

WIN, M.Z., and SCHOLTZ, R.A., 2000. Ultra-Wide Bandwidth Time-Hopping Spread-Spectrum Impulse Radio for Wireless Multiple-Access Communications, IEEE Transactions on Communications, 48: 679-691.

WU, X.H., CHEN, Z.N., and CHIA, M.Y:W., 2003. Note on Antenna Design in UWB Wireless Communication Systems, Proceedings of the 2003 IEEE Confrence on Ultra Wideband Systems and Technologies, 503-507.

WU, X.H., KISHK, A.A., and CHEN, Z.N., 2005. A Linear Antenna Array for UWB Applications, Proceedings of the 2005 IEEE International Symposium on Antennas and Propagation, 594-597.

BIOGRAPHICAL SKETCH

Şule (YENER) ÇOLAK was born in Adana, Turkey. She received her Bachelor of Science degree from the Electrical and Electronics Engineering Department at Çukurova University in Adana, Turkey, in 1997. She received the Master of Science degree from the same department at Çukurova University in 2000. She was a visiting researcher in the Electrical and Computer Engineering Department at University of Florida, Gainesville, FL, USA during 2002 and 2005. She has been working as a Research Assistant in the Electrical and Electronics Engineering Department at Çukurova University since 1997.

Sule's research interests are ultra wideband communications, antenna arrays and design, and electromagnetic theory.